ON COMPENSATING THE OFDM PHYSICAL LAYER IMPAIRMENTS USING COMPRESSIVE SENSING

BY

ANUM ALI

A Thesis Presented to the
DEANSHIP OF GRADUATE STUDIES

KING FAHD UNIVERSITY OF PETROLEUM & MINERALS
DHAHRAN, SAUDI ARABIA

In Partial Fulfillment of the
Requirements for the Degree of

MASTER OF SCIENCE

In

ELECTRICAL ENGINEERING

MARCH 2014

KING FAHD UNIVERSITY OF PETROLEUM & MINERALS
DHAHRAN 31261, SAUDI ARABIA

DEANSHIP OF GRADUATE STUDIES

This thesis, written by **ANUM ALI** under the direction of his thesis adviser and approved by his thesis committee, has been presented to and accepted by the Dean of Graduate Studies, in partial fulfillment of the requirements for the degree of **MASTER OF SCIENCE IN ELECTRICAL ENGINEERING**.

Thesis Committee

Dr. Tareq Y. Al-Naffouri (Adviser)

Dr. Oualid Hammi (Co-adviser)

Dr. Azzedine Zerguine (Member)

Dr. Wajih A. Al-Saud (Member)

Dr. Ali A. Al-Shaikhi (Member)

Dr. Ali A. Al-Shaikhi
Department Chairman

Dr. Salam A. Zummo
Dean of Graduate Studies

15/5/14
Date

© Copyright by Anum Ali 2014
All Rights Reserved

"To give and not expect return, that is what lies at the heart of love."
Oscar Wilde (1854-1900)

To My Mother and Father,
for their Endless Love, Support and Encouragement.

ACKNOWLEDGEMENTS

I am truly grateful to Allah *subhanahu-wa-ta'ala*, the Most Compassionate and the Most Merciful, for enabling me to complete this work. I pray that this work and the growth that I had at KFUPM will be used in His cause.

I thank KFUPM for giving me the opportunity to study at this prestigious institute and for the facilities and support that I received here. I also acknowledge the Deanship of Scientific Research (DSR) at KFUPM and King Abdulaziz City for Science and Technology (KACST) for partly funding my research work.

I am thankful to COMSATS Institute of Information Technology, Islamabad, and its faculty for providing me a strong undergraduate education. Specifically, my learnings from Dr. Shafayat Abrar have been a great help in my research work at KFUPM.

I would like to express my profound gratitude to my principal advisor and mentor Dr. Tareq. Y. Al-Naffouri for the guidance, trust and help I received from him. He held me to a very high standard, and pushed me very hard from time to time. In addition to being a productive supervisor, he is a splendid human being and I have been thoroughly enriched working with him. I also thank Dr. Tareq for hosting me at his research group in King Abdullah University of Science

and Technology (KAUST), several times, including a semester long visit in spring 2014.

I acknowledge my co-advisor Dr. Oualid Hammi for his careful reviews and insightful commentary on my work throughout the degree. I also thank my committee members, Dr. Azzedine Zerguine, Dr. Wajih A. Al-Saud and Dr. Ali A. Al-Shaikhi for constructive criticism that has helped in sharpening the presentation of this work.

My research work is colored with contributions from many colleagues and advisors. In that regard, I would like to thank Dr. Ayman Naguib (Qualcomm Research Silicon Valley), Dr. Samir Al-Ghadhban (KFUPM), Ebrahim B. Al-Safadi (University of Southern California), Ahmed A. Quadeer (Hong Kong University of Science and Technology (HKUST)), Muhammad S. Sohail (HKUST), Damilola S. Owodunni (Saudi Telecom Company (STC)), Mudassir Masood (KAUST) and Abdullatif Al-Rabah (STC).

I would also like to thank my friends who have made my KFUPM experience, one to cherish. My evening tours with my roommate Mujahid bhai and our colleagues Qureshi sb and Asjad bhai will always be a valuable part of my memory. I also thank Qureshi sb for letting me use his office cubicle.

I am infinitely grateful to my parents for the values that they have passed down to me. I am also thankful to my family and friends for their continuous support and encouragement throughout my studies. Without their support, it would not have been possible to complete this degree.

TABLE OF CONTENTS

ACKNOWLEDGEMENTS **iii**

LIST OF TABLES **viii**

LIST OF FIGURES **ix**

ABSTRACT (ENGLISH) **xii**

ABSTRACT (ARABIC) **xiv**

CHAPTER 1 INTRODUCTION **1**

1.1 Transmitter Impairments 2

1.1.1 Peak-to-Average Power Ratio 2

1.1.2 Amplifier Nonlinearity 3

1.2 Channel 4

1.3 Receiver Impairments 5

1.4 Compressed Sensing 5

1.5 Organization and Contributions 7

1.6 Notations 9

CHAPTER 2 POWER AMPLIFIER LINEARIZATION **11**

2.1 Motivation 11

2.1.1 Chapter Contributions 14

2.2 CS-Based Joint-Compensation for Power Efficient Linear Amplification 15

2.2.1 Principle of Joint-Compensation 15
2.2.2 Device Under Test 19
2.3 System Overview 21
2.3.1 Transceiver Model 21
2.3.2 Spectrum Allocation 27
2.4 Over-driven Amplifier's distortion 28
2.4.1 Single User Over-drive 28
2.4.2 Multiuser Over-drive 29
2.5 Compressive Sensing for
Post-Compensation 30
2.5.1 Pilot Aided Compressed Sensing Scheme 31
2.5.2 Data-Aided Compressed Sensing Scheme 32
2.6 SIMO-OFDMA System 35
2.6.1 Individual Reconstruction per Diversity Branch 37
2.6.2 Joint Reconstruction Using Diversity Branches 37
2.7 Simulation Results 39
2.7.1 Experiment 1: Single Antenna Receiver 41
2.7.2 Experiment 2: Multiple Antenna Receiver 45
2.7.3 Experiment 3: Single Antenna vs Multiple Antenna Receiver 46
2.7.4 Experiment 4: Outage Capacity 47
2.7.5 Experiment 5: Mean Square Error 49
2.7.6 Experiment 6: Channel Delay Spread 50
2.8 Chapter Conclusion 52

CHAPTER 3 PAPR REDUCTION IN OFDM 53

3.1 Motivation 53
3.1.1 Chapter Contributions 56
3.2 Data Model for Clipped OFDM 57
3.3 Proposed Clipping Reconstruction Scheme 62
3.3.1 Simulation Results 67

3.4 Clipping Reconstruction for SIMO Systems 73
3.4.1 Simulation Results 75
3.5 Multi-user Communication 76
3.5.1 Simulation Results 82
3.6 Channel Estimation in Presence of Clipping 82
3.6.1 Simulation Results 86
3.7 Chapter Conclusion 87

CHAPTER 4 NARROWBAND INTERFERENCE PROBLEM 89
4.1 Motivation 89
4.2 Chapter Contributions 93
4.3 SC-FDMA and NBI Model 94
4.3.1 The NBI impaired SC-FDMA 96
4.4 Bayesian Sparse Recovery of the NBI 98
4.4.1 Sparsifying $\mathcal{I}'$ 102
4.4.2 Simulation Results 105
4.4.3 Experiment 2: Sparsifying usnig haar transform and reconstruction accuracy 106
4.5 Augmented NBI Recovery and the concept of Reliability 109
4.5.1 Simulation Results 114
4.6 Multiple Antenna Base-station 117
4.6.1 Simulation Results 118
4.7 Chapter Conclusion 118

CHAPTER 5 CONCLUSION AND FUTURE WORK 120
5.1 Concluding Remarks 120
5.2 Future Work 122

REFERENCES 124

VITAE 135

LIST OF TABLES

2.1 Over-drive level versus efficiency of the linearized Doherty amplifier. 18

3.1 Summary of the proposed WPA-SABMP scheme 68

LIST OF FIGURES

1.1 A typical high PAPR OFDM symbol. 3

2.1 Power spectrum of linearized PA's output, as a function of amplifier over-drive. 16

2.2 Distortions' sparsity rate and magnitude as a function of amplifier over-drive. 19

2.3 Measured gain and phase characteristics of PA. 20

2.4 Measured and approximated gain and phase characteristics of PA-DPD combination. 20

2.5 Block diagram of a typical communication system. 21

2.6 Sub-carrier allocation in OFDMA system. 28

2.7 Frequency domain view of distortion from user 1. 29

2.8 Geometrical representation of adopted reliability criteria. 33

2.9 Individual reconstruction per diversity branch. 38

2.10 Joint reconstruction using all diversity branches. 39

2.11 EVM performance of single antenna receiver averaged over fading channels. 43

2.12 BER performance of single antenna receiver averaged over fading channels. 43

2.13 EVM performance of single antenna receiver for optimistic channel. 44

2.14 EVM performance of multiple antenna receiver averaged over fading channels. 45

2.15 BER performance of multiple antenna receiver averaged over fading channels. 46
2.16 EVM performance comparison of single antenna vs multiple antenna receiver averaged over fading channels. 47
2.17 BER performance comparison of single antenna vs multiple antenna receiver averaged over fading channels. 48
2.18 Outage capacity averaged over fading channels for 4 dB over-drive and 4.5 dB over-drive. 49
2.19 MSE performance averaged over fading channels. 50
2.20 EVM performance comparison of for channels with high and low delay spread. 51
2.21 BER performance comparison of for channels with high and low delay spread. 52

3.1 BER versus CR ($P = 128$,$E_b/N_0 = 27$dB). 70
3.2 BER versus E_b/N_0 (CR $= 1.61$,$P = 128$). 70
3.3 BER versus P (CR $= 1.61$,$E_b/N_0 = 27$dB). 71
3.4 BER versus CR ($P = 128$, $E_b/N_0 = 27$dB, $\rho_{\text{init}} = 0.01\rho_{\text{true}}$ and $\sigma^2_{z_\text{init}} = 0.01\sigma^2_{z_\text{true}}$). 72
3.5 Individual reconstruction per diversity branch. 74
3.6 Joint reconstruction over all diversity branches. 75
3.7 BER versus CR for SIMO-OFDM Communication Systems ($P = 77$,$E_b/N_0 = 27$dB). 76
3.8 BER versus E_b/N_0 for Multi-user clipping recovery scheme (CR $= 1.61$,$P_u = 75$). 83
3.9 E_b/N_0 MSE (dB) for data aided CIR Estimation (CR $= 1.73, Q = R = 16$). 87

4.1 NBI spreading as a result of grid mismatch between NBI sources and the SC-FDMA system. 102
4.2 BER performance as a function of E_b/N_0 ($|\mathcal{T}| = 64$). 106

4.3 SABMP reconstruction results with no grid offset ($E_b/N_0 = 20$dB). 107
4.4 GI comparison of Haar transform and windowing method. 108
4.5 BER performance comparison of Haar transform and windowing ($|\mathcal{T}| = 64$). 108
4.6 BER performance comparison of Haar transform and windowing ($E_b/N_0 = 20$dB). 109
4.7 Reconstruction accuracy of the data-aided sparse recovery with grid offset. 115
4.8 Reconstruction accuracy of the data-aided sparse recovery with no grid offset. 116
4.9 Reliability of the data-aided scheme as a function of reserved tones. The $|\mathcal{R}|\%/|\mathcal{T}|\%$ format represents the ratio of the percentage of reliable carriers picked $|\mathcal{R}|\%$ to the percentage of reserved tones $|\mathcal{T}|\%$. 116
4.10 Reconstruction accuracy of the MMV scheme ($|\mathcal{T}| = 32$). 119

THESIS ABSTRACT

NAME: Anum Ali

TITLE OF STUDY: On Compensating the OFDM Physical Layer Impairments using Compressive Sensing

MAJOR FIELD: Electrical Engineering

DATE OF DEGREE: MARCH 2014

In this thesis, compressive sensing (CS) has been used to compensate for the physical layer impairments in orthogonal frequency division multiplexing (OFDM) systems. At the transmitter of an OFDM system, we deal with high peak to average power ratio (PAPR) of the transmission signal and the nonlinear response of the power amplifier (PA). The high PAPR problem is solved by thresholding at the transmitter and clipping recovery at the receiver. A pre-compensated overdriven PA is used to simultaneously solve the problem of linearization and power efficiency. The clipped transmitted signal is passed through a frequency selective channel which causes inter-symbol interference. This channel is to be estimated and compensated for acceptable performance of the communication system. To this end, effective strategies are outlined to estimate the channel with clipped

signal transmission. At the receiver, we may experience narrow-band interference (NBI) which can deteriorate the performance of a multicarrier communication system. This problem is addressed by sparse recovery of the NBI signal at the receiver. Simulation results are presented that demonstrate the ability of CS schemes to compensate for the mentioned physical layer impairments.

مُلخّص الرسالة

الاسم الكامل: أنعم علي

عنوان الدراسة: استخدام الجس المضغوط (CS) لتعويض التدهور في الطبقة الفيزيائية في أنظمة التقسيم العامودي للتردد (OFDM)

التخصص: هندسة كهربائية

تاريخ الدرجة العلمية: مارس 2014

في هذه الأطروحة، تم استخدام تقنية الجس المضغوط (CS) للتعويض عن ضعف الطبقة الفيزيائية في أنظمة التقسيم العمودي للتردد (OFDM). عادة ما تظهر في أجهزة الإرسال لأنظمة OFDM مشاكل مثل الذروة العالية بالنسبة لمتوسط الإشارة (PAPR) والاستجابة غير الخطية لمضخمات الطاقة (PA). يتم حل مشكلة PAPR بواسطة عتبة في جهاز الارسال و بالإضافة إلى تقليم الإشارة في جهاز الاستقبال. أما بالنسبة لمشكلة الاستجابات الغير خطية (PA) فيتم معالجتها بمحاولة تعديل الاستجابة لتكون خطية وذات كفاءة طاقة عالية. يتم تمرير الإشارة المقلَّمة خلال قناة انتقائية للتردد التي تسبب تداخل بين الرموز. يجب تقدير هذه القناة ليتم التعويض عن تأثيراتها وبالتالي ينتج أداء مقبول لنظام الاتصالات. تحقيقا لهذه الغاية ، تم سرد استراتيجيات فعالة لتقدير القناة مع وجود الإشارات المقلّمة. أما في جهاز الاستقبال، فإننا قد نواجه تشويش من قبل إشارات ضيقة النطاق (NBI)، والتي من شأنها أن تدهور أداء نظام الاتصالات. تعالج هذه المشكلة عن طريق استعادة متفرقة للإشارة ضيقة النطاق NBI في جهاز الاستقبال. تم عرض نتائج المحاكاة التي تبرهن على قدرة مخططات الجس المضغوط CS للتعويض عن التدهور في الطبقة الفيزيائية.

CHAPTER 1

INTRODUCTION

With ever increasing demand of higher data throughput in wireless/wireline networks, researchers are continuously looking for innovative solutions. One scheme that is dominatingly utilized in current communication standards is orthogonal frequency division multiplexing (OFDM). OFDM provides numerous advantages including high spectral efficiency and robustness against frequency selective channels. OFDM finds applications in digital subscriber line (DSL), wireless local area network (WLAN) standards (e.g., IEEE 802.11 a/b/g and HIPERLAN/2) and digital audio and video broadcasting (DAB/DVB) [1]. Further to that, OFDM is incorporated in metropolitan area networks (IEEE 802.16e), local area networks (IEEE 802.11n), personal area networks (IEEE 802.15.3) and other emerging cellular systems e.g., third generation partnership project (3GPP), long term evolution (LTE) and 4G+. The core idea is to use simple one-tap equalizers by creating a set of parallel, orthogonal, frequency-flat sub-channels using the computationally efficient inverse fast fourier transform (IFFT)/FFT modulation/demodulation.

Despite its numerous advantages, OFDM base communication systems suffer from some physical layer impairments. These impairments can be broadly classified in the following three categories i) *Transmitter Impairments*, ii) *Channel*, and iii) *Receiver Impairments*. In the subsequent sections we give these impairments/problems a closer look.

1.1 Transmitter Impairments

At the transmitter of an OFDM communication system, we mainly have two problems which are interrelated. One is the nonlinear response of the amplifier that becomes increasingly nonlinear with higher amplitudes of the input signal. Second is the high peak-to-average power ratio (PAPR) of the transmission signal. Though high PAPR is not an impairment by itself, it is a characteristic that results in nonlinear distortions by the power amplifier.

1.1.1 Peak-to-Average Power Ratio

The time domain OFDM signal has a high PAPR (see Fig. 1.1). The high PAPR nature of the OFDM signal is troublesome as generally the power amplifiers (PA) have nonlinear response for the higher input power levels. One way to avoid this nonlinearity and hence compression is to backoff the PA. This is not a preferred choice as power backoff causes power inefficiency.

The problem of PAPR reduction has received considerable research interest. Some of the transmitter based PAPR reductions schemes include coding, partial

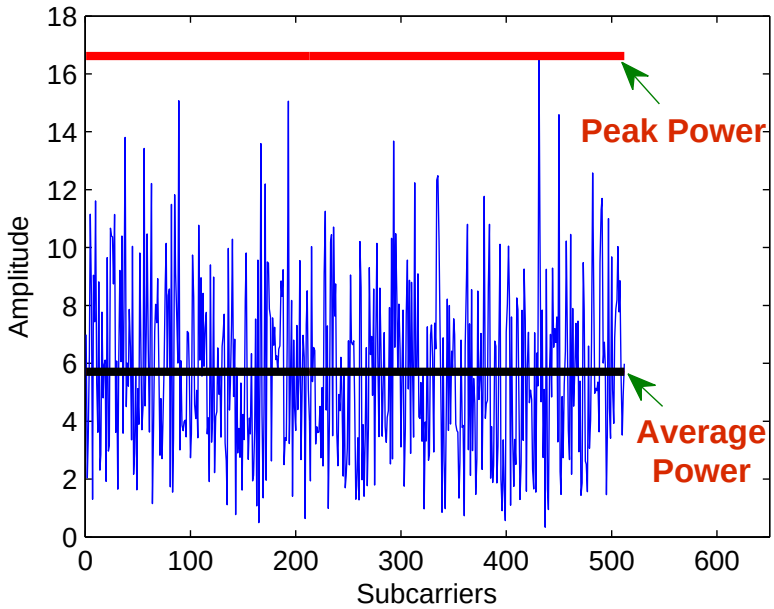

Figure 1.1: A typical high PAPR OFDM symbol.

transmit sequence (PTS), selected mapping (SLM), interleaving, tone reservation (TR), tone injection (TI) and active constellation extension (ACE) [2–5]. However, these schemes generally require an optimization algorithm, which is a source of complexity at the transmitter end. Hence, for low power mobile terminals the power efficiency obtained by the efficient operation of the PA is partly lost by running a complex optimization algorithm. Thus, there is a requirement for simple PAPR reductions scheme.

1.1.2 Amplifier Nonlinearity

Another problem at the transmitter is the nonlinear distortions generated by the PA. The amplifier has a nonlinear response especially for higher levels of the input power, hence the signals with higher power levels are generally compressed by the PA. The most commonly used methods of dealing with amplifier nonlinearity are

digital predistorter (DPD) and feedforward approaches [6–8]. The DPD consists of applying a complimentary nonlinearity (predistorter) before the nonlinear PA such that the cascade of the amplifier and predistorter behaves as a linear amplification system. However, the DPD circuit is a source of complexity at the transmitter and a power efficient solution is required.

1.2 Channel

Another source of physical layer impairments is the channel. Depending on its nature (e.g., slow fading, fast fading, flat fading or frequency selective fading), the channel introduces degradation to the transmitted signal. This is the reason why channel has to be estimated and compensated for, before the transmitted signal can be decoded.

An explanation of the matter will come in later parts of this thesis, but the frequency response of the channel per sub-carrier in OFDM systems is generally flat fading. This requires a simple one tap equalization of the channel per subcarrier at the receiver. For OFDM channel estimation, known equi-spaced pilot symbols are inserted at the transmitter and the channel frequency response is estimated using these pilot tones [9–11].

However, in presence of amplifier nonlinearity (or deliberate clipping for PAPR reduction) the performance of the channel estimation strategies based on minimum mean square error (MMSE) is not optimal and needs further investigation.

1.3 Receiver Impairments

There are some impairments that may be experienced at the receiver. One of these impairments is the narrow band interference (NBI) [12]. The OFDM signal is highly susceptible to NBI. The sources of NBI include other narrowband devices operating within the spectrum (e.g., cordless phones and garage door openers etc.). Due to the importance of NBI estimation and removal, several works were dedicated to address this issue. In [13] several tones are reserved at the transmitter and are then used at the receiver to sense the NBI. The NBI is then estimated using the linear minimum mean square error (LMMSE) approach. However, this method requires at least a rough estimate of the center frequency of the NBI, which, in general, is not available. In [14] prediction error filter (PEF) is used to eliminate the frequencies near NBI similar to a notch filter. However, the aforementioned NBI mitigation schemes do not utilize the fact that NBI is sparse. Exploiting the sparse nature of NBI will possibly result in less complex solutions towards its recovery.

1.4 Compressed Sensing

This thesis utilizes compressed sensing (CS) methodology to solve all the aforementioned problems associated with OFDM systems. CS is a tool to recover sparse signals using fewer measurements than the size of the unknown signal/system. However, the signal and the measurements have to satisfy the following two conditions:

1. The domain of signal measurements and signal sparsity are incoherrent.

2. Measurement are acquired by non-uniform sampling, i.e., measurements are obtained randomly.

Over the last few years, CS has received considerable research interests and it has been applied to many applications including OFDM communication [15–17], ultra wide band (UWB) [18, 19], image processing [20, 21] and radar [22, 23] to name a few. The main idea is to cast any problem in the form

$$\mathbf{y} = \mathbf{A}\mathbf{x} + \mathbf{n}$$

where $\mathbf{x} \in \mathbb{C}^N$ is a sparse unknown vector, $\mathbf{A} \in \mathbb{C}^{M \times N}$ is the measurement matrix and $\mathbf{y} \in \mathbb{C}^M$ is the measurement vector. Once the problem is in the aforementioned form, the signal can be reconstructed using any sparse signal reconstruction methodology e.g., ℓ_1-minimization [24], Bayesian methods [25–27] and matching pursuits [28–30]. This thesis explores the application of these CS tools to solve physical layer impairments in OFDM systems. To this end, we show how these problems can be casted as a sparse signal recovery problems and present low complexity recovery schemes. In addition, we exploit the inherent structure associated with these problems towards a better recovery of the unknown sparse signal of interest.

1.5 Organization and Contributions

From structural point of view, this thesis is divided into three portions. First portion deals with the problem of *power amplifier lienarization*, the second portion deals with the problem of *PAPR reduction* and *channel estimation* and the third portion deals with the problem of *narrow band interference cancellation*.

In the first portion (Chapter 2), linearization of user equipment PAs driven by OFDM signals is addressed. Particular attention is paid to the power efficient operation of an OFDMA cognitive radio (CR) system and realization of such a system using CS. Specifically, pre-compensated over-driven amplifiers are employed at the mobile terminal. Over-driven amplifiers result in in-band distortions and out of band interference. Out of band interference mostly occupies the spectrum of inactive users, where the in-band distortions are mitigated using CS at the receiver. It is also shown that the performance of the proposed scheme can be further enhanced using multiple measurements of the distortion signal in single-input multi-output (SIMO) systems. Numerical results verify the ability of the proposed setup to improve error vector magnitude, bit error rate, outage capacity and mean squared error.

The second portion (Chapter 3) deals with the problem of PAPR reduction. Clipping is one of the simplest PAPR reduction schemes for OFDM. Deliberately clipping the transmission signal degrades the system performance and clipping mitigation is required at the receiver for information restoration. In this chapter, we acknowledge the sparse nature of the clipping signal and propose a low

complexity Bayesian clipping estimation scheme. The proposed scheme utilizes the *a priori* information about the sparsity rate and noise variance for enhanced recovery. At the same time the proposed scheme is robust against inaccurate estimates of the clipping signal statistics. The undistorted phase property of the clipped signal as well as the clipping likelihood is utilized for enhanced reconstruction. Further, motivated by the nature of modern OFDM based communication systems, we extend our clipping reconstruction approach for i) multiple antenna receivers and ii) multi-user OFDM. We also address the problem of channel estimation from pilots contaminated by the clipping distortions. Numerical findings are presented which depict favourable results for the proposed scheme compared to the established sparse reconstruction schemes.

The third portion (Chapter 4) addresses the narrowband interference problem and a novel NBI mitigation scheme is proposed for SC-FDMA systems. The proposed NBI cancellation scheme exploits the frequency domain sparsity of the unknown signal and adopts a low complexity Bayesian sparse recovery procedure. At the transmitter a few non-uniformly placed sub-carriers are kept data free to sense the NBI signal at the receiver. Further, it is noted that in practice, the sparsity of the NBI signal is destroyed by a grid mismatch between NBI sources and the system under consideration. Towards this end, first an accurate grid mismatch model is presented that is capable of assuming independent offsets for multiple NBI sources. Secondly, prior to NBI reconstruction, the sparsity of the unknown signal is restored by employing a sparsifying transform. To improve the

spectral efficiency of the proposed scheme, a data-aided NBI recovery procedure is outlined. This data-aided scheme relies on adaptively selecting a subset of data carriers and using them as additional measurements to enhance the NBI estimation. Numerical results are presented that depict the suitability of the proposed scheme for NBI mitigation.

It is worth highlighting that the contributions of this thesis are rather diverse, tackling multiple problems (i.e., PAPR reduction, PA linearization, channel estimation and NBI mitigation) for different variants of OFDM (i.e., OFDMA, SC-FDMA, SIMO-OFDM, SIMO-SC-FDMA). Hence, it is difficult to put forth a common data model and a comprehensive literature review covering all these topics at once. To circumvent this, each chapter of this thesis is made self contained in a sense that it includes its own motivation of the problem, data model and contributions. Furthermore, as chapters 2-4 (i.e., the core of this thesis) essentially address separate problems, they are written in a manner that facilitates their individual reading, eliminating the need to go through them sequentially.

1.6 Notations

Unless otherwise noted, the scalars are represented by italic letters (e.g. N). Bold-face lower-case letters (e.g., $\mathbf{x}$) are reserved to denote time domain vectors, and frequency domain vectors are represented using bold-face upper-case calligraphic letters (e.g., $\boldsymbol{\mathcal{X}}$). Bold-face upper-case letters are associated with matrices (e.g., $\mathbf{F}$) and a hat over a variable (e.g., $\hat{\mathbf{x}}$) represents its estimate. Further, $\mathrm{x}(l)$ denotes

the lth entry of a vector $\mathbf{x}$. Underlined vectors and matrices with a number in superscript (e.g. $\underline{\boldsymbol{\mathcal{X}}}^i$) will represent the ith portion of the vector $\boldsymbol{\mathcal{X}}$, where $\boldsymbol{\mathcal{X}}$ is partitioned in I segments. The Transpose and Hermitian of a vector are denoted by T and H respectively (e.g., $\mathbf{x}^{\mathsf{T}}$ and $\mathbf{x}^{\mathsf{H}}$). The operator $|\cdot|$ operating on a scalar (e.g., $|x(i)|$) will give the absolute value and operating on a set (e.g., $|\mathcal{S}|$) will give the number of elements in $\mathcal{S}$. Further, $\mathbb{E}[\cdot]$, $\mathbf{I}$ and $\mathbf{0}$ denote the expectation operator, identity matrix and the zero vector, respectively. The operator $\text{diag}(\mathbf{X})$ forms a column vector $\mathbf{x}$ from the diagonal of $\mathbf{X}$ and $\text{diag}(\mathbf{x})$ construct a diagonal matrix $\mathbf{X}$ with $\mathbf{x}$ on its diagonal. The operators $\|\cdot\|_2, \|\cdot\|_1, \|\cdot\|_0$ define the second, first and zeroth norm respectively.

CHAPTER 2

POWER AMPLIFIER LINEARIZATION

2.1 Motivation

In this chapter, we tackle the PA linearization problem for cognitive radio (CR) systems. The CR system has the ability to adapt its transmission parameters to dynamically access the under-utilized wireless spectrum. The basic idea of the CR is to achieve spectrum efficiency by exploiting the existing wireless spectrum opportunistically [31]. This approach has the capability of utilizing the spectrum much more efficiently than the fixed spectrum assignment policy, whose typical spectral efficiency ranges from 15% to 85% with high variance in time as reported by federal communications commission's (FCC) spectrum policy task force [32]. In orthogonal frequency division multiple access (OFDMA), each user is assigned a subset of sub-carriers for use, and each carrier is assigned exclusively to one

user [33]. Hence an OFDMA-CR system operates by allocating the available subcarriers to the users on demand and opportunistically. In these systems, the use of the widespread and popular orthogonal frequency division multiplexing (OFDM) technique allows for high-speed communication over frequency selective wireless channels.

One major drawback of the OFDM scheme is the high peak to average power ratio (PAPR) of the resulting time domain signals. The amplitude modulated, high PAPR waveforms are severely affected by the nonlinear distortions when passed through the power amplifier (PA). The obvious remedy is to operate the PA in back-off, which results in poor power efficiency. Deliberate clipping is previously used to avoid the nonlinear distortions from the PA [17], however, intentional clipping produces out-of-band radiations and in-band distortions. Generally, the preferred solution to this efficiency versus linearity dilemma, is to operate the PA in its nonlinear region and then restore the linearity by means of system level architecture. For transmitter based linearization, mainly techniques like digital predistortion and feedforward are used [6,8,34,35]. In digital predistortion, the cascade of digital predistorter (DPD) and PA is employed, which behaves as a linear amplification system [6]. The main motivation behind the use of transmitter based pre-compensation techniques is to meet the stringent spectrum emission mask requirements imposed by regulatory authorities. In this work, the operating power efficiency of a wireless transmitter is extended beyond its conventional limit by over-driving digitally predistorted PAs and compensating

for the resulting distortions at the receiver side. This novel joint-compensation scheme, in which compensation of the amplifiers distortions is jointly performed between the transmitter and receiver, is shown to have two major advantages; 1) it controls the amount of spectrum regrowth at the output of the PA in order to meet the regulatory spectrum emission mask requirements, and 2) it ensures the sparsity of the distortions making it possible to use compressed sensing (CS) based techniques to compensate for the distortions at the receiver without any prior knowledge of the PA's nonlinearity.

The proposed joint-compensation technique is applied in a CR context in which the use of the radio frequency resources is optimized for power efficient rather than spectral efficient operation. This can be perceived as an attractive application of CR which is in-line with the global trend towards green communication systems. In the typical case of spectral efficiency driven CR, the available spectrum, resulting from the silence of a particular user, is allocated to other users. Conversely, in the proposed technique, the free OFDMA sub-carriers, resulting from inactive users, are kept as a guard band between active users. The active users are thus allowed to operate in a nonlinear but power efficient manner by spilling their spectrum regrowth energy mainly over the unused sub-carriers and to a lesser extent over the sub-carriers allocated for data transmission of other active users. The quality of the transmitted signals is then recovered at the receiver using CS in the context of single and multiple antenna receivers.

In this work, power efficient green CR system based on the concept of joint-

compensation is proposed. Pre-compensation is achieved using digital predistortion technique at the transmitter to ensure power efficient amplification along with sparsity of the distortions. This allows the use of sparse signal reconstruction scheme at the receiver for distortion estimation and cancellation. Furthermore, the reconstruction scheme is employed in a bandwidth efficient manner, that doesn't require tone reservation explicitly for sensing purposes, and hence avoids any hit taken on the data rate, if data carriers of the active users were to be spared. Single-input multiple-output (SIMO)-OFDMA system is considered and it is shown how the distortion recovery can be improved considerably in SIMO systems where the receiver is equipped with multiple antennas, and multiple measurements of the unknown sparse distortion vector are available. Numerical results of the performance of the entire transceiver, including the presence of a realistic communication channel, are reported.

2.1.1 Chapter Contributions

The contributions made towards power amplifier linearization can be summarized as follows:

- A joint-compensation approach, employing transmitter based digital predistortion and receiver-based CS estimation, is proposed for power efficient and linearized amplification systems.

- An OFDMA-CR communication system that emphasizes power efficient operation is proposed based on the joint-compensation technique.

- The joint-compensation based OFDMA-CR concept is extended from the case of SISO system to the case of SIMO system where the presence of multiple receiver antennas is exploited for enhanced distortion recovery.

Thanks to the digital predistortion, the distortions created by the over-driven amplifier are sparse. Over-driven amplifiers operate at a higher power efficiency but create in-band and out of band distortions. While out of band distortions mostly affect inactive users, in-band distortions are mitigated using CS at the receiver. The presence of multiple antennas further enhances the distortion recovery and hence mitigation.

2.2 CS-Based Joint-Compensation for Power Efficient Linear Amplification

2.2.1 Principle of Joint-Compensation

To linearize a PA, generally a DPD is employed at the transmitter (for pre-compensation) such that the PA-DPD combination is a linear amplification system [6]. As long as the input signal remains within the saturation limit, the use of linear PA-DPD cascade will result in distortion-free amplified signal. However, the emission mask criteria generally allows a limited amount of spectrum regrowth (as shown in Fig. 2.1). Hence, under the mask operation of linear PA, enables amplifier over-drive for enhanced power efficiency. It should be noted that an over-driven linearized PA behaves as a limiter and the sparsity of over-driven

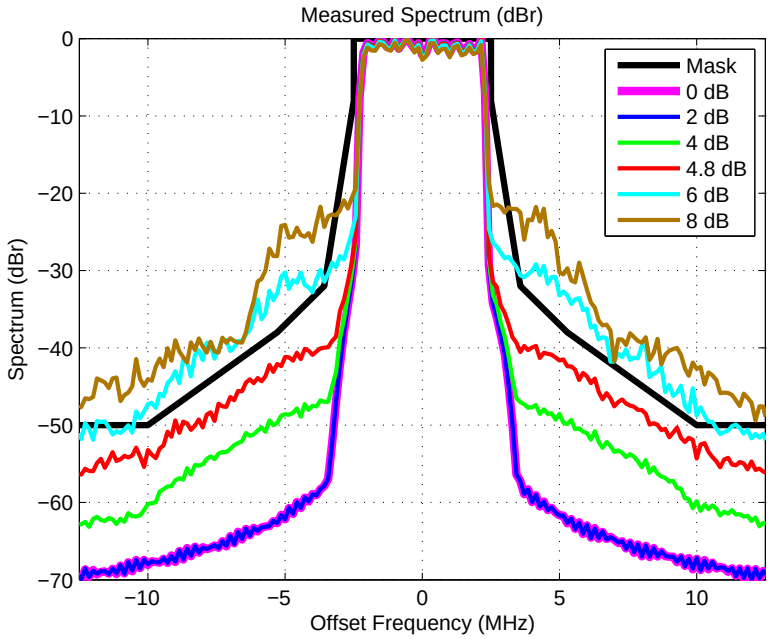

Figure 2.1: Power spectrum of linearized PA's output, as a function of amplifier over-drive.

PA's distortions can be controlled. Further, it is worthy to mention that though the amount of allowable overdrive is independent of the PA-DPD characteristics, it depends on the statistics (i.e. PAPR and complimentary cumulative distribution function (CCDF)) of the drive signal. An adjacent channel leakage ratio (ACLR) sensing algorithm can be added in the transmitter to adaptively determine, depending on the drive signal, the allowable over-drive level while meeting the linearity mask.

Fig. 2.1 compares the spectral emissions of predistorted amplification system for different values of amplifier over-drive. A normalized spectrum is presented such that the maximum in-band emissions are 0 dBr. Linearized over-driven amplifiers cause distortions which result in power spill and hence the extent to which a PA can be over-driven is determined by the spectrum emission criteria. In

this case, it is observed that a linearized PA over-driven by up to 4.8 dB will meet the spectrum mask criteria. If amplifier over-drive exceeds 4.8 dB, there will be significant distortions on the spectrum of adjacent users (as shown by the case of 6 dB and 8 dB over-drive in Fig. 2.1). However, under the mask requirement is to be met only in the case where all users are active. This is because, amplifier over-drive beyond the limit imposed by spectrum mask will cause severe distortions on the spectrum of immediate neighbours and will eventually degrade their performance. On the contrary, consider that a user is over-driving its PA while its immediate neighbours are silent. In this case, the absence of the adjacent users will alow the active user to over-drive its PA even beyond the limit imposed by the spectrum criteria without degrading the performance. In such a case, how much a user can over-drive will be dictated by the sparsity requirement on the distortion signal for it to be successfully recovered at the receiver using CS.

As the amplifier over-drive is increased, higher power efficiency is achieved. As an example when a linearized Doherty amplifier [36] is over-driven by 3 dB, its efficiency increases to 47.52%, in contrast to the case of 38.03% efficiency when no over-drive is applied. This shows around 9% increase in PA's power efficiency with 3 dB over-drive. The PA's percentage efficiency for different over-drive levels is presented in Table 2.1.

The proposed joint-compensation scheme improves the transmitter's efficiency by over-driving the PA. However, this is achieved at the expense of higher power consumption at the receiver due to additional signal processing required to miti-

Table 2.1: Over-drive level versus efficiency of the linearized Doherty amplifier.

Over-drive Level (dB)	Efficiency (%)
0	38.0
0.5	39.3
1.0	41.2
1.5	42.6
2.0	44.1
2.5	46.3
3.0	47.5

gate the amplifier's over-drive distortions. Though, the power efficiency increases with over-drive, the number of nonzero distortion samples as well as their magnitude increase. Fig. 2.2 shows the time domain distortions of an over-driven PA-DPD combination as a function of amplifier over-drive. It is apparent that the distortions increase as the over-drive is increased, both in their number and amplitude. Further, Fig. 2.2 also shows that the over-drive distortions are sparse in time domain (as expected due to the high PAPR nature of OFDM signals). Hence, given that the distortions are sparse enough, CS based scheme can be utilized at the receiver for post-compensation (i.e. estimation and cancellation) of these distortions.

Use of joint-compensation ensures that in addition to the power efficient operation, the spectrum mask is also met and over-drive distortions are sparse enough to be estimated at the receiver using CS. Further, this technique is applicable even for systems utilizing highly nonlinear amplifiers as distortions from any combination of PA and DPD are transformed into that of a quasi-perfect limiter.

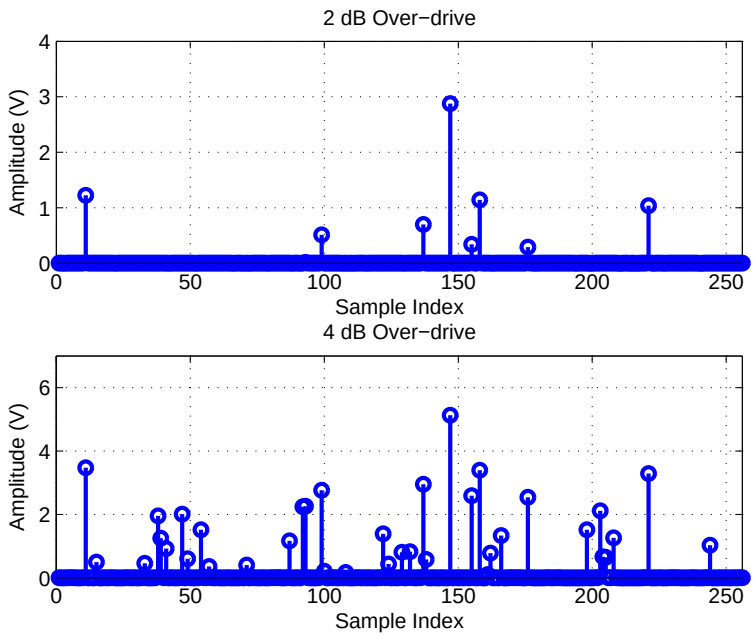

Figure 2.2: Distortions' sparsity rate and magnitude as a function of amplifier over-drive.

2.2.2 Device Under Test

The device under test (DUT) in this work is a 20 W Doherty PA designed using gallium nitride (GaN) transistor [36]. The amplifier is designed for applications in the 2110 MHz to 2170 MHz frequency band. The AM-AM and AM-PM characteristics of the DUT were measured using a 5 MHz OFDM signal centered around 2140 MHz. These are reported in Fig. 2.3. As can be seen from the AM-AM curve, the amplitude response is nonlinear, especially for high amplitude input signals, resulting in severe nonlinear distortion on the peaks. Also the phase response of the amplifier is nonlinear and varies over 20° throughout the range of operation.

A linear amplification system is obtained using the cascade of nonlinear PA and a DPD circuit matched to the characteristics of PA. The measured characteristics of the linearized amplifier are shown in Fig. 2.4. It is apparent, that the PA-DPD

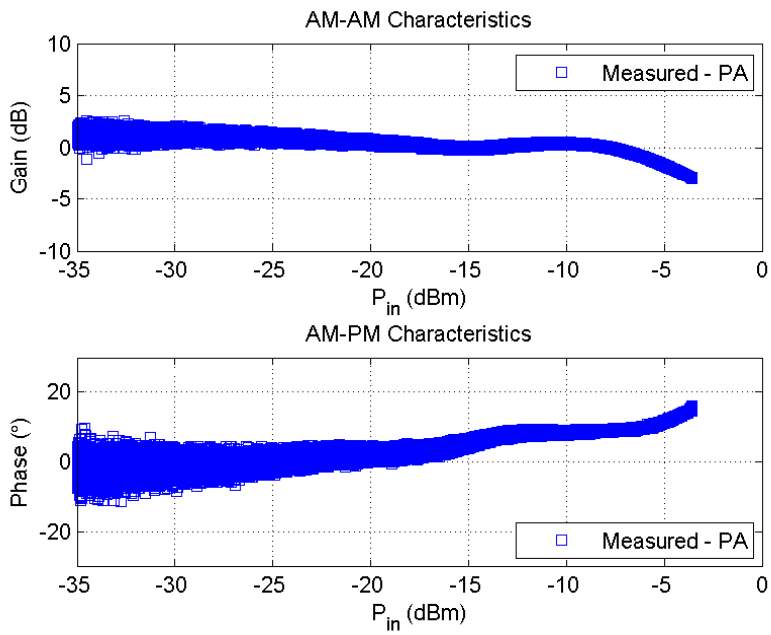

Figure 2.3: Measured gain and phase characteristics of PA.

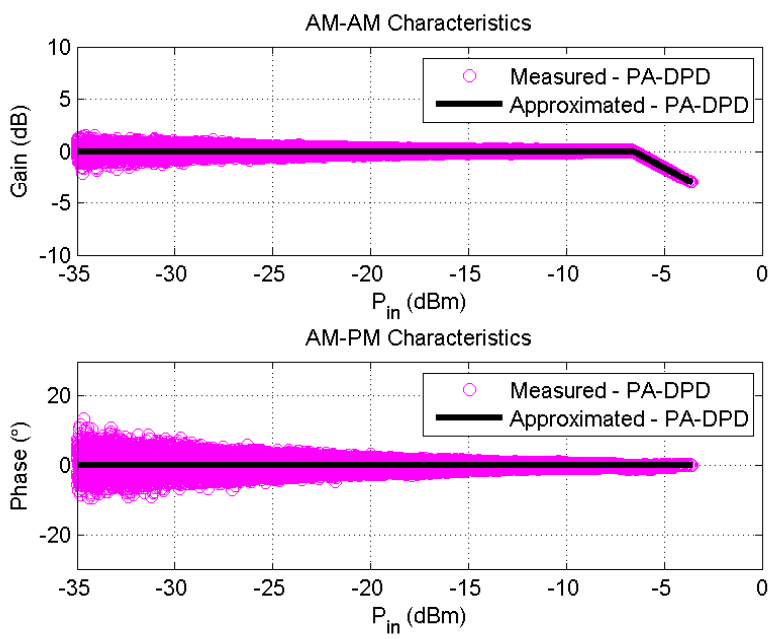

Figure 2.4: Measured and approximated gain and phase characteristics of PA-DPD combination.

cascade has a constant gain response to a point where the amplifier saturates, and starts compressing. In the saturation region, the gain of the PA-DPD combination

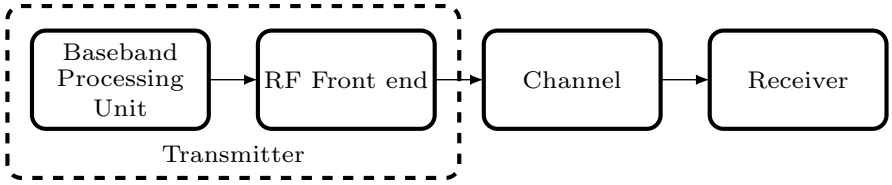

Figure 2.5: Block diagram of a typical communication system.

decreases linearly with increasing input power. However, the phase response of the linearized PA is constant throughout the range of interest. To simulate the PA, a look-up table (LUT) behavioural model, derived from the measured AM-AM and AM-PM characteristics of the linearized PA, using exponential moving average algorithm is adopted in this work [37]. The characteristics of the linearized amplifier based on the LUT model are also shown in Fig. 2.4. For any linear amplification system, if the characteristics of DPD match closely with that of the PA, a system having the characteristics such as shown in Fig. 2.4 results. The low dispersion of the AM-AM and AM-PM characteristics confirm the memoryless behavior of the DUT and the suitability of the LUT behavioral model. This is expected due to the narrowband nature of the transmission signals in handsets.

2.3 System Overview

2.3.1 Transceiver Model

A typical OFDMA-CR system can be divided into four major blocks as shown in Fig. 2.5. Each of these blocks is discussed below.

Baseband Processing Unit

In an OFDM system, serially incoming bits are divided into N low rate parallel streams. An N dimensional data vector $\boldsymbol{\mathcal{X}} = [\mathcal{X}(0), \mathcal{X}(1), \cdots, \mathcal{X}(N-1)]^{\mathsf{T}}$ results when these parallel streams are mapped to an M-ary QAM alphabet $\{\mathcal{A}_0, \mathcal{A}_1, \cdots, \mathcal{A}_{M-1}\}$. The time domain signal vector is obtained by an IFFT operation, so that $\mathbf{x} = \mathbf{F}^{\mathsf{H}}\boldsymbol{\mathcal{X}}$. Here $\mathbf{F}$ denotes the unitary discrete fourier transform (DFT) matrix with (n_1, n_2) element

$$\mathrm{f}_{n_1,n_2} = \frac{1}{\sqrt{N}} e^{-j2\pi n_1 n_2/N}, \quad n_1, n_2 \in 0, 1, \cdots, N-1$$

In the uplink of the OFDMA system, the total number of available sub-carriers N is divided among subscribers and each user will be allocated $K = N/I$ sub-carriers for data transmission. Hence at the user equipment (UE), the incoming stream of data is divided into K parallel streams followed by QAM modulation. In the context of a complete OFDMA symbol, the frequency domain signal corresponding to the ith user can be written as

$$\begin{aligned}\boldsymbol{\mathcal{X}}^i =& [\mathbf{0}, \mathcal{X}^i(0), \mathcal{X}^i(1), \cdots, \mathcal{X}^i(K-1), \mathbf{0}]^{\mathsf{T}} \\ =& [\mathbf{0}, \underline{\boldsymbol{\mathcal{X}}}^{i^{\mathsf{T}}}, \mathbf{0}]^{\mathsf{T}} \end{aligned} \tag{2.1}$$

where $\underline{\boldsymbol{\mathcal{X}}}^i = [\mathcal{X}^i(0), \mathcal{X}^i(1), \cdots, \mathcal{X}^i(K-1)]^{\mathsf{T}}$ is a length K vector corresponding to the data from i^{th} user mapped to the sub-carriers allocated to the ith user by virtue of preceding and succeeding zero vectors of appropriate dimensions. The

time domain signal for user i, i.e., $\mathbf{x}^i$ can be obtained by taking the IFFT of $\boldsymbol{\mathcal{X}}^i$.

RF Front End

The time domain signal that passes through a linear amplification system that is not over-driven will go undistorted. However, the amplifier over-drive will result in a distorted transmitted signal. This distortion can be modelled as addition of a distortion signal $\mathbf{x}_d$ to the transmission signal. Hence the output of the PA can be written as

$$\mathbf{x}_p^i = \mathbf{x}^i + \mathbf{x}_d^i \tag{2.2}$$

Here, the small signal gain of the PA is taken to be unity for simplicity, as it doesn't affect the generality of the system model.

Since the main focus of this work is to study the effects of the PA's distortions, the RF front end is considered to be ideal except for the nonlinear distortions generated by the amplifier. Thus, the RF front end is modelled using the baseband equivalent behavioral model of the PA. To take into consideration the presence of the DPD module in the baseband processing unit, while using a realistic model based on the measured data of the linearized PA, the PA-DPD combination is simulated using the LUT synthesized from the measured data presented in the previous section.

Channel

The RF front end output $\mathbf{x}_p^i$ is transmitted through a channel with impulse response $\mathbf{h}^i = [h^i(0), h^i(1), \cdots, h^i(N_c - 1)]^\mathsf{T}$, where the channel tap coefficients form an independent and identically distributed (i.i.d) collection with zero mean and independent real and imaginary parts. The time domain signal from i^{th} user at the output of the channel, can be written as

$$\mathbf{y}^i = \mathbf{H}^i \mathbf{x}_p^i \tag{2.3}$$

where $\mathbf{H}^i = \mathbf{F}^\mathsf{H} \mathbf{D}^i \mathbf{F}$ is a circulant channel matrix by virtue of the cyclic prefix in OFDM signalling and $\mathbf{D}^i$ is a diagonal matrix containing the frequency response coefficients on its diagonal and zeros on non-diagonal entries.

In a quasi-static or block fading channel environment, the impulse response of the channel associated with each user can be obtained at the receiver via training. The training symbol, also called preamble, precedes the information containing symbols in OFDM packets and is known at the receiver. The knowledge of pilot sequence and statistics of additive white Gaussian noise (AWGN) (discussed in the following section) at the receiver, mixed with realistic assumption that the channel and noise are independent, allows the reconstruction of impulse response using minimum mean squared error (MMSE) estimation. Having the knowledge of the channel impulse response, the frequency response and the circulant channel matrix can be subsequently reconstructed.

Receiver

At the base station, the signals received from all I users combine to form a time domain received signal $\mathbf{y}$ given as:

$$\mathbf{y} = \sum_{i=1}^{I} \mathbf{H}^i(\mathbf{x}^i + \mathbf{x}_d^i) + \mathbf{z} \tag{2.4}$$

where $\mathbf{z} \sim \mathcal{CN}(\mathbf{0}, \sigma_z^2 \mathbf{I}_{N\times N})$. The frequency domain received signal can be obtained by the FFT operation as

$$\boldsymbol{\mathcal{Y}} = \sum_{i=1}^{I} \mathbf{D}^i \boldsymbol{\mathcal{X}}^i + \sum_{i=1}^{I} \mathbf{D}^i \boldsymbol{\mathcal{X}}_d^i + \boldsymbol{\mathcal{Z}} \tag{2.5}$$

The last term on the right hand side (R.H.S) of eq. (2.5), $\boldsymbol{\mathcal{Z}}$, refers to the noise vector $\mathbf{z}$ linearly transformed by $\mathbf{F}$, and thus has the same statistics as $\mathbf{z}$. The product column vector $\mathbf{D}^i \boldsymbol{\mathcal{X}}^i$ will have nonzero elements only at the locations corresponding to the sub-carriers that are allocated to user i for transmission. Hence, the first summation on the R.H.S of eq. (2.5) can be written compactly as $\mathbf{D}\boldsymbol{\mathcal{X}}$, where $\boldsymbol{\mathcal{X}}$ contains non-overlapping transmitted data from all the users, and $\mathbf{D}$ contains the non-overlapping channel coefficients of all users, i.e.

$$\boldsymbol{\mathcal{X}} = \begin{bmatrix} \underline{\boldsymbol{\mathcal{X}}}^1 \\ \underline{\boldsymbol{\mathcal{X}}}^2 \\ \vdots \\ \underline{\boldsymbol{\mathcal{X}}}^I \end{bmatrix} \quad \text{and} \quad \mathbf{D} = \begin{bmatrix} \underline{\mathbf{D}}^1 & & & \\ & \underline{\mathbf{D}}^2 & & \\ & & \ddots & \\ & & & \underline{\mathbf{D}}^I \end{bmatrix}$$

Note that, although the channel frequency responses $\mathbf{D}^1, \mathbf{D}^2, \cdots, \mathbf{D}^I$ are diagonal matrices of size $N \times N$ and hence are overlapping, the matrix $\mathbf{D}$ comprises of only the portions of $\mathbf{D}^i$, belonging to the ith user band, which is denoted by $\underline{\mathbf{D}}^i$. Now we can write

$$\boldsymbol{\mathcal{Y}} = \mathbf{D}\boldsymbol{\mathcal{X}} + \sum_{i=1}^{I} \mathbf{D}^i \boldsymbol{\mathcal{X}}_d^i + \boldsymbol{\mathcal{Z}} \tag{2.6}$$

Unlike the first summation of (2.5) whose components add in a non-overlapping manner, the elements of $\boldsymbol{\mathcal{X}}_d^i$ spill over adjacent users and hence the second summation cannot be simplified like the first and needs further investigation.

In the absence of distortion (i.e. when the second term of (2.6) is zero), the receiver could easily separate the users (as they occupy different carriers) and equalize the users' channels to recover the transmitted data. Mathematically we can write

$$\underline{\boldsymbol{\mathcal{Y}}}^i = \underline{\mathbf{D}}^i \underline{\boldsymbol{\mathcal{X}}}^i + \underline{\boldsymbol{\mathcal{Z}}}^i \tag{2.7}$$

where $\underline{\boldsymbol{\mathcal{Y}}}^i$ is the portion of $\boldsymbol{\mathcal{Y}}$ confined to the carriers of the ith user (a similar definition applies to $\underline{\mathbf{D}}^i$,$\underline{\boldsymbol{\mathcal{X}}}^i$ and $\underline{\boldsymbol{\mathcal{Z}}}^i$). Upon equalizing, we obtain

$$\widehat{\underline{\boldsymbol{\mathcal{X}}}^i} = (\underline{\mathbf{D}}^i)^{-1} \underline{\boldsymbol{\mathcal{Y}}}^i \tag{2.8}$$

The noisy estimate $\widehat{\underline{\boldsymbol{\mathcal{X}}}^i}$ is then rounded to the nearest constellation point, which we denote by $\lfloor \widehat{\underline{\boldsymbol{\mathcal{X}}}^i} \rfloor$ (from here on the operator $\lfloor \cdot \rfloor$ is used to denote rounding to the nearest constellation point).

Note that the two steps of equalization and rounding could also be done in the

presence of the distortion term in (2.6). In this case, the receiver simply ignores the distortion and treats it as part of the additive noise, which will result in degraded performance. However distortions could also be estimated and cancelled, which is what we pursue in this work.

2.3.2 Spectrum Allocation

Consider the spectrum allocation in an OFDMA system, as shown in Fig. 2.6. As illustrated, the available spectrum or total number of sub-carriers in the OFDMA system are utilized to provide access to three users simultaneously. However, consider the case in which only users 1 and 3 are active, while user 2 is in silent mode (e.g. active but not transmitting). Two methods can be used to take benefit of the situation at hand:

1. A rather conventional approach of allocating the free spectrum resulting from the silence of user 2, to another user (e.g. user 1 or 3), which is true to the essence of CR.

2. An alternative approach towards utilization of the free spectrum, which allows one and possibly more of the active users to operate in a power efficient manner by over-driving their PAs.

Here onwards, attention is paid only to the case where the advantage of the silent user is taken by the power efficient operation of active users.

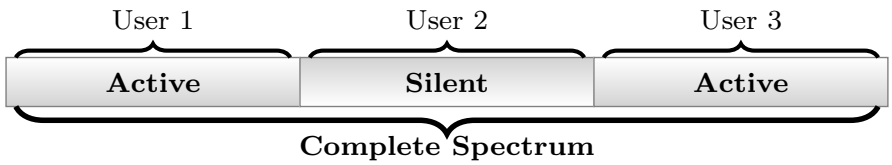

Figure 2.6: Sub-carrier allocation in OFDMA system.

2.4 Over-driven Amplifier's distortion

Both users 1 and 3 could make use of the absence of user 2 and over-drive their PAs. For clarity of exposition, let's focus first on the case when only one user is over-driving his/her PA and subsequently consider the more general case.

2.4.1 Single User Over-drive

First consider the case where only one user among the active users is transmitting by over-driving his/her PA and requires distortion estimation and cancellation at the receiver (without loss of generality we consider it to be user 1). Other users are operating their PAs in the linear region and hence only the signal from user 1 contributes to the nonlinear distortion seen at the receiver (absolute over-drive distortions coming from user 1 are shown in Fig. 2.7). Hence we can write

$$\underline{\boldsymbol{\mathcal{Y}}}^1 = \underline{\mathbf{D}}^1 \underline{\boldsymbol{\mathcal{X}}}^1 + \underline{\mathbf{D}}^1 \underline{\boldsymbol{\mathcal{X}}}_d^1 + \underline{\boldsymbol{\mathcal{Z}}}^1 \tag{2.9}$$

where by definition, $\underline{\boldsymbol{\mathcal{Y}}}^1$ and $\underline{\boldsymbol{\mathcal{Z}}}^1$ represent the portions of $\boldsymbol{\mathcal{Y}}$ and $\boldsymbol{\mathcal{Z}}$ corresponding to the carriers assigned to user 1.

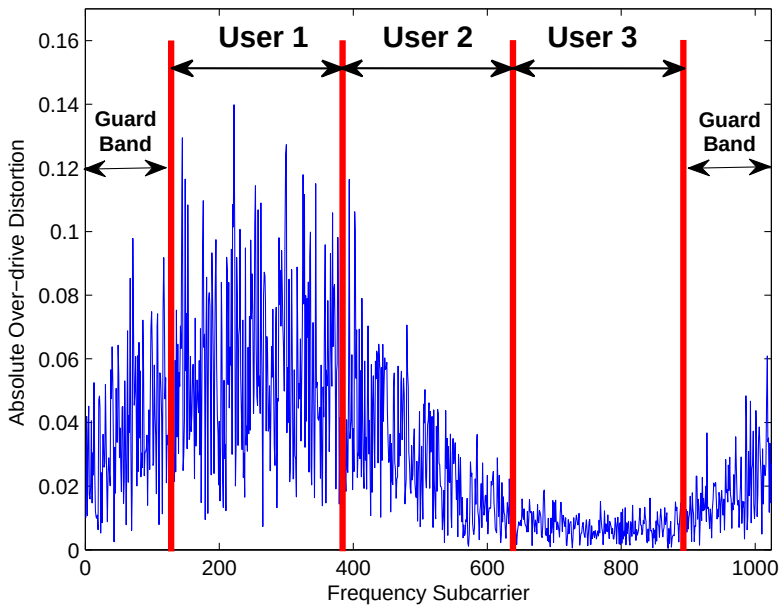

Figure 2.7: Frequency domain view of distortion from user 1.

2.4.2 Multiuser Over-drive

Now consider the case when both user 1 and user 3 are over-driving their PAs. Just like the first case, most of the distortion will be felt by the users immediately adjacent (in this case user 2). The impact of user 1's distortions on user 3 is minimal as shown in Fig. 2.7 (this can actually be controlled by limiting the degree to which the PA is over-driven). Similarly, the effect of user 3's distortion on user 1 is minimal. So the distortion of each user is felt mostly in-band and in the spectrum originally reserved for user 2.

From the discussion above, we see that the multiuser over-drive case is similar to the single user over-drive case (since most distortion is self inflicted and spills are mostly to the spectrum of user 2). Thus (2.9) applies to all users and we can

write

$$\underline{\boldsymbol{\mathcal{Y}}}^i \simeq \underline{\mathbf{D}}^i \underline{\boldsymbol{\mathcal{X}}}^i + \underline{\mathbf{D}}^i \underline{\boldsymbol{\mathcal{X}}}_d^i + \underline{\boldsymbol{\mathcal{Z}}}^i \tag{2.10}$$

where the approximate equality comes from the fact that we are ignoring distortions coming from distant users (which is also equivalent to lumping these distortions with additive noise). So the distortion model is same in the two cases of single or multiple over-driving users and most of the distortion is self inflicted. In the next section, we see how to estimate and cancel this distortion.

2.5 Compressive Sensing for Post-Compensation

Our eventual goal is to recover the data $\underline{\boldsymbol{\mathcal{X}}}^i$ from (2.10), given noise and distortion. As mentioned previously, we could ignore the presence of distortion and consider it part of the additive noise which will result in inferior performance. Alternatively, we could try to estimate and cancel this distortion which is accomplished here by utilizing the distortion's sparse nature in the time domain.

Specifically note that the distortion $\underline{\boldsymbol{\mathcal{X}}}_d^i$ experienced by the ith user is related to the time domain distortion $\mathbf{x}_d^i$ by

$$\underline{\boldsymbol{\mathcal{X}}}_d^i = \underline{\mathbf{F}}^i \mathbf{x}_d^i \tag{2.11}$$

where as per convention $\underline{\mathbf{F}}^i$ is a $K \times N$ matrix with rows corresponding to those

of the ith user. Thus, (2.10) reads

$$\underline{\boldsymbol{\mathcal{Y}}}^i - \underline{\mathbf{D}}^i \underline{\boldsymbol{\mathcal{X}}}^i = \underline{\mathbf{D}}^i \underline{\mathbf{F}}^i \mathbf{x}_d^i + \underline{\boldsymbol{\mathcal{Z}}}^i \tag{2.12}$$

or

$$\underline{\boldsymbol{\mathcal{U}}}^i = \underline{\boldsymbol{\Psi}}^i \mathbf{x}_d^i + \underline{\boldsymbol{\mathcal{Z}}}^i \tag{2.13}$$

where $\underline{\boldsymbol{\Psi}}^i \triangleq \underline{\mathbf{D}}^i \underline{\mathbf{F}}^i$ and $\underline{\boldsymbol{\mathcal{U}}}^i \triangleq \underline{\boldsymbol{\mathcal{Y}}}^i - \underline{\mathbf{D}}^i \underline{\boldsymbol{\mathcal{X}}}^i$. Assuming that $\underline{\boldsymbol{\mathcal{U}}}^i$ is known, this represents an under-determined system of K equations in the unknown *sparse* vector $\mathbf{x}_d^i$. The N dimensional unknown vector $\mathbf{x}_d^i$ is S sparse, i.e., it has S non-zero elements and $(N - S)$ zeros. The sparsity of $\mathbf{x}_d^i$ makes it possible to recover it from (2.13) using CS[1].

2.5.1 Pilot Aided Compressed Sensing Scheme

Let's reserve $\{L : L < K\}$ of the carriers in $\underline{\boldsymbol{\mathcal{X}}}^i$ and keep them data free. If we retain in eq. (2.13), the entries corresponding to these zero carriers, we obtain

$$\underline{\boldsymbol{\mathcal{U}}}_L^i = \underline{\boldsymbol{\Psi}}_L^i \mathbf{x}_d^i + \underline{\boldsymbol{\mathcal{Z}}}_L^i \tag{2.14}$$

Since we are retaining only the carriers that are free of data, we have $\underline{\boldsymbol{\mathcal{U}}}_L^i = \underline{\boldsymbol{\mathcal{Y}}}_L^i$. As mentioned before, we can now recover $\mathbf{x}_d^i$ using CS. Specifically we have

$$\begin{aligned} \text{minimize} \quad & \|\mathbf{x}_d^i\|_1, \\ \text{subject to} \quad & \|\underline{\boldsymbol{\mathcal{U}}}_L^i - \underline{\boldsymbol{\Psi}}^i \mathbf{x}_d^i\|_2 \leq \epsilon \end{aligned} \tag{2.15}$$

where ϵ restricts the amount of noise in recovered data [24]. Further, $\|\cdot\|_1$ and $\|\cdot\|_2$ represent the first and second norm of the vector, respectively. Although ℓ_1 minimization is widely used, it is not the only way of sparse signal reconstruction. There are other sparse reconstruction techniques (e.g. Bayesian methods [25–27, 38], and matching pursuits [28–30]) which can be utilized, and some of these are much less computationally intensive than ℓ_1 minimization.

2.5.2 Data-Aided Compressed Sensing Scheme

The pilot aided scheme described above does not make the most efficient use of bandwidth. So in this subsection, we pursue a data-aided approach which essentially uses the most reliable data to form enough equations to recover the sparse vector $\mathbf{x}_d^i$ from (2.13). We call this approach data-aided compressed sensing (DACS). The DACS algorithm is based on the assumption that after getting corrupted by the distortion of the over-driven PA, part of the data samples still remain within their corresponding correct decision regions.

For example in Fig. 2.8, $\hat{\mathcal{X}}_1$ and $\hat{\mathcal{X}}_2$ are perturbed versions of $\mathcal{X}$ and both are reliable because they remain within the ML decision region of $\mathcal{X}$. Note also that while $\hat{\mathcal{X}}_1$ and $\hat{\mathcal{X}}_2$ have the same distance to $\mathcal{X}$, $\hat{\mathcal{X}}_2$ is more reliable than $\hat{\mathcal{X}}_1$. The reason is that the distance of $\hat{\mathcal{X}}_2$ to the next nearest constellation point $\mathcal{X}_b$ is larger than the distance of $\hat{\mathcal{X}}_1$ to its next nearest constellation point $\mathcal{X}_a$. To be more precise, consider (2.10) which we can use to equalize the received data $\widehat{\underline{\boldsymbol{\mathcal{X}}}}^i = (\underline{\mathbf{D}}^i)^{-1}\underline{\boldsymbol{\mathcal{Y}}}^i$. In the absence of noise and distortions, we would have $\widehat{\underline{\boldsymbol{\mathcal{X}}}}^i = \underline{\boldsymbol{\mathcal{X}}}^i$.

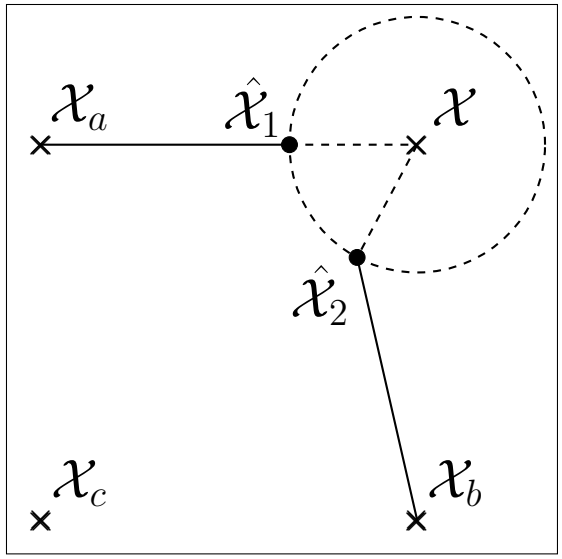

Figure 2.8: Geometrical representation of adopted reliability criteria.

In general, however, only some elements of $\widehat{\underline{\boldsymbol{\mathcal{X}}}^i}$ will remain within the correct decision region (we call the corresponding carriers reliable while the remaining are unreliable). For the set of reliable carriers, we have $\lfloor\widehat{\underline{\boldsymbol{\mathcal{X}}}^i_R}\rfloor = \underline{\boldsymbol{\mathcal{X}}}^i_R$, where $\widehat{\underline{\boldsymbol{\mathcal{X}}}^i_R}$ is $\widehat{\underline{\boldsymbol{\mathcal{X}}}^i}$ confined to the set of reliable carriers R ($\underline{\boldsymbol{\mathcal{X}}}^i_R$ is similarly defined).

Now we use a similar strategy to what we did in the pilot-aided case. We use (2.13) and confine our attention to the set of reliable carriers. At these carriers, we have

$$\begin{aligned}\underline{\boldsymbol{\mathcal{U}}}^i_R =& \underline{\boldsymbol{\mathcal{Y}}}^i_R - \underline{\mathbf{D}}^i_R \underline{\boldsymbol{\mathcal{X}}}^i_R \\ =& \underline{\boldsymbol{\mathcal{Y}}}^i_R - \underline{\mathbf{D}}^i_R \lfloor\widehat{\underline{\boldsymbol{\mathcal{X}}}^i_R}\rfloor \end{aligned} \tag{2.16}$$

where equality follows from the fact that at the reliable carriers, we have that $\lfloor\widehat{\underline{\boldsymbol{\mathcal{X}}}^i_R}\rfloor = \underline{\boldsymbol{\mathcal{X}}}^i_R$. In other words, the reliable carriers are as good as pilot carriers. In the pilot carriers case, we know that zeros are transmitted. In the reliable data

carriers case, we know which constellation point is being transmitted.

When confined to the set of reliable carriers, (2.13) reads

$$\underline{\boldsymbol{\mathcal{U}}}_R^i = \underline{\boldsymbol{\Psi}}_R^i \mathbf{x}_d^i + \underline{\boldsymbol{\mathcal{Z}}}_R^i \tag{2.17}$$

where $\underline{\boldsymbol{\Psi}}_R^i$ is the matrix $\underline{\boldsymbol{\Psi}}^i$ with rows confined to the set of reliable carriers R. Note that (2.17) is an under-determined system of equations in the sparse vector $\mathbf{x}_d^i$ and hence can be recovered by ℓ_1 optimization similar to (2.15) or by utilizing any other sparse signal recovery method.

The DACS algorithm developed above assumes that the set of reliable carriers is available to us. It is important to note first that we need not to determine the set of all reliable carriers R. Rather, it is sufficient to determine a large enough subset[2] $R' \subset R$ and use that subset to recover the distortion

$$\begin{aligned} \text{minimize} \quad & \|\mathbf{x}_d^i\|_1, \\ \text{subject to} \quad & \|\underline{\boldsymbol{\mathcal{U}}}_{R'}^i - \underline{\boldsymbol{\Psi}}_{R'}^i \mathbf{x}_d^i\|_2 \leq \epsilon \end{aligned} \tag{2.18}$$

The reconstruction of R' is necessary for successful implementation of DACS and in this work, a geometrical approach is pursued to select the most reliable set of carriers from the observed data.

In order to explain the adopted approach, we consider as a motivating example the constellation shown in Fig. 2.8. Here $\hat{\mathcal{X}}_1$ and $\hat{\mathcal{X}}_2$ are two equalized data samples which are equidistant from the closest constellation point $\mathcal{X}$. However, in spite

of being equidistant from $\mathcal{X}$, $\hat{\mathcal{X}}_1$ and $\hat{\mathcal{X}}_2$ have different reliability values. This is because the distances of these two points from their respective next nearest neighbours are different. Specifically, note that $\mathcal{X}_a$ is next nearest neighbour of $\hat{\mathcal{X}}_1$ and $\mathcal{X}_b$ is next nearest neighbour of $\hat{\mathcal{X}}_2$, respectively. Given that $\hat{\mathcal{X}}_1$ and $\hat{\mathcal{X}}_2$ are equidistant from $\mathcal{X}$, $\hat{\mathcal{X}}_2$ is considered more reliable than $\hat{\mathcal{X}}_1$ since in relative terms we have

$$\frac{|\hat{\mathcal{X}}_2 - \mathcal{X}|}{|\hat{\mathcal{X}}_2 - \mathcal{X}_b|} < \frac{|\hat{\mathcal{X}}_1 - \mathcal{X}|}{|\hat{\mathcal{X}}_1 - \mathcal{X}_a|} \tag{2.19}$$

This motivates the following reliability metric $\mathfrak{R}(n)$,

$$\mathfrak{R}(n) = -\log\left(\frac{|\hat{\mathcal{X}} - \lfloor\hat{\mathcal{X}}\rfloor|}{|\hat{\mathcal{X}} - \lfloor\hat{\mathcal{X}}\rfloor_{NN}|}\right) \tag{2.20}$$

where as defined before, $\lfloor\hat{\mathcal{X}}\rfloor$ denotes rounding to the nearest constellation point while $\lfloor\hat{\mathcal{X}}\rfloor_{NN}$ denotes rounding to the next nearest constellation point.

Thus, it is possible to calculate the reliability of all N carriers, sort the reliabilities in descending order $\mathfrak{R}(n_1) \geq \mathfrak{R}(n_2) \geq \cdots \geq \mathfrak{R}(n_K)$ and choose the R' carriers with the highest reliability.

2.6 SIMO-OFDMA System

Let us consider an OFDMA receiver equipped with multiple antennas, i.e., a SIMO communication system. Base station of the SIMO-OFDMA system receives multiple copies of the same transmitted signal via different paths. These multiple received signals contain the same distortion signal convoluted with different chan-

nel impulse responses. For acceptable performance of the communication system, the distortion needs to be eliminated from all diversity branches before signals are combined to obtain the estimate of transmitted signal. Further, the availability of multiple measurement vectors of the same distortion can be exploited to gain enhanced recovery of the sparse distortion signal. After removing the distortions, the distortion free independent versions of the received signal can be combined using any of the well known diversity combining methods e.g., equal gain combining (EGC), selection combining (SC) and maximal ratio combining (MRC) [39] to obtain the estimate of transmitted signal.

Now, we need to generalize (2.10) to the case of multiple antenna receiver. We see that in a P branch diversity system, the received signal of the ith user, on p^{th} antenna can be written as

$$\underline{\boldsymbol{\mathcal{Y}}}_p^i = \underline{\mathbf{D}}_p^i \underline{\boldsymbol{\mathcal{X}}}^i + \underline{\mathbf{D}}_p^i \underline{\boldsymbol{\mathcal{X}}}_d^i + \underline{\boldsymbol{\mathcal{Z}}}^i \tag{2.21}$$

Here, $\underline{\mathbf{D}}_p^i$ is the frequency response of the ith user's sub-carriers associated with p^{th} channel. Note that $\underline{\boldsymbol{\mathcal{X}}}^i$ and $\underline{\boldsymbol{\mathcal{X}}}_d^i$ in (2.21) are free of subscript p, as these quantities *are same for all diversity branches*. If we consider a receiver that does not eliminate the distortions and uses MRC for combining the signals from each diversity branch, then the estimate of transmitted signal is given as

$$\widehat{\underline{\boldsymbol{\mathcal{X}}}^i} = \sum_{p=1}^{P} (\underline{\mathbf{D}}_p^i)^{\mathsf{H}} \underline{\boldsymbol{\mathcal{Y}}}_p^i \tag{2.22}$$

On the other hand, a receiver equipped with CS algorithm will first estimate the distortions, will remove them and then use MRC combiner to achieve improved performance. From (2.21), using the reasoning which led us from (2.10) to (2.13), we can write for each diversity branch

$$\underline{\boldsymbol{\mathcal{U}}}_p^i = \underline{\Psi}_p^i \mathbf{x}_d^i + \underline{\boldsymbol{\mathcal{Z}}}_p^i \tag{2.23}$$

Having a total of P systems of linear equations of the form (2.23), the following two approaches can be pursued towards reconstruction of $\mathbf{x}_d^i$ via CS.

2.6.1 Individual Reconstruction per Diversity Branch

In this method, linear system associated with each diversity branch is treated as an individual system and the procedure discussed in Section 2.5 is applied for sparse signal reconstruction. Initially, estimation of distortion vector is carried individually (with the help of reliable carriers) in each branch as shown in Fig. 2.9. Having a total of P recovered versions of the unknown sparse vector, the distortion associated with p^{th} diversity branch is subtracted from the received signal on p^{th} branch. This will yield a total of P distortion free received vectors, which can be combined using MRC to obtain the estimate of the transmitted signal.

2.6.2 Joint Reconstruction Using Diversity Branches

Under-determined system of linear equations of the form (2.23) coming from each diversity branch can be used jointly to estimate the distortions as shown

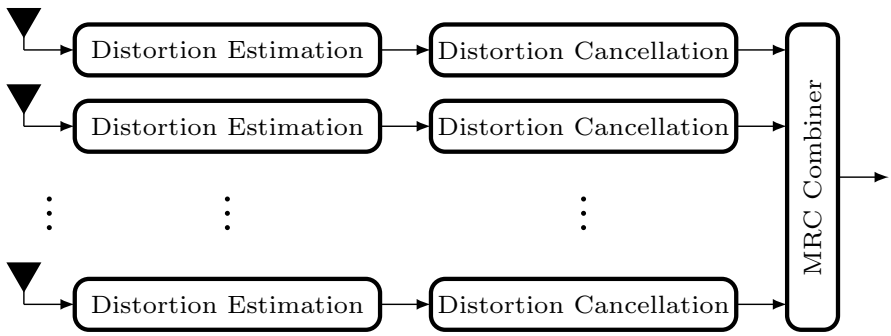

Figure 2.9: Individual reconstruction per diversity branch.

in Fig. 2.10. First, we will find reliable carriers for each diversity branch resulting in P systems of the following form:

$$\underline{\boldsymbol{\mathcal{U}}}^i_{p,R'} = \underline{\boldsymbol{\Psi}}^i_{p,R'}\mathbf{x}^i_d + \underline{\boldsymbol{\mathcal{Z}}}^i_{p,R'} \tag{2.24}$$

where $\underline{\boldsymbol{\mathcal{U}}}^i_{p,R'}$ denotes the subset of most reliable measurements on the pth diversity branch for i^{th} user ($\underline{\Psi}^i_{p,R'}$ and $\underline{\boldsymbol{\mathcal{Z}}}^i_{p,R'}$ are defined similarly). All these P systems can be concatenated and setup into the following form:

$$\begin{bmatrix} \underline{\boldsymbol{\mathcal{U}}}^i_{1,R'} \\ \underline{\boldsymbol{\mathcal{U}}}^i_{2,R'} \\ \vdots \\ \underline{\boldsymbol{\mathcal{U}}}^i_{P,R'} \end{bmatrix} = \begin{bmatrix} \underline{\Psi}^i_{1,R'} \\ \underline{\Psi}^i_{2,R'} \\ \vdots \\ \underline{\Psi}^i_{P,R'} \end{bmatrix} \mathbf{x}^i_d + \begin{bmatrix} \underline{\boldsymbol{\mathcal{Z}}}^i_{1,R'} \\ \underline{\boldsymbol{\mathcal{Z}}}^i_{2,R'} \\ \vdots \\ \underline{\boldsymbol{\mathcal{Z}}}^i_{P,R'} \end{bmatrix} \tag{2.25}$$

which can be written more compactly as

$$\underline{\boldsymbol{\mathcal{U}}}^i_{R'} = \underline{\Psi}^i_{R'}\mathbf{x}^i_d + \underline{\boldsymbol{\mathcal{Z}}}^i_{R'} \tag{2.26}$$

It is evident in this case, that having R' measurements per diversity branch, a total of PR' measurements, are available for the reconstruction of the same unknown sparse vector $\mathbf{x}_d^i$. Having more measurements helps in better reconstruction of the unknown distortion signal. Here on, proceeding in the manner adopted previously, this reconstructed signal is subtracted from each diversity branch to obtain P distortion free signals. These distortion free versions can then be combined via MRC to obtain the estimate of the transmitted signal.

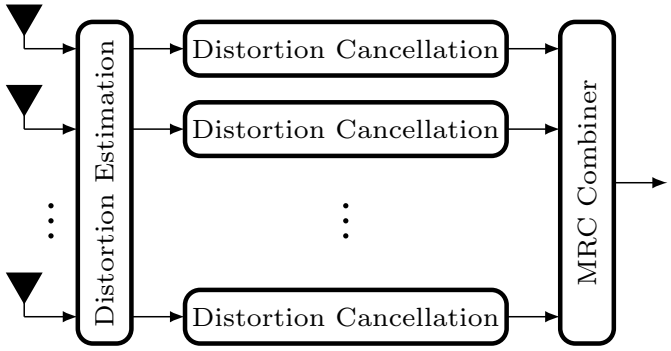

Figure 2.10: Joint reconstruction using all diversity branches.

2.7 Simulation Results

The transceiver model was implemented in co-simulation between Advanced Design System (ADS) software (from Agilent Technologies, Santa Clara, CA) and MATLAB software (from MathWorks Inc., Natick, MA). For simulation a 1024 sub-carrier OFDMA is utilized. Each of the 3 users is allocated 256 sub-carriers with no data transmission on DC subcarrier. All the remaining sub-carriers are distributed equally among upper side and lower side guard bands. An OFDM packet consists of 15 symbols with preamble containing the binary pilot symbols

10dB below the information signal level. The low power transmission of the pilot signal is required to ensure distortionless transmission of the pilot and hence correct estimation of the channel at receiver. Channel impulse response for each user is 7 tap long, and is generated independently using complex normal distribution. As MMSE estimation is employed at the receiver, it is worth mentioning that the channel covariance matrix reduces to a diagonal matrix due to the i.i.d nature of the channel taps. A normalized 64 QAM constellation is used for data transmission. The resulting OFDM signals at the UE are used to over-drive the PA according to results presented earlier, unless noted otherwise. For measurements 100 most reliable carriers are used, making the under-sampling factor 100/1024. The simulation results are averaged over 200 Rayleigh channels, unless otherwise stated.

A Bayesian approach entitled support agnostic Bayesian matching pursuit (SABMP) is utilized to reconstruct the unknown sparse signal in this work [40]. The SABMP scheme estimates the unknown signal without any assumption on the distribution of the active taps. This approach utilizes the *a priori* information about the sparsity rate of the unknown over-drive distortion signal and the noise variance. However, if such estimates are not available, the SABMP scheme can bootstrap itself and estimate the required statistics (sparsity rate and noise variance). It was shown in [40], that the SABMP scheme outperforms most algorithms in estimation accuracy as well as time taken to estimate the unknown sparse signal. The complexity incurred by the use of the SABMP is of order

$\mathcal{O}(KNS)$, when an N dimensional signal with S nonzero elements is estimated using K measurements. Further if exact estimates of the signal parameters are not available and the greedy algorithm is run $E_{\max}$ times, the complexity increases to an order of $\mathcal{O}(E_{\max}KNS)$.

The metrics used for performance comparison in experiments (1-3 and 6) are error vector magnitude (EVM) and bit error rate (BER).

- Error Vector Magnitude is defined by [41, 42]:

$$\text{EVM} = \sqrt{\frac{\frac{1}{N}\sum_{n=1}^{N}\left|\mathcal{X}(n) - \hat{\mathcal{X}}(n)\right|^2}{\frac{1}{N}\sum_{n=1}^{N}\left|\mathcal{X}(n)\right|^2}} \tag{2.27}$$

  where $\mathcal{X}(n)$ and $\hat{\mathcal{X}}(n)$ are the original and estimated data symbols, respectively. The EVM (dB) is obtained by EVM (dB)=$10\log_{10}$(EVM).

- Bit Error Rate is given by:

$$\text{BER} = \frac{\textit{total number of erroneous bits received}}{\textit{total number of bits received}} \tag{2.28}$$

2.7.1 Experiment 1: Single Antenna Receiver

To quantify the impact of over-drive distortions from only user 1 or combined distortions from users 1 and 3, EVM and BER results are generated for both cases, and are reported in Fig. 2.11 and Fig. 2.12, respectively. For each case, the performances of the communication system were evaluated before and after applying CS based recovery technique for the distortions' post-compensation. Fig. 2.11 reports

the EVM performance of the communication system as a function of the received signal's signal-to-noise ratio (SNR). Similarly, Fig. 2.12 presents the BER results as a function of the received signal's SNR obtained under the same conditions. As apparent from the results reported in Fig. 2.11 and Fig. 2.12, there is very little or no difference between the EVM and BER for cases of user 1 over-driving and both user 1 and user 3 over-driving. This confirms the observations presented in Section 2.4 about the effects of distortions on non-adjacent users. Indeed, the presence or the absence of distortions from user 3 do not have a significant impact on the EVM and BER of user 1. Further, it can be seen from the results reported in Fig. 2.11 and Fig. 2.12, that CS can be used to improve the EVM and BER performance of the communication system. It is further observed that the increase in performance is limited by the channel state. In an optimistic scenario of a less severe channel, significant improvement can be obtained as shown by the EVM results in Fig. 2.13.

It can be noted however, that the proposed scheme gives significant improvement only for high SNR regime. This is due to the fact that a highly dense two dimensional signal constellation (i.e 64 QAM) is utilized keeping in view its bandwidth efficient characteristics. As the order of constellation increases, the required SNR for any given BER is increased. For example, WiMAX forum specifies 19.9dB to be the minimum SNR required for 64 QAM with 5/6 forward error correction (FEC) coding on the downlink [43]. In another work, it is shown that an SNR of 30dB or more is required for an intentionally clipped signal to achieve acceptable

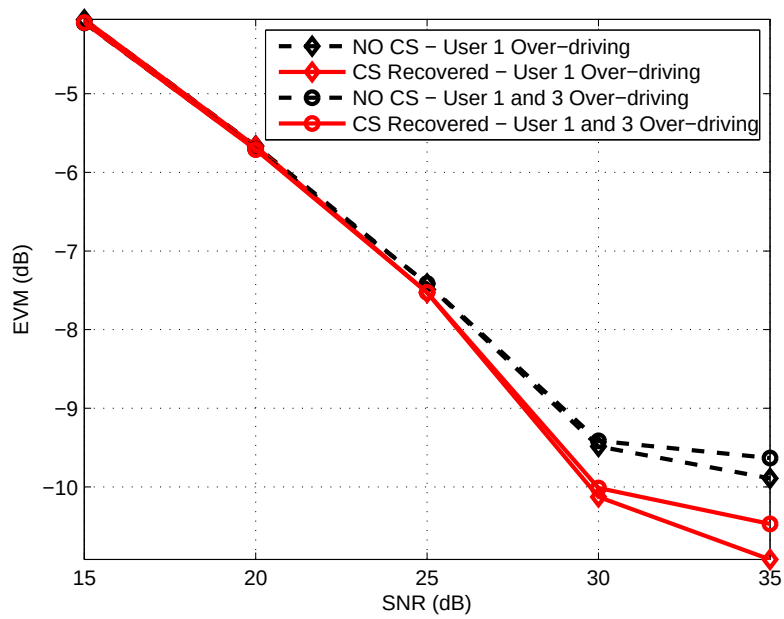

Figure 2.11: EVM performance of single antenna receiver averaged over fading channels.

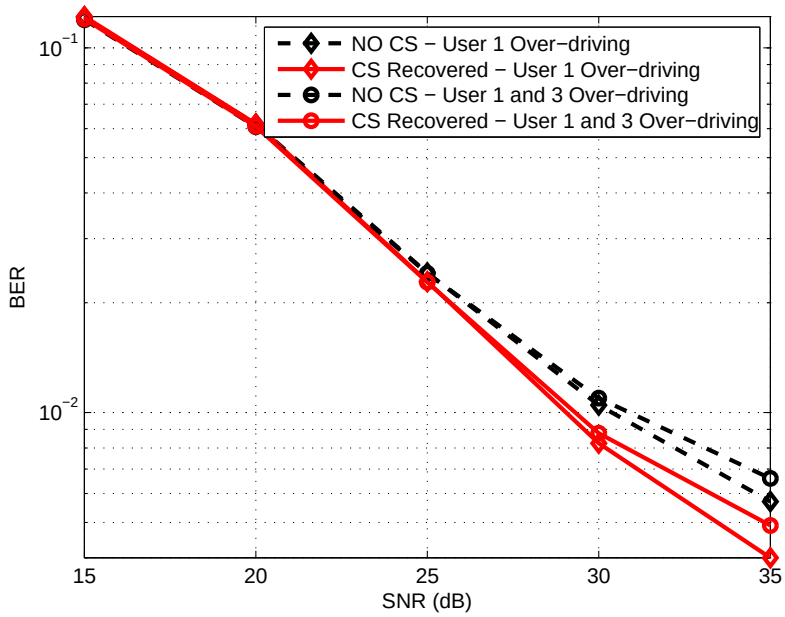

Figure 2.12: BER performance of single antenna receiver averaged over fading channels.

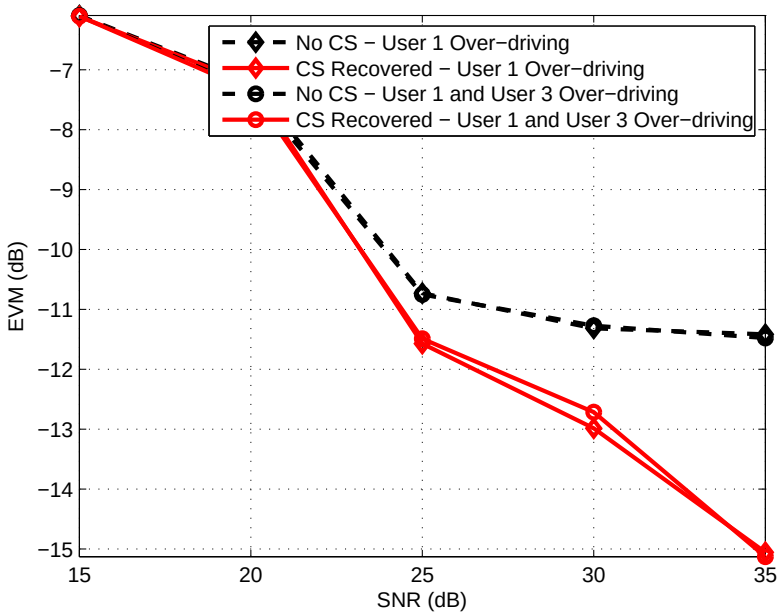

Figure 2.13: EVM performance of single antenna receiver for optimistic channel.

symbol error rate (SER) performance with 64 QAM and 1024 sub-carriers on a static inter-symbol interference (ISI) channel [44]. Furthermore, the transmitted signal is extracted at the receiver via coherent detection which depends on the channel estimation of a rayleigh fading channel. Hence any channel estimation error resulting from MMSE estimation reflects in the performance of overall communication system. The task of sparse signal reconstruction is challenging if we note that though the signal at SNR 10dB is 10 times higher than the noise, the distortions (that need to be reconstructed) are certainly not that high. The situation is further worsened by the fact that measurements of these distortions are taken in frequency domain, hence, a sparse distortion vector in time domain is spread throughout the frequency domain, with power not very high above the noise floor.

2.7.2 Experiment 2: Multiple Antenna Receiver

This experiment is carried to test the applicability of proposed sparse signal reconstruction scheme in multiple antenna receiver scenario. In SIMO-OFDMA scenario, 3 diversity branches are combined at the receiver using MRC and proposed distortion cancellation scheme is implemented. Once again, as shown in Fig. 2.14, not only for the case where there is no post-compensation but also for the case where there is post-compensation, it is true that the difference between the case of over-drive distortions only from 1 user, and distortions from both user 1 and user 3 is marginal. Further to that, the joint-estimation of the over-drive distortion using multiple measurements jointly led to improved EVM performance. BER results are shown in Fig. 2.15, which demonstrate the ability of proposed scheme to significantly improve the BER of the communication system.

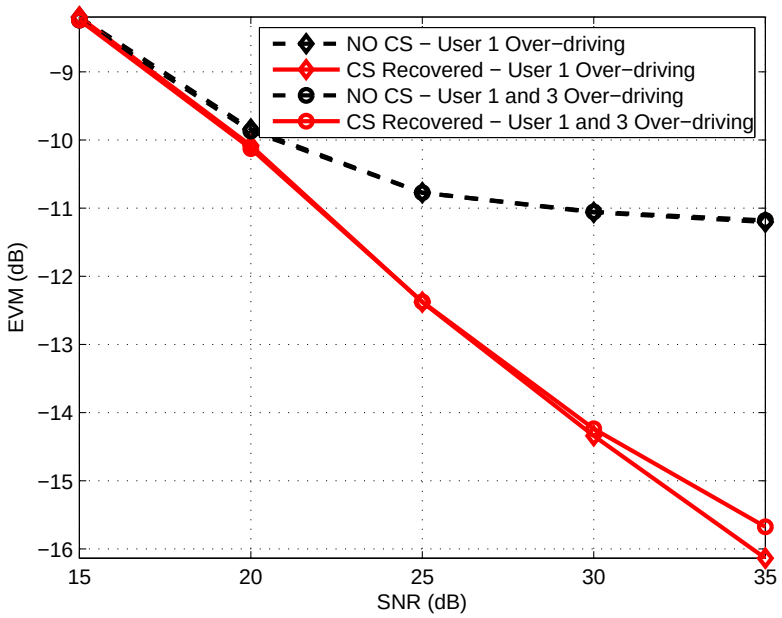

Figure 2.14: EVM performance of multiple antenna receiver averaged over fading channels.

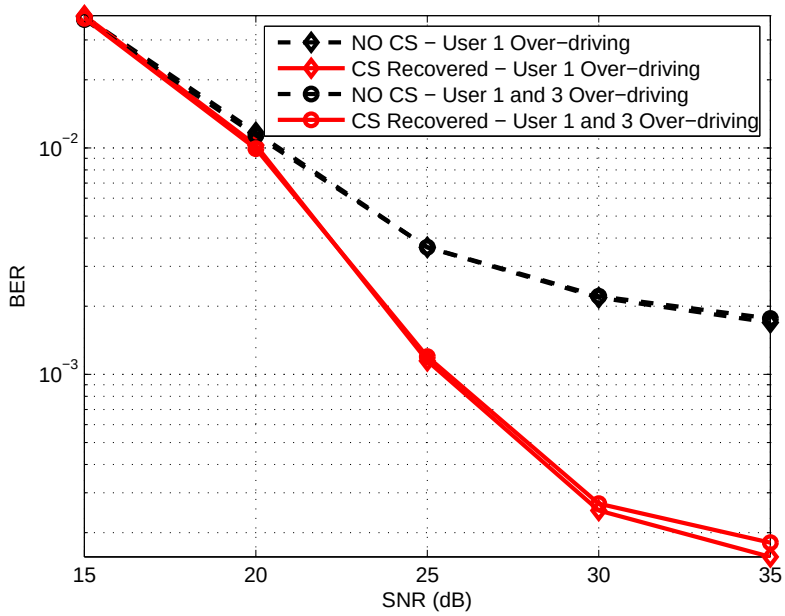

Figure 2.15: BER performance of multiple antenna receiver averaged over fading channels.

2.7.3 Experiment 3: Single Antenna vs Multiple Antenna Receiver

This experiment is carried to compare the results of single antenna and multiple antenna receiver systems. Only the case of over-drive distortions from both user 1 and user 3 is used for comparison. Diversity combining causes the low EVM floor for multiple antenna receiver system, as evident from Fig. 2.16. Though, the advantage of MRC is significant on low SNR values, it diminishes with increasing SNR if CS based post-compensation is not used. However, the use of the proposed post-compensation technique maintains the superior performance of the SIMO configuration. Furthermore, the performance enhancement obtained fol-

lowing the use of CS based technique is more pronounced in the region of interest corresponding to an SNR of 25 dB or higher. These findings are further validated using to the BER results shown in Fig. 2.17.

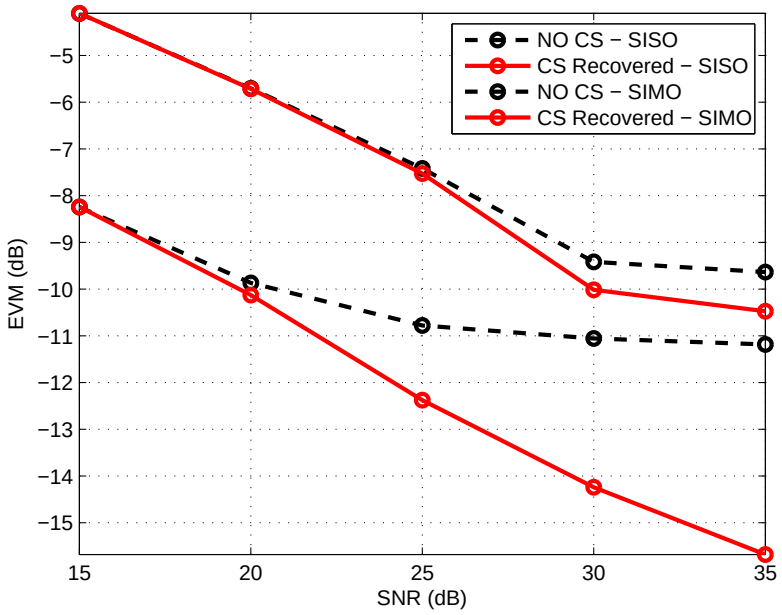

Figure 2.16: EVM performance comparison of single antenna vs multiple antenna receiver averaged over fading channels.

2.7.4 Experiment 4: Outage Capacity

In this experiment, the outage capacity of the communication system on hand, with and without the proposed distortion recovery scheme is studied. The largest rate of reliable communication at a certain outage probability is called the outage capacity [45]. It is well known that error correcting codes (i.e. block codes and convolutional codes) can be used to correct erroneous bits at the receiver [46]. Depending on the code type and rate, an error correcting code can achieve maximum capacity if the bit error rate is low enough. In this experiment, a coded communi-

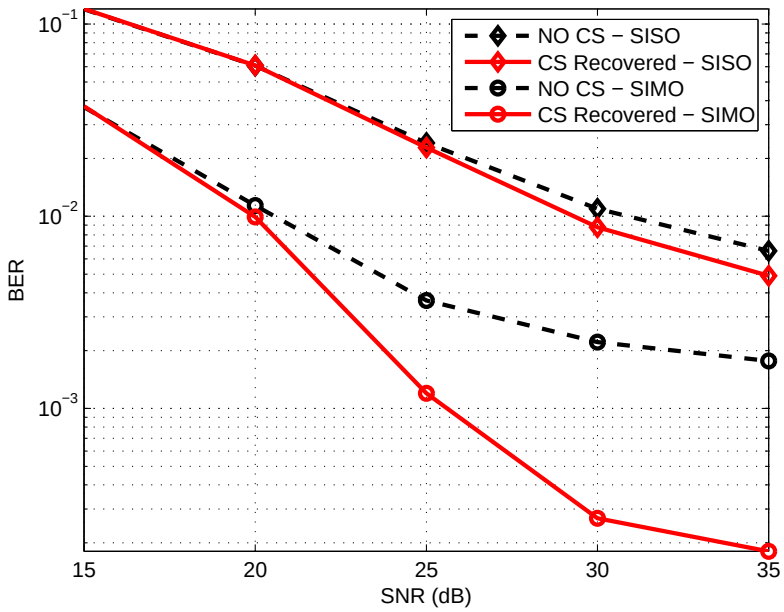

Figure 2.17: BER performance comparison of single antenna vs multiple antenna receiver averaged over fading channels.

cation system with multiple receiver antennas and distortions coming from both users is used. The targeted BER for error correction is $10^{-2.5}$; any BER below the targeted threshold will result in maximum capacity throughput whereas, BER above the threshold results in zero throughput. The outage capacity is studied at over-drive levels of 4 dB and 4.5 dB and is plotted against SNR in Fig. 2.18. It is observed that the communication system without distortion recovery will achieve maximum capacity with SNR more than 22.6 dB, whereas with distortion recovery, maximum capacity is achieved at SNR as low as 20.9 dB, in the case of 4 dB over-drive. Hence, the use of the proposed distortion recovery scheme gives a margin of around 1.7 dB in required SNR. Similarly, as shown in Fig. 2.18, with 4.5 dB over-drive no distortion recovery requires 33.1 dB, in comparison with 28.5 dB required for CS recovery, which makes the SNR margin 4.6 dB.

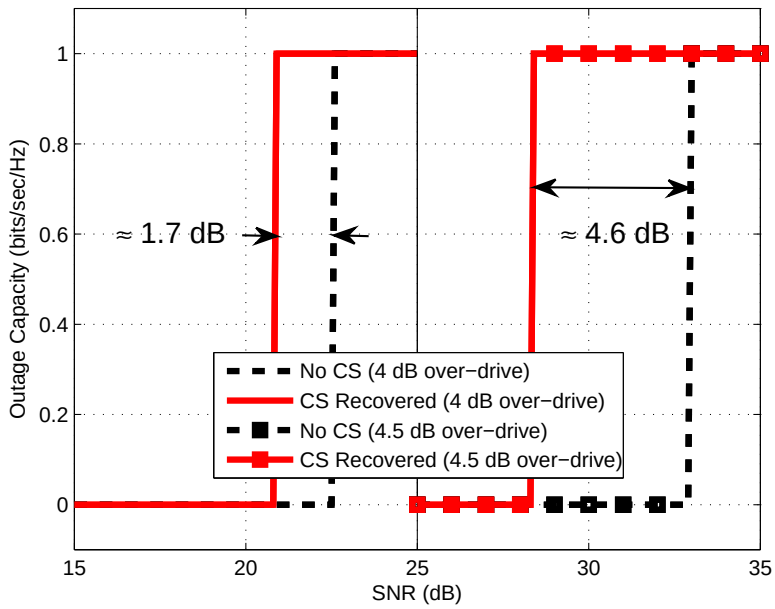

Figure 2.18: Outage capacity averaged over fading channels for 4 dB over-drive and 4.5 dB over-drive.

2.7.5 Experiment 5: Mean Square Error

In this experiment, the mean squared error (MSE) between the transmitted signal and the received signal is evaluated. The MSE is defined as

$$\text{MSE} = \frac{1}{N}\sum_{n=1}^{N}\left|\mathcal{X}(n) - \hat{\mathcal{X}}(n)\right|^2 \tag{2.29}$$

The MSE is evaluated for the case of multiple antenna receiver and over-drive distortions coming from both users. From the results shown in Fig. 2.19, it can be observed that the proposed distortion recovery scheme can significantly reduce the MSE between the transmitted signal and received recovered signal. Though performance enhancement is achieved throughout the range of interest, advantage of using the proposed scheme is more pronounced for high SNR values. It is worth

mentioning that the distortion recovery using CS is probabilistic and not certain. However, considering a large number of corrupted OFDM signals requiring distortion mitigation, CS has shown satisfactory results as demonstrated unanimously by all the experiments.

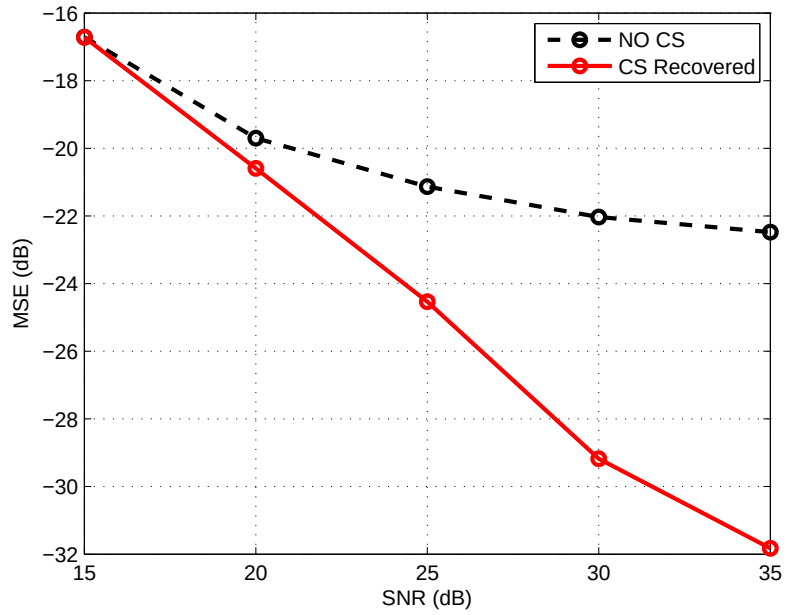

Figure 2.19: MSE performance averaged over fading channels.

2.7.6 Experiment 6: Channel Delay Spread

In this experiment, the effect of channel delay spread on the performance of proposed over-driven distortion recovery scheme is analyzed. Channels with 10 and 128 complex i.i.d taps coming from uniform normal distribution are generated for comparison. To avoid ISI between successive OFDM symbols, the length of the cyclic prefix is adjusted according to the length of channel impulse response and perfect channel knowledge is assumed at the receiver. The results shown in

Fig. 2.20 and Fig. 2.21 depict no significant difference in performance for channels with high and low delay spread. This is expected because as the cyclic prefix ensures no ISI between OFDM symbols, the channel frequency response per subcarrier is essentially flat fading. Hence, irrespective of the channel delay spread the proposed distortion recovery scheme works satisfactorily. It is worth mentioning that though in this experiment perfect channel knowledge is assumed at the receiver, this information can be easily obtained using MMSE estimation as reflected through the results of experiments 1 to 5. As channel estimation in quasi-static scenario is done via low power preamble signal (full of pilots and not influenced by the amplifier's distortions), the MMSE estimate will be sufficiently good for any channel irrespective of the delay spread.

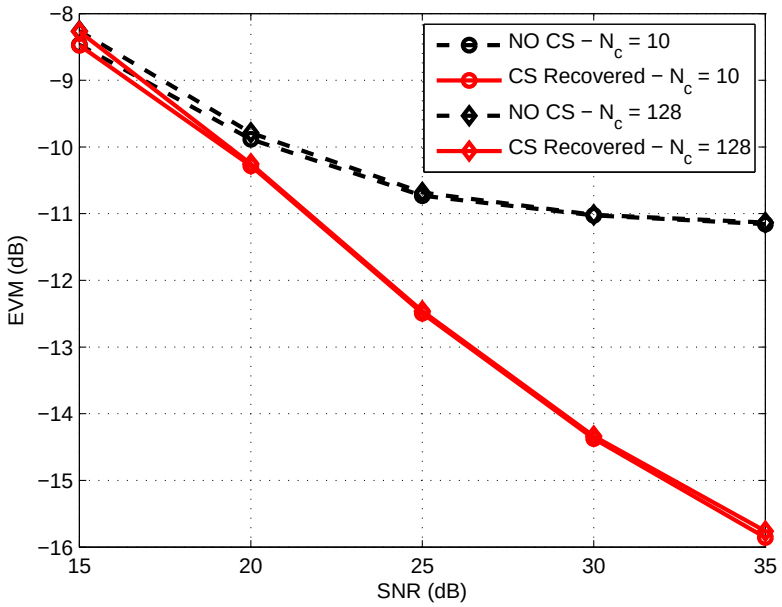

Figure 2.20: EVM performance comparison of for channels with high and low delay spread.

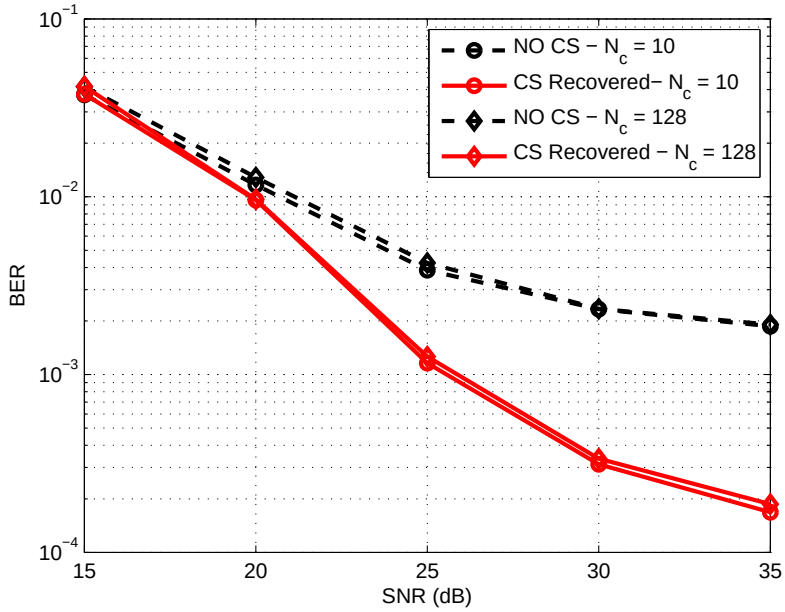

Figure 2.21: BER performance comparison of for channels with high and low delay spread.

2.8 Chapter Conclusion

In this chapter, a power efficient OFDMA-CR system is presented. Power efficiency is achieved by applying the proposed joint-compensation technique to an amplifier operating beyond saturation. Such an operation caused over-drive distortions which required to be estimated at the receiver. Hence sparse signal reconstruction scheme was employed at the receiver for distortion estimation. It was shown by numerical results for the entire communication system including channel effects, that proposed formulation leads to improved EVM and BER performance. Further, the proposed technique was successfully applied in SIMO configuration. The results illustrate that, compared to the SISO case, additional performance enhancement can be obtained when multiple antennas are used at the receiver with MRC.

CHAPTER 3

PAPR REDUCTION IN OFDM

3.1 Motivation

The problem of high peak-to-average power ratio (PAPR) in orthogonal frequency division multiplexing (OFDM) has received considerable research interest in the past. As the power amplifiers (PA) have a nonlinear response for higher input levels, the inflated PAPR causes nonlinear distortions. Though power back-off in the operating point of the PA will reduce the nonlinear distortions, it is not desirable as it results in inefficient operation of the PA and reduced battery life of the mobile terminal. Hence PAPR reduction in OFDM signalling is a necessity for the linear and power efficient operation of the PA. Some of the transmitter based PAPR reduction schemes include coding, partial transmit sequence (PTS), selected mapping (SLM), interleaving, tone reservation (TR), tone injection (TI) and active constellation extension (ACE) [2–5]. The computational requirement of the aforementioned transmitter based schemes make them unsuitable for appli-

cations where the transmitter complexity is a bottleneck.

Clipping is one simple and low complexity PAPR reduction method. The clipping operation is performed such that the magnitude of the time domain OFDM signal is limited to a pre-specified threshold. The clipping operation, however, is nonlinear and causes out-of-band radiations as well as in-band distortions. The out-of-band power spill interferes with adjacent channels and reduces power spectral efficiency. Though filtering can be used to significantly reduce the out-of-band radiations, it results in peak regrowth. A compromise between out-of-band spill and peak regrowth can be reached by iterative clipping and filtering operations [47–49]. Unlike out-of-band radiations, the in-band distortions can be taken care of at the receiver. However, if not, they result in significant performance loss evidenced e.g., by the high bit error rate (BER).

Recently the sparsity of the clipping signal has been exploited and compressed sensing (CS) schemes were used for clipping recovery at the receiver. The sparse nature of the clipping signal is evident as it originates when a high PAPR signal (with only a few high peaks) is subjected to a thresholding operation. Here it is noteworthy that the performance and applicability of any CS based PAPR reduction schemes is mainly limited by two factors: the complexity of the sparse signal reconstruction scheme and the number of reserved/measurement tones. In [17] Al-Safadi and Al-Naffouri utilized augmented CS for signal recovery in severe clipping scenarios. However, the drawback of [17] is the severe hit taken on the data rate due to dedicated measurement tones. A CS based approach using reliable carriers

(RC) as measurement tones with no compromise on data rate is proposed in [50]. However, this method is tailored for one-user single-input-single-output system. Hence it lacks the generality required by multiple receiver antenna systems and multi-user communications.

In this work, we focus on deliberate clipping based PAPR reduction. The time domain OFDM signal is limited to a pre-specified threshold and sparse clipping signal is reconstructed at the receiver using a low complexity Bayesian recovery algorithm. The proposed reconstruction scheme is agnostic to the signal statistics and utilizes *a priori* information about the additive noise, sparsity rate of the signal and the clipping threshold. However, if accurate estimates of these quantities are not available, it can bootstrap itself and estimate them from the data. The proposed scheme also utilizes the *a priori* information about undistorted phase of the clipped signal for enhanced recovery. Further, the recovery algorithm focuses on the most probable clipping locations by obtaining the clipping likelihood from a comparison between the magnitude of the received data samples and the clipping threshold. At the receiver, some of the data sub-carriers are designated as RCs for sensing the clipping distortion (based on the criteria proposed in [50]) and hence there is no data loss in using the proposed clipping reconstruction scheme. Considering that most modern communication standards use multiple antennas at the receiver, the proposed scheme is extended to the case of single-input multiple-output (SIMO) systems. It is also highlighted that the problem of clipping estimation in multi-user communications (i.e., orthogonal frequency

division multiple access (OFDMA) systems) is not straight forward. The complications arise due to the fact that clipping distortions from different users overlap in frequency domain and are indistinguishable from one another. In light of this, a clipping reconstruction scheme for OFDMA systems is also framed. The proposed multi-user clipping recovery scheme initially performs the joint-estimation of clipping distortions from all users. This is followed by the decoupling stage, in which subsystems belonging to each users are formed such that they are interference free from other users' distortions. Then the clipping is individually recovered on each decoupled subsystem. Lastly we consider the channel estimation problem for clipped OFDM and present two data aided channel estimation schemes. The main idea is to use RCs in addition to the pilot sub-carriers for enhanced minimum mean square error (MMSE) estimation.

3.1.1 Chapter Contributions

The main contributions of this chapter can be summarized as follows

- A low complexity Bayesian clipping recovery scheme is presented, that has the following features
  - It is agnostic to the signal statistics.
  - It uses *a priori* information about the additive noise, sparsity rate and threshold. Further, it can bootstrap itself if accurate estimates of these parameters are not available.
  - It utilizes the *a priori* information of the undistorted phase and the

clipping support from the vicinity of the received signal to the clipping level.

  - It has a data aided version that makes use of the RCs in place of reserved carriers hence conserving the data rate.

- It is able to make use of the multiple receive antennas for enhanced clipping recovery.

- It can be extended to the multi-user OFDMA systems.

In addition, in this chapter effective channel estimation strategies are proposed that work in spite of pilot contamination from clipping distortion.

3.2 Data Model for Clipped OFDM

In OFDM transmission the incoming bitstream is first divided into N parallel streams and is then modulated using an M-QAM constellation $\{\mathcal{A}_0, \mathcal{A}_1, \cdots, \mathcal{A}_{M-1}\}$. The modulated data $\boldsymbol{\mathcal{X}} = [\mathcal{X}(0), \mathcal{X}(1), \cdots, \mathcal{X}(N-1)]^{\mathsf{T}}$ is converted to the time domain using the inverse discrete Fourier transform (IDFT) i.e., $\mathbf{x} = \mathbf{F}^{\mathsf{H}}\boldsymbol{\mathcal{X}}$. Here $\mathbf{F}$ is the DFT matrix whose (n_1, n_2) element is given by

$$\mathrm{f}_{n_1,n_2} = N^{-1/2} e^{-\jmath 2\pi n_1 n_2/N}, \quad n_1, n_2 \in 0, 1, \cdots, N-1.$$

The time domain signal $\mathbf{x}$ has a high PAPR and is subjected to an amplitude

limiter for PAPR reduction. The resulting clipped signal $\mathbf{x}_p$ is described by

$$x_p(i) = \begin{cases} \gamma \exp(\jmath \angle x(i)) & \text{if } \ |x(i)| > \gamma \\ \\ x(i) & \text{otherwise,} \end{cases} \tag{3.1}$$

where $|\cdot|$ denotes the absolute value, $x_p(i)$ is the ith element of the signal after clipping, γ is the limiting threshold and $\angle x(i)$ is the phase of $x(i)$. The clipping ratio (CR) and threshold γ are related by $\text{CR} = \gamma/\sigma_x$, where σ_x is the root mean squared power of the OFDM signal. The hard clipping in (3.1) is equivalent to the addition of a *sparse* signal $\mathbf{c}$ (with active elements only at the clipping locations) to the time domain signal $\mathbf{x}$. The clipped signal $\mathbf{x}_p$ is then given as

$$\mathbf{x}_p = \mathbf{x} + \mathbf{c}. \tag{3.2}$$

The equivalence of (3.1) and (3.2) dictates that $\mathbf{c}$ must be anti-phased with $\mathbf{x}$ on the clipping locations and zero everywhere else. Thus, the addition of $\mathbf{c}$ leaves the phase unaltered i.e., $\angle x_p(i) = \angle x(i) = -\angle c(i) \ \forall \ i$. This undistorted phase property is important and is exploited in the development of the proposed reconstruction scheme.

The clipped signal $\mathbf{x}_p$ is transmitted through a channel of length N_c with impulse response $\mathbf{h} = [h(0), h(1), \cdots, h(N_c - 1)]^{\mathsf{T}}$, where the channel tap coefficients form a zero mean complex Gaussian independent and identically distributed (i.i.d)

collection. The received time domain signal can be written as

$$\mathbf{y} = \mathbf{H}\mathbf{x}_p + \mathbf{z}, \tag{3.3}$$

where $\mathbf{H}$ is the circulant channel matrix and $\mathbf{z}$ is the additive white Gaussian noise (AWGN) with $\mathbf{z} \sim \mathcal{CN}(\mathbf{0}, \sigma_z^2\mathbf{I})$. The circulant nature of $\mathbf{H}$ allows us to diagonalize it using the DFT matrix $\mathbf{F}$ and write $\mathbf{H} = \mathbf{F}^{\mathsf{H}}\mathbf{D}\mathbf{F}$, where $\mathbf{D}$ is a diagonal matrix with channel frequency response on its diagonal. The data model and proposed reconstruction scheme are developed assuming channel knowledge at the receiver. The procedure for acquiring the channel impulse response (CIR) in clipped OFDM is outlined in Section 3.6 further ahead.

The frequency domain received signal can be obtained from (3.3) by the DFT operation as

$$\boldsymbol{\mathcal{Y}} = \mathbf{D}\boldsymbol{\mathcal{X}}_p + \boldsymbol{\mathcal{Z}} = \mathbf{D}(\boldsymbol{\mathcal{X}} + \boldsymbol{\mathcal{C}}) + \boldsymbol{\mathcal{Z}}, \tag{3.4}$$

where $\boldsymbol{\mathcal{Y}} = \mathbf{F}\mathbf{y}$ and $\boldsymbol{\mathcal{X}}_p, \boldsymbol{\mathcal{X}}, \boldsymbol{\mathcal{C}}, \boldsymbol{\mathcal{Z}}$ are similarly defined. Equalizing the received data in (3.4) results in

$$\widehat{\boldsymbol{\mathcal{X}}} = \mathbf{D}^{-1}\boldsymbol{\mathcal{Y}} = \boldsymbol{\mathcal{X}} + \underbrace{\boldsymbol{\mathcal{C}} + \mathbf{D}^{-1}\boldsymbol{\mathcal{Z}}}_{:=\boldsymbol{\mathcal{Z}}^{\dagger}} = \boldsymbol{\mathcal{X}} + \boldsymbol{\mathcal{Z}}^{\dagger}, \tag{3.5}$$

here $\boldsymbol{\mathcal{Z}}^{\dagger}$ is the combined additive noise and clipping distortion. A naive receiver will disregard the presence of clipping noise in (3.5) and will make the maximum

likelihood (ML) decisions on $\widehat{\boldsymbol{\mathcal{X}}}$ to obtain the estimated transmitted signal $\lfloor \widehat{\boldsymbol{\mathcal{X}}} \rfloor$ (the operator $\lfloor \cdot \rfloor$ is used to denote the ML decisions or equivalently rounding to the nearest QAM constellation point). However, a receiver employing CS reconstruction will exploit the sparse nature of $\mathbf{c}$ for its estimation and hence removal.

As the clipping signal $\mathbf{c}$ is sparse in the time domain, its frequency domain counterpart $\boldsymbol{\mathcal{C}}$ perturbs all sub-carriers alike as the time and frequency domains are maximally incoherent. Utilizing this incoherence via CS, it is possible to reconstruct an N dimensional time domain sparse vector with only P random projections on frequency domain, where $P << N$. These projections can be made using randomly allocated pilot tones as done in [17] but doing so reduces the data rate. In this work, we avoid this and use a data aided approach to estimate $\mathbf{c}$ as we describe below.

Given the equalized signal $\widehat{\boldsymbol{\mathcal{X}}}$ at the receiver we expect the following: for some sub-carriers, the perturbation $\mathcal{Z}^{\dagger}(i)$ is strong enough to take $\mathcal{X}(i)$ out of its correct decision region i.e. $\lfloor \widehat{\mathcal{X}(i)} \rfloor \neq \mathcal{X}(i)$, while for others with a milder perturbation, we expect to have $\lfloor \widehat{\mathcal{X}(i)} \rfloor = \mathcal{X}(i)$. The subset of data carries which satisfy $\lfloor \widehat{\mathcal{X}(i)} \rfloor = \mathcal{X}(i)$ are called RCs and fortunately constitute a major part of all sub-carriers. To select this subset, we note that the major source of perturbation is the clipping distortion, especially for high signal-to-noise ratio (SNR). Hence, from (3.5), we can write the reliability function of the ith sub-carrier in terms of

$\mathcal{Z}^{\dagger}(i)$ as

$$\mathfrak{R}(\mathrm{i}) = \frac{\mathrm{p}(\mathcal{Z}^{\dagger}(i) = \widehat{\mathcal{X}(i)} - \lfloor \widehat{\mathcal{X}(i)} \rfloor)}{\sum_{k=0,\mathcal{A}(k)\neq\lfloor\widehat{\mathcal{X}(i)}\rfloor}^{M-1} \mathrm{p}(\mathcal{Z}^{\dagger}(i) = \widehat{\mathcal{X}(i)} - \mathcal{A}(k))}, \tag{3.6}$$

where $\mathrm{p}(\cdot)$ represents the pdf of $\boldsymbol{\mathcal{Z}}^{\dagger}$, which is assumed to be zero mean Gaussian with variance σ_z^2 (see [50] for details). In (3.6), the numerator is the probability that $\mathcal{Z}^{\dagger}(i)$ does not take $\mathcal{X}(i)$ beyond its correct decision region and the denominator sums the probabilities of all possible incorrect decisions that $\mathcal{Z}^{\dagger}(i)$ can cause. The detailed investigation of this reliability criteria is reported in [50]. After obtaining the reliability $\mathfrak{R}(i)$ for each carrier i, we pick the P sub-carriers with highest reliability values and use them as measurement tones to recover sparse clipping vector $\mathbf{c}$. Consider an $N \times N$ binary selection matrix $\mathbf{S}$, with P ones along its diagonal, corresponding to the locations of the most reliable P sub-carriers. Using $\mathbf{S}$ we construct a $P \times N$ matrix $\mathbf{S}_P$ by pruning $\mathbf{S}$ of its zero rows. Subtracting $\mathbf{D}\lfloor\widehat{\boldsymbol{\mathcal{X}}}\rfloor$ from (3.4) and using $\mathbf{S}_P$, we have

$$\begin{aligned} \mathbf{S}_P(\boldsymbol{\mathcal{Y}} - \mathbf{D}\lfloor\widehat{\boldsymbol{\mathcal{X}}}\rfloor) &= \mathbf{S}_P\mathbf{D}(\boldsymbol{\mathcal{X}} - \lfloor\widehat{\boldsymbol{\mathcal{X}}}\rfloor) + \mathbf{S}_P\mathbf{D}\mathbf{F}\mathbf{c} + \mathbf{S}_P\boldsymbol{\mathcal{Z}}, \\ \boldsymbol{\mathcal{Y}}' &= \boldsymbol{\Psi}\mathbf{c} + \boldsymbol{\mathcal{Z}}', \end{aligned} \tag{3.7}$$

where $\boldsymbol{\mathcal{Y}}' = \mathbf{S}_P(\boldsymbol{\mathcal{Y}} - \mathbf{D}\lfloor\widehat{\boldsymbol{\mathcal{X}}}\rfloor)$, $\boldsymbol{\Psi} = \mathbf{S}_P\mathbf{D}\mathbf{F}$ and $\boldsymbol{\mathcal{Z}}' = \mathbf{S}_P\boldsymbol{\mathcal{Z}}$. To establish the equality in aforementioned equation, we have used the fact that on RCs $\lfloor\widehat{\mathcal{X}(i)}\rfloor = \mathcal{X}(i)$, and hence $\mathbf{S}_P\mathbf{D}(\boldsymbol{\mathcal{X}} - \lfloor\widehat{\boldsymbol{\mathcal{X}}}\rfloor) = \mathbf{0}$. A typical CS problem of the form (3.7), with P measurements and N dimensional sparse unknown ($P << N$) can be solved using

any sparse reconstruction algorithm e.g., [25–30, 38]. However, these schemes are complex and do not utilize the clipping likelihood and undistorted phase property of the clipped signal.

3.3 Proposed Clipping Reconstruction Scheme

From (3.1) and (3.2), and the discussion that followed, it is known that the clipping vector $\mathbf{c}$ and the signal vector $\mathbf{x}$ are anti-phased. Hence, the phase information can be deduced at the receiver from the time domain equivalent of (3.5), i.e., $\hat{\mathbf{x}} = \mathbf{x}+\mathbf{c}+\mathbf{H}^{-1}\mathbf{z}$. Since $\angle c(i) = -\angle x(i)\ \forall\, i$, only the support and the magnitudes of the active clipping elements are left unknown. Hence we can rewrite (3.7) as

$$\begin{aligned} \boldsymbol{\mathcal{Y}}' &= \boldsymbol{\Psi}\boldsymbol{\Theta}_{\mathbf{c}}\mathbf{c}_m + \boldsymbol{\mathcal{Z}}', \\ &= \boldsymbol{\Phi}\mathbf{c}_m + \boldsymbol{\mathcal{Z}}', \end{aligned} \tag{3.8}$$

where $\boldsymbol{\Phi} = \boldsymbol{\Psi}\boldsymbol{\Theta}_{\mathbf{c}}$. Here the matrix $\boldsymbol{\Theta}_{\mathbf{c}}$ contains the phases of $\mathbf{c}$ on its diagonal, i.e., $\boldsymbol{\Theta}_{\mathbf{c}} \approx -\boldsymbol{\Theta}_{\hat{\mathbf{x}}} = -\text{diag}(\angle\hat{x}(0), \angle\hat{x}(1), \cdots, \angle\hat{x}(N-1))$ and the vector $\mathbf{c}_m$ consists of the magnitudes of the elements of $\mathbf{c}$. Since the aforementioned system of equations is complex with real unknown, we can split the real and imaginary parts (designated as $\text{Re}\{\cdot\}$ and $\text{Im}\{\cdot\}$, respectively) to obtain a system with $2P$

equations

$$\begin{bmatrix} \mathrm{Re}\{\boldsymbol{\mathcal{Y}}'\} \\ \mathrm{Im}\{\boldsymbol{\mathcal{Y}}'\} \end{bmatrix} = \begin{bmatrix} \mathrm{Re}\{\boldsymbol{\Phi}\} \\ \mathrm{Im}\{\boldsymbol{\Phi}\} \end{bmatrix} \mathbf{c}_m + \begin{bmatrix} \mathrm{Re}\{\boldsymbol{\mathcal{Z}}'\} \\ \mathrm{Im}\{\boldsymbol{\mathcal{Z}}'\} \end{bmatrix},$$

$$\bar{\boldsymbol{\mathcal{Y}}} = \bar{\boldsymbol{\Phi}}\mathbf{c}_m + \bar{\boldsymbol{\mathcal{Z}}}. \tag{3.9}$$

From hereon, we simply use $\mathbf{c}$ and not $\mathbf{c}_m$ to denote the unknown signal, with the understanding that $\mathbf{c}$ contains only the magnitudes and rewrite (3.9) as

$$\bar{\boldsymbol{\mathcal{Y}}} = \bar{\boldsymbol{\Phi}}\mathbf{c} + \bar{\boldsymbol{\mathcal{Z}}}. \tag{3.10}$$

To solve the under-determined system in (3.10), we employ a Bayesian sparse reconstruction scheme. A tractable Bayesian approach e.g., [26] assumes Gaussian distribution on active elements of the unknown signal. However, this is not the case here, as the nonzero elements of $\mathbf{c}$ are the differences of a Rayleigh distributed elements $|x(i)|$ and a constant γ. As the unknown is clearly non-Gaussian, we pursue a Bayesian approach introduced in [51] that does not make any assumption on the statistics of the nonzero elements of $\mathbf{c}$.

Let us compute the MMSE estimate of $\mathbf{c}$ given the observation $\bar{\boldsymbol{\mathcal{Y}}}$ as

$$\hat{\mathbf{c}}_{\mathrm{mmse}} \triangleq \mathbb{E}[\mathbf{c}|\bar{\boldsymbol{\mathcal{Y}}}] = \sum_{\mathcal{S}} \mathrm{p}(\mathcal{S}|\bar{\mathcal{Y}})\mathbb{E}[\mathbf{c}|\bar{\boldsymbol{\mathcal{Y}}}, \mathcal{S}], \tag{3.11}$$

where the sum is executed over all possible 2^N support sets $\mathcal{S}$ of $\mathbf{c}$. Now assuming

that the support $\mathcal{S}$ is perfectly known, (3.10) reduces to

$$\bar{\boldsymbol{\mathcal{Y}}} = \bar{\boldsymbol{\Phi}}_{\mathcal{S}}\mathbf{c}_{\mathcal{S}} + \bar{\boldsymbol{\mathcal{Z}}}, \tag{3.12}$$

where $\bar{\boldsymbol{\Phi}}_{\mathcal{S}}$ is formed by selecting the columns of $\bar{\boldsymbol{\Phi}}$ indexed by support $\mathcal{S}$. Similarly, $\mathbf{c}_{\mathcal{S}}$ is formed by selecting entries of $\mathbf{c}$ indexed by $\mathcal{S}$. Since the distribution of $\mathbf{c}$ is unknown, computing $\mathbb{E}[\mathbf{c}|\bar{\boldsymbol{\mathcal{Y}}}, \mathcal{S}]$ is very difficult, if possible at all. Thus, we resort to the best linear unbiased estimate (BLUE) as an estimate of $\mathbf{c}$, as given below

$$\mathbb{E}[\mathbf{c}|\bar{\boldsymbol{\mathcal{Y}}}, \mathcal{S}] \leftarrow (\bar{\boldsymbol{\Phi}}_{\mathcal{S}}^{\mathsf{H}}\bar{\boldsymbol{\Phi}}_{\mathcal{S}})^{-1}\bar{\boldsymbol{\Phi}}_{\mathcal{S}}^{\mathsf{H}}\bar{\boldsymbol{\mathcal{Y}}}. \tag{3.13}$$

Using Bayes rule, the posterior in (3.11) can be written as

$$\mathrm{p}(\mathcal{S}|\bar{\boldsymbol{\mathcal{Y}}}) = \frac{\mathrm{p}(\bar{\boldsymbol{\mathcal{Y}}}|\mathcal{S})\mathrm{p}(\mathcal{S})}{\mathrm{p}(\bar{\boldsymbol{\mathcal{Y}}})}, \tag{3.14}$$

where $\mathrm{p}(\bar{\boldsymbol{\mathcal{Y}}})$ is common to all posteriors, and hence can be ignored. Note that Bayesian reconstruction schemes (e.g., support agnostic Bayesian matching pursuit (SABMP) [51] and fast Bayesian matching pursuit (FBMP) [26]) assume that the elements of the unknown are activated according to a Bernoulli distribution with success probability ρ. Hence, $\mathrm{p}(\mathcal{S})$ is calculated as $\mathrm{p}(\mathcal{S}) = \rho^{|\mathcal{S}|}(1-\rho)^{N-|\mathcal{S}|}$. However, for problem on hand it is reasonable to assume that $c(i)$ is an active element if the received sample $\hat{x}(i)$ is in close proximity to γ. So, instead of assigning a uniform probability ρ to all samples, we assign higher probabilities to the samples which correspond to the elements of $\mathbf{x}$ that are more likely to have been

clipped. To do so, we define a weight vector $\mathbf{w}$ with elements $w(i) = \gamma - |\hat{x(i)}|$, and assign higher probabilities to the locations where the aforementioned difference is small. One such assignment is $\rho_i = e^{-w(i)}$, where, ρ_i is the probability of a clip on ith element (ρ_i's are normalized to have $\max(\rho_i) = 1$). This gives us

$$\mathrm{p}(\mathcal{S}) = \prod_{i \in \mathcal{S}} \rho_i \prod_{k \in \bar{\mathcal{S}}} (1 - \rho_k), \tag{3.15}$$

where $\mathcal{S} \cap \bar{\mathcal{S}} = \varnothing$ and $\mathcal{S} \cup \bar{\mathcal{S}} = \{1, 2, \cdots, N\}$.

We are left with the calculation of $\mathrm{p}(\bar{\boldsymbol{\mathcal{Y}}}|\mathcal{S})$, which is difficult owing to the non-Gaussian nature of $\mathbf{c}_{\mathcal{S}}$. To go around, we note that $\bar{\boldsymbol{\mathcal{Y}}}$ is formed by a vector in the subspace spanned by the columns of $\bar{\boldsymbol{\Phi}}_{\mathcal{S}}$ plus a Gaussian noise vector $\bar{\boldsymbol{\mathcal{Z}}}$. This motivates us to eliminate the non-Gaussian component by projecting $\bar{\boldsymbol{\mathcal{Y}}}$ onto the orthogonal complement space of $\bar{\boldsymbol{\Phi}}_{\mathcal{S}}$. This is done by pre-multiplying $\bar{\boldsymbol{\mathcal{Y}}}$ by a projection matrix $\mathbf{P}_{\bar{\mathcal{S}}}^{\perp}$ defined as

$$\mathbf{P}_{\bar{\mathcal{S}}}^{\perp} = \mathbf{I} - \mathbf{P}_{\mathcal{S}} = \mathbf{I} - \bar{\boldsymbol{\Phi}}_{\mathcal{S}} \left(\bar{\boldsymbol{\Phi}}_{\mathcal{S}}^{\mathsf{H}} \bar{\boldsymbol{\Phi}}_{\mathcal{S}} \right)^{-1} \bar{\boldsymbol{\Phi}}_{\mathcal{S}}^{\mathsf{H}}.$$

This leaves us with $\mathbf{P}_{\bar{\mathcal{S}}}^{\perp} \bar{\boldsymbol{\mathcal{Y}}} = \mathbf{P}_{\bar{\mathcal{S}}}^{\perp} \bar{\boldsymbol{\mathcal{Z}}}$, which is Gaussian with zero mean and covariance

$$\begin{aligned} \mathbf{K} &= \mathbb{E}[(\mathbf{P}_{\bar{\mathcal{S}}}^{\perp} \bar{\boldsymbol{\mathcal{Z}}})(\mathbf{P}_{\bar{\mathcal{S}}}^{\perp} \bar{\boldsymbol{\mathcal{Z}}})^{\mathsf{H}}] \\ &= \mathbf{P}_{\bar{\mathcal{S}}}^{\perp} \mathbb{E}[\bar{\boldsymbol{\mathcal{Z}}} \bar{\boldsymbol{\mathcal{Z}}}^{\mathsf{H}}] \mathbf{P}_{\bar{\mathcal{S}}}^{\perp\mathsf{H}} = \mathbf{P}_{\bar{\mathcal{S}}}^{\perp} \sigma_z^2 \mathbf{P}_{\bar{\mathcal{S}}}^{\perp\mathsf{H}} \\ &= \sigma_z^2 \mathbf{P}_{\bar{\mathcal{S}}}^{\perp}. \end{aligned} \tag{3.16}$$

Thus we have,

$$\mathrm{p}(\bar{\boldsymbol{\mathcal{Y}}}|\mathcal{S}) = \frac{1}{\sqrt{(2\pi\sigma_z^2)^{2P}}} \exp\left(-\frac{1}{2}(\mathbf{P}_{\mathcal{S}}^{\perp}\bar{\boldsymbol{\mathcal{Y}}})^{\mathsf{H}}\mathbf{K}^{-1}(\mathbf{P}_{\mathcal{S}}^{\perp}\bar{\boldsymbol{\mathcal{Y}}})\right). \tag{3.17}$$

Simplifying and dropping the pre-exponential factor yields,

$$\mathrm{p}(\bar{\boldsymbol{\mathcal{Y}}}|\mathcal{S}) \simeq \exp\left(-\frac{1}{2\sigma_z^2}\|\mathbf{P}_{\mathcal{S}}^{\perp}\bar{\boldsymbol{\mathcal{Y}}}\|^2\right). \tag{3.18}$$

Substituting (3.15) and (3.18) in (3.14) gives the expression for posterior probability, which is then used to compute the sum in (3.11). However, this computation is challenging as the number of support sets is large (typical values of N in OFDM are 256 and 512). The computational burden can be reduced with slight compromise on the performance, if this sum is computed only on the support sets corresponding to the significant posteriors $\mathcal{S}_d$ (see [51] for details). Thus, we can write the approximated MMSE estimate of $\mathbf{c}$ as

$$\hat{\mathbf{c}}_{\text{ammse}} \triangleq \mathbb{E}[\mathbf{c}|\bar{\boldsymbol{\mathcal{Y}}}] = \sum_{\mathcal{S}_d} \mathrm{p}(\mathcal{S}|\bar{\mathcal{Y}})\mathbb{E}[\mathbf{c}|\bar{\boldsymbol{\mathcal{Y}}}, \mathcal{S}], \tag{3.19}$$

Now, we pursue a greedy approach [26,51] to find a subset of the dominant support $\mathcal{S}_d$. Note that though this approach of sparse signal reconstruction was presented in [51], the proposed clipping recovery scheme has two differentiating characteristics. First is the use of weighted $\mathrm{p}(\mathcal{S})$ in (3.15), which helps to find the dominant support much faster than the un-weighted case. Second is the phase augmentation which results in improved reconstruction accuracy.

The Bayesian reconstruction approach discussed above relies on the *a priori* information about the sparsity rate ρ, the noise variance σ_z^2 and the clipping threshold γ to reconstruct the vector $\mathbf{c}$. The threshold γ can be communicated to the receiver during the signalling period, ρ can be obtained from previously accumulated data and any SNR estimation scheme can be used to find σ_z^2. Nonetheless, if accurate estimates of these quantities are not available, the proposed scheme can bootstrap itself and estimate these parameters from the data. Specifically, in the absence of accurate estimates, we start with initial rough estimates of the parameters and obtain $\hat{\mathbf{c}}$. The estimate of $\mathbf{c}$ is then used to refine the parameters $\hat{\sigma}_z^2$ and $\hat{\rho}$, and these parameters are now used to obtain an improved estimate of $\mathbf{c}$. This procedure can continue iteratively, until a predetermined criteria is satisfied. The computational complexity of the proposed reconstruction scheme is of the order $\mathcal{O}(E_{\max}\rho P N^2)$, if an N dimensional signal with ρN non-zero elements is estimated using P measurements and the parameter refinement is performed $E_{\max}$ number of times [51]. As the proposed scheme uses weighting and phase augmentation we term it weighted and phase augmented (WPA)-SABMP. An algorithmic description of the WPA-SABMP reconstruction scheme is provided in Table 3.1.

3.3.1 Simulation Results

The SABMP algorithm was proposed in [51] and was shown to outperform other Bayesian and ℓ_1 based sparse recovery algorithms. Hence in this work we com-

Table 3.1: Summary of the proposed WPA-SABMP scheme

1. *Equalize:* $\hat{\mathbf{x}} = \mathbf{F}^{\mathsf{H}}\mathbf{D}^{-1}\mathbf{F}\mathbf{y}$
2. *Estimate clipping level:* $\hat{\gamma} = \max(\hat{\mathbf{x}})$
3. *Calculate the weight:* $\mathbf{w} = \hat{\gamma} - |\hat{\mathbf{x}}|$
4. *Find Reliable Carriers:* Calculate $\mathfrak{R}$ and choose P carriers with highest reliability.
5. *Estimate sparsity rate:* $\hat{\rho}(0) = \mathsf{Q}\left(\frac{\hat{\gamma} - \mu}{\sigma}\right)$, an initial estimate, where μ and σ are the mean and standard deviation of $\hat{\mathbf{x}}$, respectively.
6. $t = 1, 2, \cdots,$ *repeat*
   (a) $\hat{\rho}(t)_i = \hat{\rho}(t)e^{-w(i)},\ i = 1, 2, \cdots, N$
   (b) *Compute:* $\hat{\mathbf{c}}_{\text{mmse}}$ and $\hat{\rho}(t)$ using the technique discussed in [51] *until* $\left(\frac{|\hat{\rho}(t) - \hat{\rho}(t-1)|}{\hat{\rho}(t-1)} < 0.02\right)$
   (c) *Phase augment:* $\hat{\mathbf{c}} = \mathbf{\Theta}_c|\hat{\mathbf{c}}_{\text{ammse}}|$
   (d) *Remove distortion:* $\hat{\mathbf{x}}(t+1) = \hat{\mathbf{x}}(t) - \hat{\mathbf{c}}$

pare the proposed WPA-SABMP scheme with SABMP [51], the phase augmented version of FBMP i.e., PA-FBMP and weighted and phase augmented-LASSO (WPAL) [17]. As a benchmark we use the oracle-least squares (LS) solution (i.e., the case when the support is perfectly known and LS solution is calculated on the known support). In all simulations it is assumed that the statistics (i.e., the mean and the variance) of the clipping signal are not known. These schemes are compared for their BER performance and practical complexity. The practical complexity is calculated as the average runtime for signal recovery and is presented by subgraphs within the main figures (the independent axes of the subgraph and the corresponding main figure are always identical).

An OFDM system with 512 sub-carriers is simulated. The 64-QAM alphabet is used for modulation and the data is passed through a channel with 10 i.i.d taps of unit variance. All simulation results are averaged over 5000 bit errors unless otherwise noted.

Experiment 1

In this experiment, the performance of the proposed scheme is tested vs the CR while keeping the E_b/N_0 and P fixed. It is natural that the performance of the reconstruction schemes improves as the clipping is reduced (i.e., higher CR values). However, as shown in Fig. 3.1 the proposed WPA-SABMP scheme performs better than SABMP and PA-SABMP for all CR values and better than WPAL for most CR values. Further, observe that WPA-SABMP scheme recovers the clipping in a small time irrespective of the CR.

Experiment 2

In this experiment, sparse reconstruction schemes are tested for their BER performance. The CR is kept fixed at CR = 1.61 and the number of RCs is set to $P = 128$. It can be observed from the results in Fig. 3.2 that the proposed scheme provides significant gain over existing reconstruction schemes and attains BER very close to the oracle-LS. Further, it can be noticed from the subgraph that among the compared schemes, WPA-SABMP is the least complex clipping reconstruction scheme.

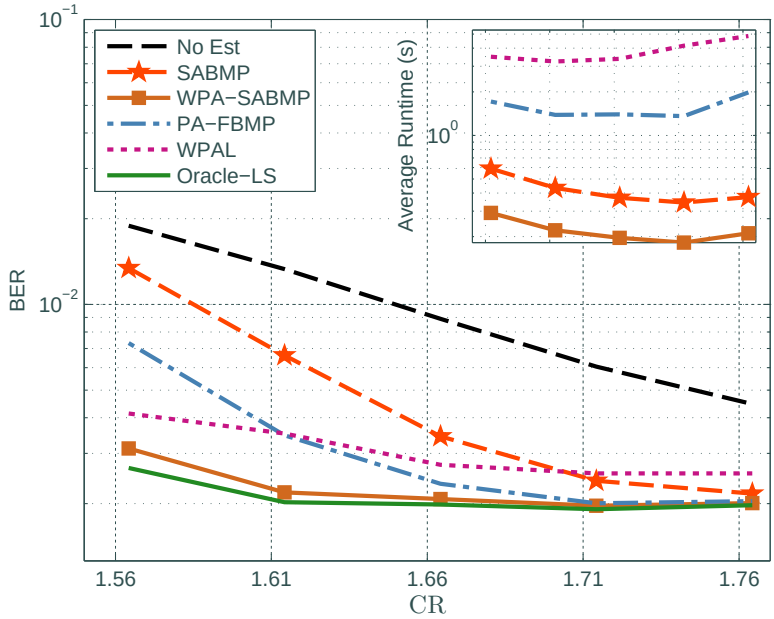

Figure 3.1: BER versus CR ($P = 128$,$E_b/N_0 = 27$dB).

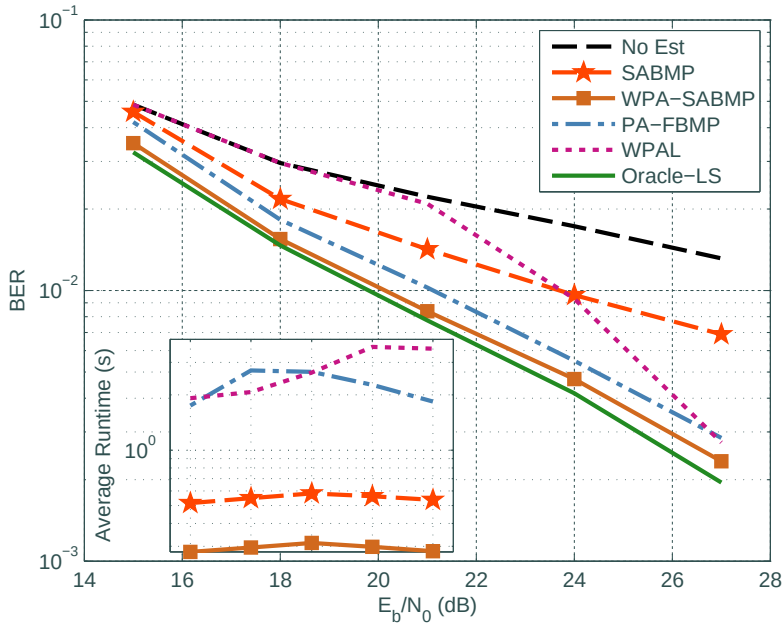

Figure 3.2: BER versus E_b/N_0 (CR $= 1.61$,$P = 128$).

Experiment 3

In this experiment, the E_b/N_0 is kept fixed at 27 dB and the number of RCs P used for reconstruction is varied from 75 to 175. Observe that if P is reduced,

the reconstruction accuracy of SABMP and PA-FBMP is reduced, however, WPA-SABMP and WPAL show robustness against reduced P. Though WPAL has good reconstruction accuracy through the range of interest, it is the most complex algorithm among the compared schemes. Further, this complexity is elevated with increasing P. The time graph also shows that the WPA-SABMP has least complexity that varies slightly with P.

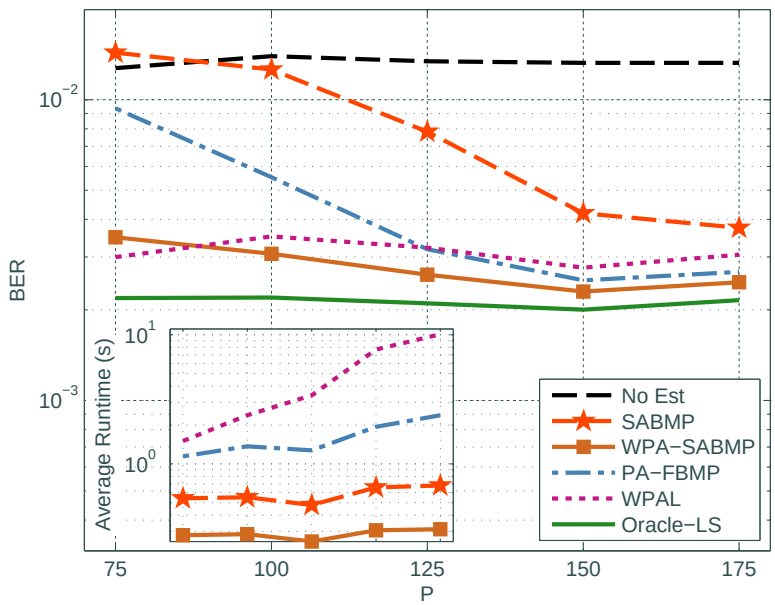

Figure 3.3: BER versus P (CR = 1.61,E_b/N_0 = 27dB).

Experiment 4

In this experiment, we compare the performance of the proposed scheme in absence of the accurate estimates of the signal statistics (i.e., the threshold γ, the noise variance σ_z^2 and the sparsity rate ρ are not known). The results of this experiments are depicted in Fig. 3.4. The WPA-SABMP (True) scheme in Fig. 3.4 represents the case when the actual estimates are available, WPA-SABMP (Est)

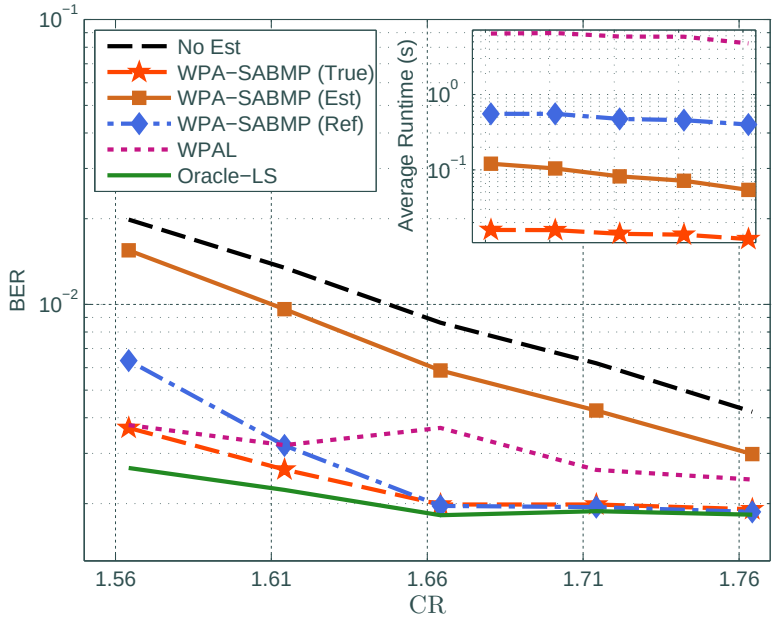

Figure 3.4: BER versus CR ($P = 128$, $E_b/N_0 = 27$dB, $\rho_{\text{init}} = 0.01\rho_{\text{true}}$ and $\sigma^2_{z_\text{init}} = 0.01\sigma^2_{z_\text{true}}$).

represents the case where the actual estimates are not available but no refinement is performed and WPA-SABMP (Ref) represents the case where the proposed scheme is run $E_{\max} = 5$ time for refinement of the initial estimates. The proposed refinement based scheme is compared with WPAL as it does not require any signal statistics. The initial estimates of the signal sparsity and noise variance are $\rho_{\text{init}} = 0.01\rho_{\text{true}}$ and $\sigma^2_{z_\text{init}} = 0.01\sigma^2_{z_\text{true}}$. It is observed that using the refinement procedure, even in the absence of accurate statistics, performance very close to the oracle-LS can be obtained. However, as the refinement procedure runs $E_{\max}$ times, it take more execution time than the non-refined counterpart.

3.4 Clipping Reconstruction for SIMO Systems

Let us consider an OFDM communication system equipped with L receiver antennas. At the receiver we have L independent copies of the transmitted signal. All diversity branches contain the same distortion signal $\mathbf{c}$, convoluted with the channel impulse response $\mathbf{h}_l$ of the lth branch. For acceptable performance of the communication system, the distortion needs to be eliminated from all diversity branches before signals are combined to obtain an estimate of the transmitted signal. The distortion free independent versions of the received signal can be combined using any of the well known diversity combining methods (e.g., equal gain combining (EGC), selection combining (SC) and maximal ratio combining (MRC) [39]) to obtain an estimate of the transmitted signal.

To pursue the reconstruction of $\mathbf{c}$ using the scheme proposed in Section 3.3, a system of equations of the form (3.10) is formulated for each diversity branch. In general, for the lth branch we have

$$\bar{\boldsymbol{\mathcal{Y}}}_l = \bar{\boldsymbol{\Phi}}_l \mathbf{c} + \bar{\boldsymbol{\mathcal{Z}}}_l, \tag{3.20}$$

where, $\bar{\boldsymbol{\mathcal{Y}}}_l$ is the measurement vector associated with the lth diversity branch of the system (similar definitions apply to $\bar{\Phi}_l$ and $\bar{\boldsymbol{\mathcal{Z}}}_l$). Note that $\mathbf{c}$ is free of subscript l, as it is same *for all diversity branches*.

One rather obvious approach towards estimation of $\mathbf{c}$ given L systems of the form (3.20) is *individual reconstruction* per diversity branch as shown in Fig. 3.5.

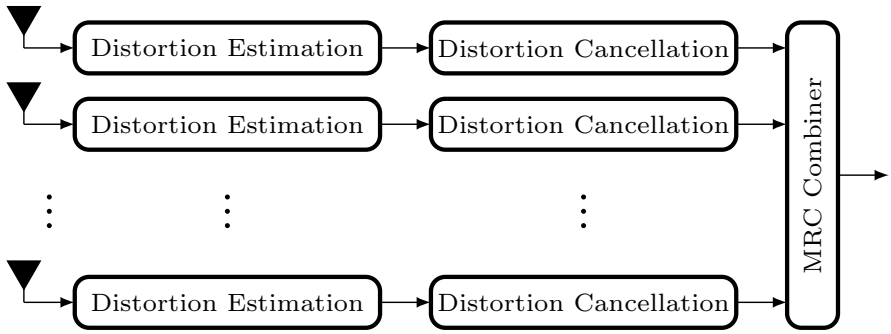

Figure 3.5: Individual reconstruction per diversity branch.

Once the estimates of the clipping distortion are available, these estimates are subtracted from the respective branches to obtain the distortion free versions $\check{\boldsymbol{\mathcal{Y}}}_l = \boldsymbol{\mathcal{Y}}_l - \hat{\mathbf{c}}$ of the transmitted signal corresponding to each branch. These signals are then combined by MRC to obtain $\widehat{\boldsymbol{\mathcal{X}}}$ using the following definition

$$\widehat{\boldsymbol{\mathcal{X}}} = \sum_{l=1}^{L} \mathbf{D}_l^{\mathsf{H}} \check{\boldsymbol{\mathcal{Y}}}_l, \tag{3.21}$$

where $\mathbf{D}_l$ is the diagonal frequency response matrix corresponding to the lth branch. An alternative and a more effective approach is to utilize the fact that the clipping signal is same over all diversity branches. As such, the L systems of linear equations (3.20) can be concatenated and setup in the following form:

$$\begin{bmatrix} \bar{\boldsymbol{\mathcal{Y}}}_1 \\ \bar{\boldsymbol{\mathcal{Y}}}_2 \\ \vdots \\ \bar{\boldsymbol{\mathcal{Y}}}_L \end{bmatrix} = \begin{bmatrix} \bar{\boldsymbol{\Phi}}_1 \\ \bar{\boldsymbol{\Phi}}_2 \\ \vdots \\ \bar{\boldsymbol{\Phi}}_L \end{bmatrix} \mathbf{c} + \begin{bmatrix} \bar{\boldsymbol{\mathcal{Z}}}_1 \\ \bar{\boldsymbol{\mathcal{Z}}}_2 \\ \vdots \\ \bar{\boldsymbol{\mathcal{Z}}}_L \end{bmatrix}, \tag{3.22}$$

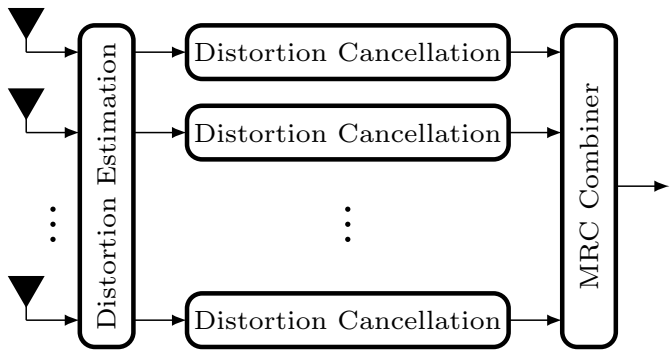

Figure 3.6: Joint reconstruction over all diversity branches.

which can be written more compactly as

$$\vec{\mathcal{Y}} = \vec{\mathbf{\Phi}}\mathbf{c} + \vec{\mathcal{Z}}. \tag{3.23}$$

It is evident that with $2P$ measurements per diversity branch, a total of $2LP$ measurements are now available to reconstruct the sparse unknown (see Fig. 3.6). Once $\hat{\mathbf{c}}$ is obtained as done in Section 3.3 for single antenna case, the subsequent distortion removal and MRC combining is identical to the case of individual reconstruction.

3.4.1 Simulation Results

In this experiment, the performance of the proposed joint reconstruction scheme is compared with individual reconstruction for two receiver antenna systems i.e., $L = 2$. The CR is varied while E_b/N_0 and P are kept fixed. The simulation is averaged over 500 bit errors. The results in Fig. 3.7 show that the joint reconstruction scheme achieves an error rate much lower than individual reconstruction. Further to compare the computational complexity, we note that individual reconstruction

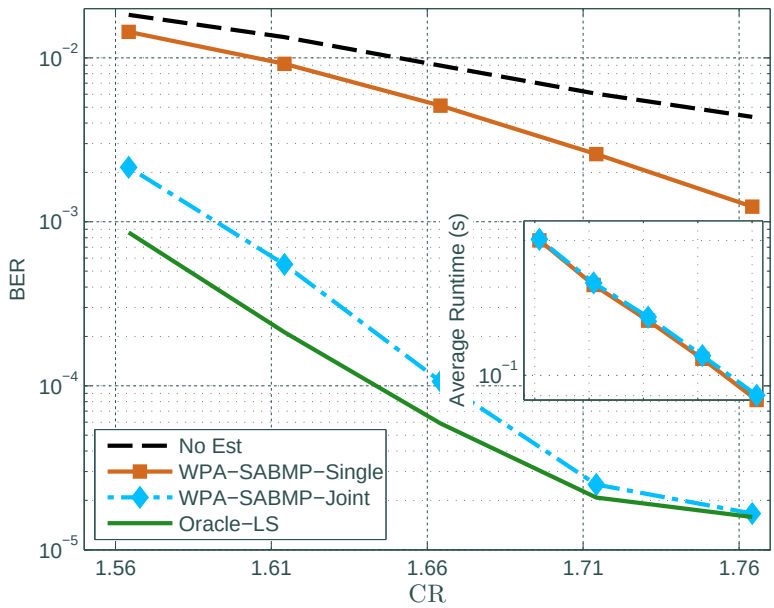

Figure 3.7: BER versus CR for SIMO-OFDM Communication Systems ($P = 77$,$E_b/N_0 = 27$dB).

can be performed in parallel, so we consider the time required for signal reconstruction in one branch only. It is observed from the subgraph that the average time taken by the joint and individual reconstruction is almost the same.

3.5 Multi-user Communication

In multi-user OFDM systems i.e., OFDMA, each user is assigned a subset of sub-carriers, and each carrier is assigned exclusively to one user [33]. The time domain signal resulting from IDFT on each user are clipped for PAPR reduction. Clipping multiple users simultaneously complicates the estimation process at the receiver. This is because the distortions from each user are spread over all sub-carriers and hence overlap. The frequency domain overlap of distortions render many of the

assumptions made in the single user scenario invalid. To be specific, weighting and phase augmentation cannot be applied in multi-user clipping estimation directly. Further, as the data on each sub-carrier is corrupted by clipping distortions from all users (and additive noise), the perturbations are generally strong enough to take the data out of the corresponding decision regions and hence the RCs method is inapplicable. Hence, in multi-user clipping estimation we resort to the data free pilot tones for measuring the clipping distortions.

Let us commence the formulation of a multi-user clipping estimation strategy by generalizing the data model presented in Section 3.2 for OFDMA systems. In this work, we consider the two user case for clarity of exposition, however, the proposed scheme is easily extendable to the general U user case. In the uplink of an OFDMA system, the total number of available sub-carriers N is divided between the two subscribers and each user will be allocated $K = N/2$ sub-carriers for data transmission. The sub-carriers can be allocated adjacently (sub-carriers $(u-1)N/K$ to $uN/K-1$ reserved for uth user) or in an interleaved manner (user u is allocated sub-carriers $u+dK-(K+1), \quad d \in \{1, 2, \cdots, N/K\}$). In this work, we focus solely on the interleaved carrier allocation. In the context of a complete OFDMA symbol, the frequency domain signal corresponding to the first user can be written as

$$\boldsymbol{\mathcal{X}}^1 = [\mathcal{X}^1(0), 0, \mathcal{X}^1(1), 0, \cdots, \mathcal{X}^1(N/2-1), 0]^{\mathsf{T}},$$

and signal corresponding to the second user is given by

$$\boldsymbol{\mathcal{X}}^2 = [0, \mathcal{X}^2(0), 0, \mathcal{X}^2(1), 0, \cdots, \mathcal{X}^2(N/2-1)]^{\mathsf{T}},$$

The time domain signal for uth user (i.e., $\mathbf{x}^u$) is obtained by taking the IDFT of $\boldsymbol{\mathcal{X}}^u$. To reduce the PAPR, the signals $\mathbf{x}^u$ are clipped as given by (3.1) and at the receiver we have $\mathbf{y} = \mathbf{H}^1(\mathbf{x}^1 + \mathbf{c}^1) + \mathbf{H}^2(\mathbf{x}^2 + \mathbf{c}^2) + \mathbf{z}$. The frequency domain received signal can be obtained by the DFT operation as

$$\boldsymbol{\mathcal{Y}} = \mathbf{D}^1\boldsymbol{\mathcal{X}}^1 + \mathbf{D}^1\boldsymbol{\mathcal{C}}^1 + \mathbf{D}^2\boldsymbol{\mathcal{X}}^2 + \mathbf{D}^2\boldsymbol{\mathcal{C}}^2 + \boldsymbol{\mathcal{Z}}. \tag{3.24}$$

Note that, although the channel frequency responses $\mathbf{D}^u$ are diagonal matrices of size $N \times N$ and hence are overlapping, the matrix $\mathbf{D}$ comprises of only the portions of $\mathbf{D}^u$, belonging to the uth user band, which is denoted by $\underline{\mathbf{D}}^u$. Hence we can write

$$\boldsymbol{\mathcal{Y}} = \mathbf{D}\boldsymbol{\mathcal{X}} + \mathbf{D}^1\boldsymbol{\mathcal{C}}^1 + \mathbf{D}^2\boldsymbol{\mathcal{C}}^2 + \boldsymbol{\mathcal{Z}}, \tag{3.25}$$

where $\boldsymbol{\mathcal{X}} = \boldsymbol{\mathcal{X}}^1 + \boldsymbol{\mathcal{X}}^2$. In the absence of distortion (i.e., when $\mathbf{D}^1\boldsymbol{\mathcal{C}}^1 = \mathbf{D}^2\boldsymbol{\mathcal{C}}^2 = \mathbf{0}$), the receiver could easily separate the users (as they occupy different carriers) and equalize the users' channels (as in (3.5)) to recover the transmitted data. Mathematically, we can write $\underline{\boldsymbol{\mathcal{Y}}}^u = \underline{\mathbf{D}}^u\underline{\boldsymbol{\mathcal{X}}}^u + \underline{\boldsymbol{\mathcal{Z}}}^u$, where $\underline{\boldsymbol{\mathcal{Y}}}^u$ is the portion of $\boldsymbol{\mathcal{Y}}$ confined to the carriers of the uth user (a similar definition applies to $\underline{\mathbf{D}}^u$,$\underline{\boldsymbol{\mathcal{X}}}^u$ and

$\underline{\mathcal{Z}}^u$). Upon equalizing, we obtain

$$\underline{\widehat{\mathcal{X}}}^u = (\underline{\mathbf{D}}^u)^{-1}\underline{\mathcal{Y}}^u = \underline{\mathcal{X}}^u + (\underline{\mathbf{D}}^u)^{-1}\underline{\mathcal{Z}}^u, \tag{3.26}$$

The noisy estimate $\underline{\widehat{\mathcal{X}}}^u$ is then rounded to the nearest constellation point ($\lfloor\underline{\widehat{\mathcal{X}}}^u\rfloor$). However, in presence of the distortions, clipping needs to be estimated and cancelled before the equalization step of (3.26).

Now to demonstrate how clipping distortions can be estimated, we re-write (3.25) as

$$\mathcal{Y}=\mathbf{D}\mathcal{X}+[\mathbf{D}^1\mathbf{D}^2]\begin{bmatrix}\mathcal{C}^1\\ \mathcal{C}^2\end{bmatrix}+\mathcal{Z}=\mathbf{D}\mathcal{X}+[\mathbf{D}^1\mathbf{D}^2]\mathbf{F}\begin{bmatrix}\mathbf{c}^1\\ \mathbf{c}^2\end{bmatrix}+\mathcal{Z}, \tag{3.27}$$

where we have made the substitution $\mathcal{C}^u = \mathbf{F}\mathbf{c}^u$. Using a selection matrix $\mathbf{S}_P$ we proceed by projecting $\mathcal{Y}$ onto the subspace spanned by the reserved carriers. This yields

$$\mathbf{S}_P\mathcal{Y}=\mathbf{S}_P(\mathbf{D}\mathcal{X}+[\mathbf{D}^1\mathbf{D}^2]\mathbf{F}\mathbf{c}+\mathcal{Z}) \text{ i.e., } \mathcal{Y}'=\mathbf{\Psi}\mathbf{c}+\mathcal{Z}'. \tag{3.28}$$

The clipping $\mathbf{c}$ can be recovered from the under-determined systems in (3.28) by sparse signal reconstruction. However, the assumptions used for weighting and phase augmentation in earlier parts of this chapter are no longer valid. Though the signal can be recovered using sparse signal recovery tools (e.g., FBMP, SABMP and ℓ_1-optimization), however, in multiuser scenario it is not really effective espe-

cially as the number of users gets larger. For example, in the two user scenario of (3.25), the sparse vector is twice as large and could have twice the number of active elements. As such to maintain the quality of the estimate in two-user scenario, we need to double the number of free carriers, which will reduce the throughput. Alternatively here, we get by with the estimate obtained from (3.28) and once these estimates are available we proceed in a decoupled manner to improve these estimates.

Once the clipping signals are initially reconstructed using (3.28) (i.e., the joint estimation), it is possible to setup two uncoupled systems of equations for user 1 and 2 respectively. After the isolated systems are formed, the sparse clipping reconstruction can be performed for each user for enhanced recovery. Therefore, the crux of the proposed reconstruction scheme can be summarized in the following two steps: 1) Estimate $\mathbf{c} = [\mathbf{c}^{1\mathsf{T}}\mathbf{c}^{2\mathsf{T}}]^{\mathsf{T}}$ via joint sparse reconstruction using (3.28) and 2) Decouple the two systems of linear equations corresponding to user 1 and user 2 and perform clipping reconstruction for each user.

To obtain the decoupled systems, we modify the approach initially proposed for channel estimation [52] (we term this approach the contaminated pilot approach). It was noted that as the clipped signal is transmitted (transmitted pilots are also clipped) hence it is not optimal to use ideal pilot sequence at the receiver as a reference for channel estimation. Instead, the clipped pilot sequence was first estimated at the receiver and then used for enhanced channel estimation. As the clipped pilots are used in [52] instead of clean pilot signals, we call this scheme

the contaminated pilot approach. In this work, we use the idea of reconstructing the clipped version of the transmitted signal at the receiver to form the decoupled systems. To do that, the initial estimate of $\mathbf{c}$ obtained using (3.28) is subtracted from (3.25) to get

$$\boldsymbol{\mathcal{Y}}_{\text{cs}} = \boldsymbol{\mathcal{Y}} - [\mathbf{D}^1\mathbf{D}^2]\mathbf{F}\hat{\mathbf{c}} = \mathbf{D}\boldsymbol{\mathcal{X}} + \boldsymbol{\mathcal{Z}}'. \tag{3.29}$$

We proceed by extracting the carriers allocated to user u and get $\underline{\boldsymbol{\mathcal{Y}}}^u_{\text{cs}}$, which is then equalized using (3.26) to obtain $\widehat{\underline{\boldsymbol{\mathcal{X}}}^u} = (\underline{\mathbf{D}}^u)^{-1}\underline{\boldsymbol{\mathcal{Y}}}^u_{\text{cs}}$. Now, we estimate the transmitted frequency domain signal by making the ML decisions $\lfloor\widehat{\underline{\boldsymbol{\mathcal{X}}}^u}\rfloor$. The time domain signal is obtained by IDFT as $\widehat{\mathbf{x}^u} = \mathbf{F}^{\mathsf{H}}\lfloor\widehat{\underline{\boldsymbol{\mathcal{X}}}^u}\rfloor$. This time domain signal is then clipped using (3.1) to get $\widehat{\mathbf{x}^u_p}$. Now the difference between the clipped and un-clipped versions of $\widehat{\mathbf{x}}^u$ i.e., $\widehat{\mathbf{c}}^u = (\widehat{\mathbf{x}}^u_p - \widehat{\mathbf{x}}^u)$ is entrusted as the improved estimate of the clipping distortion and is subtracted from (3.25) to form the decoupled systems. The stepwise procedure for formulation of the decoupled system is outlined below,

1. Do the joint sparse signal reconstruction based on (3.28).

2. Subtract the estimated distortion $\hat{\mathbf{c}}$ from (3.25) to obtain

   $\boldsymbol{\mathcal{Y}}_{\text{cs}} = \boldsymbol{\mathcal{Y}} - [\mathbf{D}^1\mathbf{D}^2]\mathbf{F}\hat{\mathbf{c}} = \mathbf{D}\boldsymbol{\mathcal{X}} + \boldsymbol{\mathcal{Z}}$

3. Get $\underline{\boldsymbol{\mathcal{Y}}}^u_{\text{cs}} = \underline{\mathbf{D}}^u\boldsymbol{\mathcal{X}}^u + \underline{\boldsymbol{\mathcal{Z}}}^u$ by extracting user u's carriers.

4. Equalize $\underline{\boldsymbol{\mathcal{Y}}}^u_{\text{cs}}$ using (3.26) and obtain $(\lfloor\widehat{\underline{\boldsymbol{\mathcal{X}}}^u}\rfloor)$.

5. Using pilots and $\lfloor\widehat{\underline{\boldsymbol{\mathcal{X}}}^u}\rfloor$, form a time domain signal $\widehat{\mathbf{x}^u}$.

6. Obtain $\widehat{\mathbf{x}_p^u}$ from $\widehat{\mathbf{x}^u}$ using (3.1) and obtain $\widehat{\boldsymbol{\mathcal{C}}^u} = \widehat{\boldsymbol{\mathcal{X}}}_p^u - \widehat{\boldsymbol{\mathcal{X}}^u}$.

7. Obtain $\boldsymbol{\mathcal{Y}}^{\bar{u}} = \boldsymbol{\mathcal{Y}} - \mathbf{D}^u\widehat{\boldsymbol{\mathcal{C}}^u} = \mathbf{D}\boldsymbol{\mathcal{X}} + \mathbf{D}^u\boldsymbol{\mathcal{C}}^u + \boldsymbol{\mathcal{Z}},\ \bar{u} \neq u$ based on (3.25).

Note that $\boldsymbol{\mathcal{Y}}^{\bar{u}}$ is decoupled from user u's clipping. Now with this decoupled system for user $\bar{u}$, we can extract sub-carriers allocated to user $\bar{u}$ to form $\underline{\boldsymbol{\mathcal{Y}}}^{\bar{u}} = \underline{\mathbf{D}}^{\bar{u}}\underline{\boldsymbol{\mathcal{X}}}^{\bar{u}} + \underline{\mathbf{D}}^{\bar{u}}\boldsymbol{\mathcal{C}}^{\bar{u}} + \underline{\boldsymbol{\mathcal{Z}}}^{\bar{u}}$ and reconstruct $\mathbf{c}^{\bar{u}}$ using sparse recovery.

3.5.1 Simulation Results

The OFDMA system with two users is simulated using 512 sub-carriers and 64-QAM modulation. Each user is assigned a total of 256 sub-carriers in an interleaved fashion. The number of reserved tones used for CS measurements is $P_u = 75$ for $u = 1, 2$. The threshold for both users is chosen such that CR = 1.61. For sparse signal reconstruction FBMP [26] is used and results are presented in Fig. 3.8. The results compare the proposed (two stage recovery) scheme with the joint estimation scheme. It can be seen that the joint reconstruction of the clipping distortions gives very little gain in BER. However, the proposed decoupling based two stage multi-user clipping reconstruction scheme significantly improves the BER and achieves the no clipping rate for high E_b/N_0.

3.6 Channel Estimation in Presence of Clipping

Clipping the transmission signal results in pilot contamination, hence the MMSE estimation based on these pilot signals is not optimum. In this section we discuss

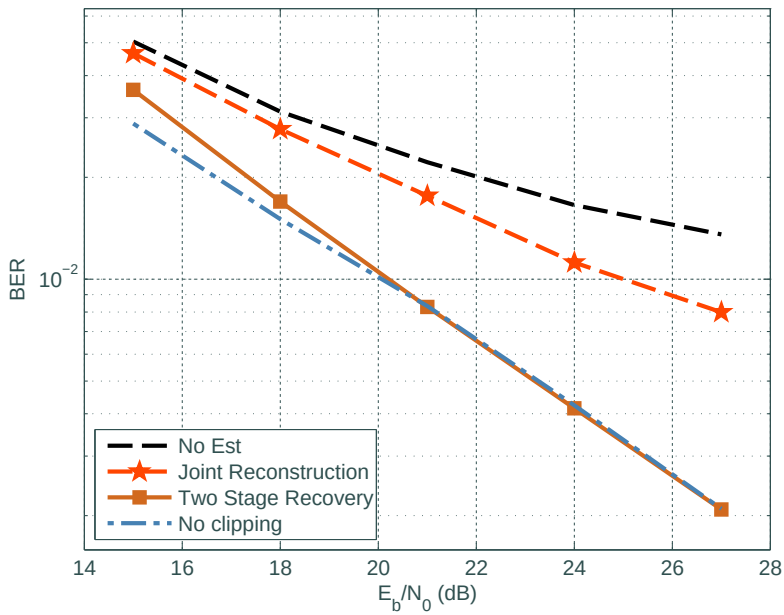

Figure 3.8: BER versus E_b/N_0 for Multi-user clipping recovery scheme (CR = 1.61,$P_u = 75$).

the channel estimation problem for clipped OFDM and present data aided CIR estimation strategies.

The received OFDM signal is given in (3.4) and can be written as

$$\boldsymbol{\mathcal{Y}} = \mathbf{D}\boldsymbol{\mathcal{X}} + \mathbf{D}\boldsymbol{\mathcal{C}} + \boldsymbol{\mathcal{Z}} = \mathbf{D}\boldsymbol{\mathcal{X}} + \boldsymbol{\mathcal{Z}}^{`}, \tag{3.30}$$

where $\boldsymbol{\mathcal{Z}}^{`} = \mathbf{D}\boldsymbol{\mathcal{C}} + \boldsymbol{\mathcal{Z}}$ is the combined AWGN noise and clipping distortion. Let us define $\boldsymbol{\mathcal{D}} \triangleq \text{diag}(\mathbf{D}) = \sqrt{N}\bar{\mathbf{F}}\mathbf{h}$ (where, $\bar{\mathbf{F}}$ represents the $N \times N_c$ partial DFT matrix obtained by pruning $\mathbf{F}$ of its last $N - N_c$ columns). Now note that, $\mathbf{D}\boldsymbol{\mathcal{X}}$ is a product of a diagonal matrix and a column vector, and hence we can exchange

the roles of $\mathbf{D}$ and $\boldsymbol{\mathcal{X}}$ by rewriting (3.30) as

$$\begin{aligned}\boldsymbol{\mathcal{Y}} &= \text{diag}(\boldsymbol{\mathcal{X}})\text{diag}(\mathbf{D}) + \boldsymbol{\mathcal{Z}}' = \text{diag}(\boldsymbol{\mathcal{X}})\boldsymbol{\mathcal{D}} + \boldsymbol{\mathcal{Z}}' \\ &= \sqrt{N}\text{diag}(\boldsymbol{\mathcal{X}})\bar{\mathbf{F}}\mathbf{h} + \boldsymbol{\mathcal{Z}}' = \mathbf{X}\mathbf{h} + \boldsymbol{\mathcal{Z}}', \end{aligned} \tag{3.31}$$

where $\mathbf{X} \triangleq \sqrt{N}\text{diag}(\boldsymbol{\mathcal{X}})\bar{\mathbf{F}}$. For channel estimation in OFDM, Q equally spaced pilot signals are inserted at the transmitter [9–11]. Based on this known pilot sequence, the receiver finds the MMSE estimate of the channel. Let $\mathcal{I}_q$ denote the index set of the pilot locations, then we can write $\boldsymbol{\mathcal{Y}}_{\mathcal{I}_q} = \mathbf{X}_{\mathcal{I}_q}\mathbf{h} + \boldsymbol{\mathcal{Z}}'_{\mathcal{I}_q}$, where $\boldsymbol{\mathcal{U}}_{\mathcal{I}_q}$ prunes $\boldsymbol{\mathcal{U}}$ of all rows except for the rows belonging to $\mathcal{I}_q$. Now the MMSE estimate of $\mathbf{h}$ can be obtained by solving the regularized LS problem $\hat{\mathbf{h}} = \arg\max_{\mathbf{h}}\{\|\boldsymbol{\mathcal{Y}}_{\mathcal{I}_q} - \mathbf{X}_{\mathcal{I}_q}\mathbf{h}\|^2_{\mathbf{R}^{-1}_{\mathcal{Z}'}} + \|\mathbf{h}\|^2_{\mathbf{R}^{-1}_h}\}$ where $\mathbf{R}_h = \mathbb{E}[\mathbf{h}\mathbf{h}^{\mathsf{H}}] = \sigma_h^2\mathbf{I}$. Further, ignoring the clipping noise component of $\boldsymbol{\mathcal{Z}}'$ we can write $\mathbf{R}_{\mathcal{Z}'} = \mathbb{E}[\boldsymbol{\mathcal{Z}}'\boldsymbol{\mathcal{Z}}'^{\mathsf{H}}] = \sigma_z^2\mathbf{I}$ (the subscript $\mathcal{I}_q$ of $\boldsymbol{\mathcal{Z}}'$ is dropped here for notational convenience). Solving this LS problem yields [53]

$$\hat{\mathbf{h}} = \mathbf{X}^{\mathsf{H}}_{\mathcal{I}_q}(\mathbf{X}_{\mathcal{I}_q}\mathbf{X}^{\mathsf{H}}_{\mathcal{I}_q} + (\sigma_z^2/\sigma_h^2)\mathbf{I})^{-1}\boldsymbol{\mathcal{Y}}_{\mathcal{I}_q}. \tag{3.32}$$

Increasing the number of pilot tones for CIR estimation results in improved estimation accuracy. However, generally it is not feasible to spare additional pilots as it reduces the data rate. In this work, we increase the number of measurements without increasing the number of reserved pilots by using RCs (for the procedure to find the RCs see the discussion following (3.5)). Let $\mathcal{I}_r$ denote the index set of the RCs and the pilot carriers. We can now retain these carriers in estimating $\mathbf{h}$

and prune all other sub-carriers from (3.31). This yields

$$\boldsymbol{\mathcal{Y}}_{\mathcal{I}_r} = \mathbf{X}_{\mathcal{I}_r}\mathbf{h} + \boldsymbol{\mathcal{Z}}'_{\mathcal{I}_r}, \tag{3.33}$$

Now we can obtain the refined estimate of $\mathbf{h}$ based on (3.32) by replacing the pilot index set $\mathcal{I}_q$ with enhanced set $\mathcal{I}_r$ consisting of the pilots and RCs. The enhanced MMSE estimation procedure based on RCs can be summarized in the following three steps: 1) Find the initial MMSE estimate of the CIR using (3.32), 2) Find reliability $\mathfrak{R}$ for all sub-carriers using (3.6) and select R sub-carriers with highest reliability index as RCs and 3) Use RCs as additional measurements (by using (3.33)) and find MMSE estimate using (3.32).

It is important to note that however many pilots and RCs we use to enhance the channel estimate, we are bottle-necked by the clipping distortions. Another way to look at this is to notice that what passes through the channel is not the pure signal or pilots but their clipped versions. As such, motivated by the work of [52], we first estimate the contaminated (pilots + RCs) and use them for enhanced MMSE estimation. The proposed data aided CIR estimation scheme can be summarized as:

1. Obtain the initial MMSE estimate by using (3.32).

2. Equalize the received data and make ML decisions on the equalized data i.e., $\lfloor \mathcal{Y}(i)/\hat{\mathcal{D}}(i) \rfloor = \lfloor \hat{\mathcal{X}}(i) \rfloor$.

3. Find reliability $\mathfrak{R}$ for all sub-carriers and select R sub-carriers with highest

reliability index as RCs.

4. Construct time domain signal $\hat{\mathbf{x}} = \mathbf{F}^{\mathsf{H}} \lfloor \hat{\mathcal{X}}(i) \rfloor$.

5. Find $\hat{\mathbf{x}}_p$ by clipping $\hat{\mathbf{x}}$ using (3.1) and obtain $\hat{\boldsymbol{\mathcal{X}}}_p = \mathbf{F}\hat{\mathbf{x}}_p$.

6. Obtain (clipped pilot sequence + RCs) $\boldsymbol{\mathcal{X}}_{p_{\mathcal{I}_r}}$ and $\mathbf{X}_{p_{\mathcal{I}_r}} = \text{diag}(\boldsymbol{\mathcal{X}}_{p_{\mathcal{I}_r}})$.

7. Use $\mathbf{X}_{p_{\mathcal{I}_r}}$ in (3.32) to obtain the improved CIR estimate.

3.6.1 Simulation Results

For channel estimation 256 sub-carrier OFDM and 64-QAM modulation is used. A total of 16 equispaced pilots are inserted for channel estimation and the number of RCs is chosen to be 16 (i.e., $Q = R = 16$). Fig. 3.9 shows the mean squared error (MSE) results of simple MMSE estimation (MMSE), the RCs approach (RC), the contaminated pilot approach (CPA) [52], the proposed scheme (RC+CPA) and the MMSE for unclipped OFDM (No clipping). The MSE as a function of E_b/N_0 results are generated by keeping CR = 1.73. The results show that for high E_b/N_0 the proposed scheme provides upto 7.2 dB advantage over simple MMSE estimation. Further, considering a 7.8dB difference between E_b/N_0 and SNR, the findings are consistent with the general observation that the MSE cannot go below the noise floor.

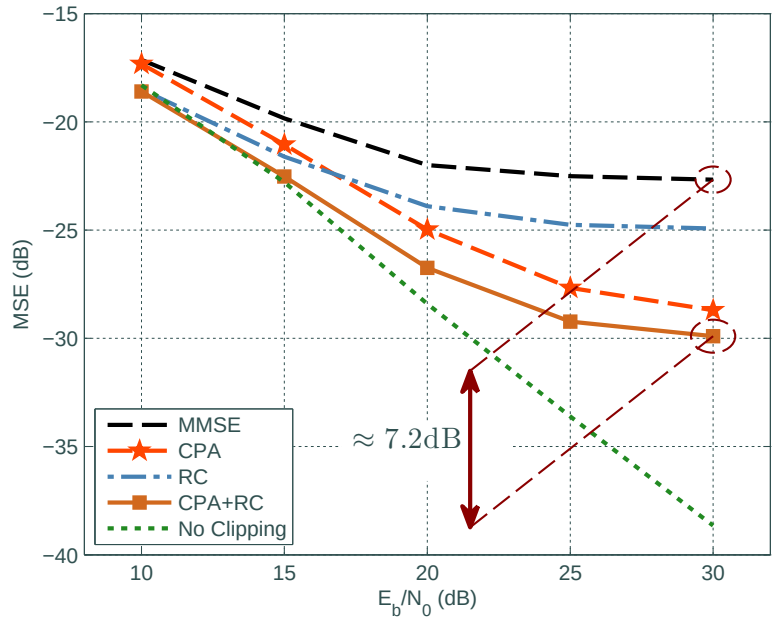

Figure 3.9: E_b/N_0 MSE (dB) for data aided CIR Estimation (CR $= 1.73, Q = R = 16$).

3.7 Chapter Conclusion

In this chapter, a low complexity Bayesian clipping recovery scheme was presented. The proposed WPA-SABMP scheme utilizes the undistorted phase property and weighting for enhanced clipping recovery. The proposed approach is agnostic to the non-Gaussian distribution of the clipping signal and so outperforms other traditional Bayesian approaches and ℓ_1 sparse recovery schemes. The WPA-SABMP scheme also utilizes the available statistics for enhanced recovery, however, when these statistics were unavailable the proposed scheme bootstrapped itself and successfully estimated the clipping distortions. Simulation results showed significant performance enhancement for WPA-SABMP scheme in both the error rate and complexity. The proposed scheme was then extended for the SIMO-OFDM sys-

tems and numerical findings were presented. In addition, a multi-user clipping recovery scheme was proposed and channel estimation strategies were presented for clipped OFDM signal. The simulation results for OFDMA clipping mitigation and data aided channel estimation also showed favourable results.

CHAPTER 4

NARROWBAND INTERFERENCE PROBLEM

4.1 Motivation

In this chapter, we tackle the problem of narrow band interference mitigation in a multi-carrier communication system. Orthogonal frequency division multiplexing (OFDM) has been the modulation of choice in modern wireless/wireline communication standards [1]. The popularity of OFDM based communication systems is due to their robustness against multipath fading, high data rates and single tap equalization. To benefit from these characteristics, a multi-user version of OFDM, i.e., orthogonal frequency division multiple access (OFDMA), has been extensively used for uplink communications. However, the transmission signal in OFDMA is the sum of orthogonal sinusoids (with random amplitudes and phases), causing high peak-to-average power ratio (PAPR). The conflicting inter-

est between linearity and power efficiency of the power amplifier renders the high PAPR an intolerable characteristic. The consequences of high PAPR are more pronounced in the uplink as inefficient operation of the power amplifier limits the battery life of the mobile terminal. Thus, peak reduction has received considerable research interest and multiple (transmitter/receiver based) schemes have been proposed [4,5,17,54]. The high PAPR problem has also motivated the development of a modified OFDMA system, namely Fourier pre-coded OFDMA. The Fourier pre-coded OFDMA (more commonly known as single carrier - frequency division multiple access (SC-FDMA)) retains the positives of the OFDMA, while eliminating the problem of high PAPR. Due to these characteristics, SC-FDMA has been adopted as the uplink multiple access scheme in 3GPP long term evolution (LTE) [55].

The wideband nature of SC-FDMA makes it highly susceptible to narrow band interference (NBI). The NBI sources include other devices operating in the same spectrum (e.g., cordless phones, garage openers etc.) and other communication systems operating in a cognitive manner. Here it is worth mentioning that though OFDMA is equally susceptible to these NBI sources, there is a fundamental difference in the way NBI affects the data in SC-FDMA and OFDMA. To this end, consider a single NBI source (aligned with the grid of the system under consideration) that affects only one sub-carrier in OFDMA, perturbs all data points in SC-FDMA system. This makes NBI mitigation in SC-FDMA vital for reliable performance of the communication system. At high signal-to-interference ratio

(SIR), coding can be relied on to mitigate the errors introduced by the NBI. However, at low SIR levels, the interference begins to overwhelm the code and necessitates a receiver that is able to intelligently deal with it.

Intensive studies have been carried to circumvent the impact of NBI in multi-carrier systems and numerous strategies are devised. The NBI mitigation schemes available in the literature commonly adopt one of the following three methodologies: *spreading* [12, 56], *avoidance* [57–59], and *subtraction* [60–63]. Avoidance relies on spectrum sculpting or shaping, through filtering or subcarrier nulling. Spreading offers inherent robustness against NBI and hence OFDM combined with Walsh sequence is termed interference suppressing OFDM (IS-OFDM) [56], and other spreading codes such as carrier interferometry spreading are also explored [12]. Subtraction either involves an iterative procedure for successive interference cancellation [60, 61] or NBI estimation followed by mitigation [62, 63]. Beyond this tertiary classification, more recently weighted-type fractional Fourier transform (WFRFT) pre-coding is studied in the context of NBI mitigation [64]. However, among the aforementioned NBI removal strategies only [62, 63] exploit the *a priori* information about the sparsity of the unknown signal. Gomma and Al-Dahir [62], opted for ℓ_1-optimization based recovery of the unknown signal, which is prohibitively complex for real time implementation. Though Sohail *et al.* [63], proposed a low complexity solution for NBI recovery, their methodology is tailer made for zero padded-OFDM (ZP-OFDM) and is unsuitable for cyclic prefix based multi-carrier communication systems.

In this work, we exploit the sparse nature of the NBI to recover it using a low complexity Bayesian sparse reconstruction procedure. Specifically, we utilize the support agnostic Bayesian matching pursuit (SABMP) algorithm for NBI recovery [51]. The SABMP is agnostic to the distribution of active elements, a characteristic that plays a vital role in NBI-impaired signal restoration. The practical scenario of grid mismatch is considered and the spreading effect is more realistically modelled by allowing all NBI sources to have independent grid offset. It is noted that the spectral spillover caused by the grid mismatch destroys the sparsity of the unknown signal. A well-accepted methodology to spectrally contain the spread NBI is windowing [65]. However, in this work, we adopt a rather unconventional sparsity restoration approach that utilizes *Haar wavelet* transformation. Further, to justify this choice, the Haar transform and windowing are numerically compared for their ability to sparsify the NBI. Due to the devastating effect of the NBI in low SIR regime, we presume (throughout this work) that sparing a small subset of data points for measurements is a reasonable choice. However, to minimize the number of reserved tones (and hence to maximize the spectral efficiency) a data-aided NBI mitigation technique is proposed. Using the proposed data-aided technique, the receiver probabilistically assigns a confidence level to each data point. A few data points (with highest confidence levels) are then selected and used in conjunction with reserved tones to enhance the NBI estimation accuracy. Finally, we extend the proposed reconstruction scheme for base-stations (BS) employing multiple-receiving antennas (i.e., single-input multi-

output (SIMO) systems). This extension is motivated by the observation that NBI on each antenna will have the same support (due to the spatial proximity of antenna elements) and possibly different magnitudes and phases (as the NBI signal may experience different fades). Therefore, a collaborative attempt is made towards finding the support of the NBI signal, resulting in a better estimate of the support and hence the NBI signal.

4.2 Chapter Contributions

The main contributions of this chapter can be summarized as follows:

- A low complexity, sparsity aware, Bayesian NBI reconstruction methodology is proposed.
- A realistic model for grid mismatch is used that allows all NBI sources to have independent grid offsets.
- Haar wavelet transformation is utilized to sparsify the unknown spread NBI signal.
- A data-aided approach for NBI recovery is presented to improve the spectral efficiency of the proposed scheme.
- The proposed scheme is extended for SIMO systems by exploiting the joint sparsity of NBI signals over all antenna elements.

4.3 SC-FDMA and NBI Model

Consider an N dimensional SC-FDMA system shared between U users. In such a system, the uth user converts the incoming high rate bit stream into $P = N/U$ parallel streams. These low rate bit streams are then modulated using a Q-ary QAM alphabet $\{\mathcal{A}_0, \mathcal{A}_1, \cdots, \mathcal{A}_{Q-1}\}$, resulting in a P dimensional data vector $\boldsymbol{\mathcal{X}}_u$. The data $\boldsymbol{\mathcal{X}}_u$ is Fourier pre-coded to lower the PAPR of the transmission signal. Owing to the linearity of discrete Fourier transform (DFT), the pre-coding can be achieved by a matrix vector product of $\mathbf{F}_P$ and $\boldsymbol{\mathcal{X}}_u$. Here $\mathbf{F}_P$ is the $P \times P$ DFT matrix whose (k, l)th element is given by

$$\mathbf{F}_{P,(k,l)} = P^{-1/2} \exp\left(-\jmath \frac{2\pi kl}{P}\right), \; k, l \in 0, 1, \cdots, P-1. \tag{4.1}$$

The pre-coded data $\mathbf{F}_P \boldsymbol{\mathcal{X}}_u$ is now mapped to the sub-carriers designated for the uth user. The sub-carrier/resource allocation can be done in a localized or distributed manner (see [55] for details). In this work, we only consider *interleaved* SC-FDMA, a special case of distributed SC-FDMA in which sub-carriers allocated to any user are spread over the entire signal band in equi-spaced fashion. The motivation behind the use of interleaved allocation is the robustness of this setting to frequency selective fading [55]. For interleaved assignment, the $N \times P$ resource

allocation matrix $\mathbf{R}_u$ is defined as

$$\mathbf{R}_{u,(k,l)} = \begin{cases} 1, & k = (u-1) + Ul, \quad 0 \leq l \leq P-1, \\ 0, & \text{otherwise.} \end{cases} \tag{4.2}$$

Further, for different users $\mathbf{R}_u$ are orthonormal, i.e.,

$$\mathbf{R}_i^{\mathsf{T}} \mathbf{R}_j = \begin{cases} \mathbf{I}_P, & i = j, \\ \mathbf{0}_P, & i \neq j. \end{cases} \tag{4.3}$$

The resource allocation is followed by the time domain conversion of the N dimensional signal $\mathbf{R}_u \mathbf{F}_P \boldsymbol{\mathcal{X}}_u$. This conversion is accomplished by pre-multiplying the signal of interest by the $N \times N$ inverse DFT (IDFT) matrix $\mathbf{F}_N^{\mathsf{H}}$. After adding the cyclic prefix, the time domain signal is fed to a finite impulse response channel of length N_c, $\mathbf{h}_u = [h_u(0), h_u(1), \cdots, h_u(N_c - 1)]^{\mathsf{T}}$. The channel tap coefficients form a zero mean, complex Gaussian, independent and identically distributed (i.i.d) collection. At the BS, after removing the cyclic prefixes, the received time domain signal (in absence of NBI) can be written as

$$\mathbf{y} = \sum_{u=0}^{U-1} \mathbf{H}_u \mathbf{F}_N^{\mathsf{H}} \mathbf{R}_u \mathbf{F}_P \boldsymbol{\mathcal{X}}_u + \mathbf{z}, \tag{4.4}$$

where $\mathbf{H}_u$ is the circulant channel matrix for the uth user and $\mathbf{z}$ is the additive white Gaussian noise (AWGN) with $\mathbf{z} \sim \mathcal{CN}(\mathbf{0}, \sigma_z^2 \mathbf{I})$. The circulant nature of $\mathbf{H}_u$ allows us to diagonalize it using the DFT matrix $\mathbf{F}_N$ and write $\mathbf{H}_u = \mathbf{F}_N^{\mathsf{H}} \boldsymbol{\Lambda}_u \mathbf{F}_N$,

where $\mathbf{\Lambda}_u$ is a diagonal matrix with channel frequency response on its diagonal. In this work, the channel impulse response (CIR) knowledge is assumed at the receiver and hence $\mathbf{H}_u$ and $\mathbf{\Lambda}_u$ are readily available. The frequency domain received data vector $\boldsymbol{\mathcal{Y}}$ is now given by

$$\boldsymbol{\mathcal{Y}} = \mathbf{F}_N \mathbf{y} = \sum_{u=0}^{U-1} \mathbf{\Lambda}_u \mathbf{R}_u \mathbf{F}_P \boldsymbol{\mathcal{X}}_u + \boldsymbol{\mathcal{Z}}, \tag{4.5}$$

where $\mathbf{\Lambda}_u = \mathbf{F}_N \mathbf{H}_u \mathbf{F}_N^{\mathsf{H}}$ and $\boldsymbol{\mathcal{Z}} = \mathbf{F}_N \mathbf{z}$. Utilizing (4.3) and the diagonal nature of $\mathbf{\Lambda}_u$, the data vector $\boldsymbol{\mathcal{X}}_u$ can be estimated by projecting $\boldsymbol{\mathcal{Y}}$ on $\mathbf{F}_P^{\mathsf{H}} \mathbf{R}_u^{\mathsf{T}} \mathbf{\Lambda}_u^{-1}$. This projection results in the following estimate

$$\widehat{\boldsymbol{\mathcal{X}}}_u = \boldsymbol{\mathcal{X}}_u + \mathbf{F}_P^{\mathsf{H}} \mathbf{R}_u^{\mathsf{T}} \mathbf{\Lambda}_u^{-1} \boldsymbol{\mathcal{Z}}. \tag{4.6}$$

Though (4.6) provides a good estimate of $\boldsymbol{\mathcal{X}}_u$ in NBI free regime, it is not suitable for systems experiencing NBI. To contemplate this idea, let us develop the model for an SC-FDMA system impaired by NBI.

4.3.1 The NBI impaired SC-FDMA

Let us consider the received signal impaired by the interference caused by a single or multiple time-varying NBI sources. In practice, these sources may have a grid offset with the SC-FDMA system, causing the energy of the NBI to spill over all tones. A spreading matrix $\mathbf{H}_{fo} = \mathbf{F}_N \mathbf{\Lambda}_{fo} \mathbf{F}_N^{\mathsf{H}}$ is commonly used to model the grid offset between the NBI signal and the system under consideration [62, 63]. The

diagonal matrix $\mathbf{\Lambda}_{fo}$ is defined as $\mathbf{\Lambda}_{fo} = \text{diag}(1, \exp(\jmath\frac{2\pi\alpha(1)}{N}, \cdots, \exp(\jmath\frac{2\pi\alpha(N-1)}{N}))$, where α is a random number uniformly distributed over the interval $[-\frac{1}{2}, \frac{1}{2}]$. A fundamental limitation of this model is its inability to assume independent grid offsets for multiple NBI sources. To overcome this limitation, we define the frequency domain NBI signal as

$$\boldsymbol{\mathcal{I}} = \mathbf{F}_N \mathbf{F}_{con}^{\mathsf{H}} \boldsymbol{\mathcal{I}}_L, \tag{4.7}$$

where $\boldsymbol{\mathcal{I}}_L$ is an L dimensional NBI vector (L is the number of active NBI sources). Further, $\mathbf{F}_{con}$ is the $L \times N$ continuous DFT matrix, with (f_l, k)th entry

$$\mathbf{F}_{con,(f_l,k)} = N^{-1/2} \exp\left(-\jmath\frac{2\pi f_l k}{N}\right), \quad \begin{array}{l} l \in 0, 1, \cdots, L-1, \\ k \in 0, 1, \cdots, N-1. \end{array} \tag{4.8}$$

As the normalized frequencies $f_l/N \in [0, 1)$ are drawn independently, they emulate independent grid offsets for different NBI sources. Recently, Tang *et al.* used a similar modelling approach in an attempt to estimate continuous frequencies and amplitudes of a mixture of complex sinusoids [66]. Here, it is important to understand that channels between NBI sources and the BS are concealed within $\boldsymbol{\mathcal{I}}_L$. In other words, we can say that $\boldsymbol{\mathcal{I}}_L = \mathbf{\Lambda}_{NBI}\bar{\boldsymbol{\mathcal{I}}}_L$, where $\mathbf{\Lambda}_{NBI}$ is a diagonal $L \times L$ matrix containing the frequency domain channel gains and $\bar{\boldsymbol{\mathcal{I}}}_L$ represents NBI sources. Hence, a simple addition of (4.7) in (4.5) will yield the NBI impaired

SC-FDMA received signal. This received signal is given as

$$\boldsymbol{\mathcal{Y}} = \sum_{u=0}^{U-1} \boldsymbol{\Lambda}_u \mathbf{R}_u \mathbf{F}_P \boldsymbol{\mathcal{X}}_u + \boldsymbol{\mathcal{I}} + \boldsymbol{\mathcal{Z}}. \tag{4.9}$$

Ignoring the presence of NBI and estimating $\boldsymbol{\mathcal{X}}_u$ along the lines of (4.6) will yield

$$\widehat{\boldsymbol{\mathcal{X}}}_u = \boldsymbol{\mathcal{X}}_u + \mathbf{F}_P^{\mathsf{H}} \mathbf{R}_u^{\mathsf{T}} \boldsymbol{\Lambda}_u^{-1} (\boldsymbol{\mathcal{I}} + \boldsymbol{\mathcal{Z}}), \tag{4.10}$$

which is not a reliable estimate of $\boldsymbol{\mathcal{X}}_u$ owing to $\boldsymbol{\mathcal{I}}$. Further, note that $\boldsymbol{\mathcal{I}}$ perturbs $\boldsymbol{\mathcal{X}}_u$ through an IDFT operation, hence, even in the more optimistic case (i.e., a single NBI source with no grid offset) all data points are corrupted. In low SIR scenarios, the interference might be strong enough to take a majority of data symbols out of their correct decision regions, resulting in an intolerably high BER. Thus, our task is the estimation/mitigation of $\boldsymbol{\mathcal{I}}$, which we pursue using a Bayesian sparse recovery procedure.

4.4 Bayesian Sparse Recovery of the NBI

To motivate the Bayesian sparse NBI recovery, we start with the case of no grid offset, i.e., when $f_l \in 0, 1, \cdots, N-1$, and later extend it to the general case of $f_l \in [0, N)$. In the simplistic case of no offset, the unknown N dimensional vector $\boldsymbol{\mathcal{I}}$ is L sparse, i.e., it has only L active elements. As time-frequency basis are maximally incoherent, the impact of the sparse NBI is felt on each data point. It is for this reason that only a small number of randomly observed measurements

(i.e., data points) will be enough to reconstruct $\boldsymbol{\mathcal{I}}$ using CS. With this in mind, we keep a randomly chosen subset of vector $\boldsymbol{\mathcal{X}}_u$ data free and index this subset using $\mathcal{T}$. Now a $|\mathcal{T}| \times P$ binary selection matrix $\mathbf{S}_{\mathcal{T}}$ can be used to obtain the projection of $\widehat{\boldsymbol{\mathcal{X}}}_u$ (in (4.10)) onto the subspace spanned by the reserved points, as given below

$$\underbrace{\mathbf{S}_{\mathcal{T}}\widehat{\boldsymbol{\mathcal{X}}}_u}_{\boldsymbol{\mathcal{X}}'_{u,\mathcal{T}}} = \mathbf{S}_{\mathcal{T}}\boldsymbol{\mathcal{X}}_u + \underbrace{\mathbf{S}_{\mathcal{T}}\mathbf{F}_P^{\mathsf{H}}\mathbf{R}_u^{\mathsf{T}}\boldsymbol{\Lambda}_u^{-1}}_{\boldsymbol{\Psi}_{u,\mathcal{T}}}\underbrace{(\boldsymbol{\mathcal{I}} + \boldsymbol{\mathcal{Z}})}_{\boldsymbol{\mathcal{I}}'},$$

$$\implies \boldsymbol{\mathcal{X}}'_{u,\mathcal{T}} = \boldsymbol{\Psi}_{u,\mathcal{T}}\boldsymbol{\mathcal{I}}', \tag{4.11}$$

where $\mathbf{S}_{\mathcal{T}}\boldsymbol{\mathcal{X}}_u = \mathbf{0}$. At this stage, we drop the subscript u for notational convenience and simply write $\boldsymbol{\mathcal{X}}'_{\mathcal{T}} = \boldsymbol{\Psi}_{\mathcal{T}}\boldsymbol{\mathcal{I}}'$ (the subscript u will reappear when required). To recover $\boldsymbol{\mathcal{I}}$, the aforementioned under-determined system of equations can be solved using any compressed sensing (CS) reconstruction algorithm (e.g., [24, 25, 28–30]). One such scheme is the SABMP algorithm by Masood and Al-Naffouri, which has been shown to outperform many existing algorithms, both for reconstruction accuracy and computational complexity (see [51] for details). However, the main motivation of employing SABMP in this work is its agnostic nature towards the distribution of active taps. This agnosticism is in sharp contrast with all contemporary Bayesian schemes that assume a known prior (see e.g., [26, 67]). Further, this characteristic is vital for NBI recovery as i) we may not know the distribution of $\boldsymbol{\mathcal{I}}$ and ii) even if we did know the distribution, it might be difficult to estimate its parameters (i.e., moments). Towards this end,

let us recall that $\boldsymbol{\mathcal{I}}_L$ represents the joint channel-NBI source i.e., $\boldsymbol{\mathcal{I}}_L = \boldsymbol{\Lambda}_{NBI}\bar{\boldsymbol{\mathcal{I}}}_L$. Here, an appropriate treatment would be to assume circularly symmetric complex Gaussian prior for both $\bar{\boldsymbol{\mathcal{I}}}_L$ and $\boldsymbol{\Lambda}_{NBI}$. This implies that the entries of $\boldsymbol{\mathcal{I}}_L$ are formed by the product of two independent complex normal random variables. O'Donoughue and Moura coined the term *complex Double Gaussian* for such a distribution [68]. Hence, in this case, though the distribution is known, its parameter estimation is relatively difficult. Further, if non-Gaussianity is assumed on the NBI-BS channel model, it may yield more complex statistical behaviour for $\boldsymbol{\mathcal{I}}_L$. As we are interested in recovering $\boldsymbol{\mathcal{I}}$, we note that for no grid offset, the active elements of $\boldsymbol{\mathcal{I}}$ will assume the distribution of $\boldsymbol{\mathcal{I}}_L$. However, grid offset will make the statistical characterization of $\boldsymbol{\mathcal{I}}$ even more challenging. For these reasons, a suitable reconstruction scheme would be able to work regardless of the distribution of unknown signal and whether this distribution is known or not. As the SABMP algorithm possesses these qualities and incurs low computational complexity, we employ SABMP as a sparse reconstruction scheme for NBI mitigation.

Another important observation is that (in (4.11)) $\boldsymbol{\mathcal{Z}}$ is considered to be a part of the unknown $\boldsymbol{\mathcal{I}}'$, and the NBI reconstruction problem is casted as a noiseless case. In other words, in recovering $\boldsymbol{\mathcal{I}}'$ we are actually estimating the NBI plus noise. This interpretation has important implications, as the sensing matrix $\boldsymbol{\Psi}_{\mathcal{T}}$ contains the inverse channel $\boldsymbol{\Lambda}_u^{-1}$ (or simply $\boldsymbol{\Lambda}^{-1}$). Before commenting further on the $\boldsymbol{\Lambda}^{-1}$ contained sensing matrix, let us highlight the impact of weak channels on the bit error rate (BER) of an SC-FDMA system. The noise corresponding to a

spectral null (i.e., a weak channel) is greatly enhanced upon zero-forcing equalization. As the enhanced noise impacts the data points through an IDFT operation, a single spectral null can considerably increase the BER. To address this issue, turbo equalizers and feedback decision equalizers are explored as replacements for the simple frequency domain linear equalization [69, 70]. Solving the system of equations in (4.11) (i.e., the joint NBI plus noise recovery) offers an alternative solution to the noise enhancement problem. To comprehend this assertion, note that due to the presence of $\boldsymbol{\mathcal{Z}}$, the unknown signal $\boldsymbol{\mathcal{I}}'$ is not truly sparse, but rather *compressible*. Hence, though none of the entries is exactly zero, only a few elements (corresponding to the active locations of $\boldsymbol{\mathcal{I}}$) constitute almost all of the signal energy. Further, the presence of $\boldsymbol{\Lambda}^{-1}$ enhances the $\boldsymbol{\Psi}_{\mathcal{T}}$ columns corresponding to the weak channels. As the measurement vector $\boldsymbol{\mathcal{X}}'_{\mathcal{T}}$ is a linear combination of the columns of $\boldsymbol{\Psi}_{\mathcal{T}}$, the stronger columns have a significant contribution in $\boldsymbol{\mathcal{X}}'_{\mathcal{T}}$. In other words, the entries of $\boldsymbol{\mathcal{I}}'$ corresponding to the weak channels are seen much more prominently in $\boldsymbol{\mathcal{X}}'_u$, and hence have a high probability of recovery. Due to the sparsity of $\boldsymbol{\mathcal{I}}$ and dense nature of $\boldsymbol{\mathcal{Z}}$, it is likely that some noise-only entries correspond to the weak channels and are recovered while solving (4.11). Recall that it is the noise at exactly these weak channels that inflates the BER. Now, that this noise is recovered and taken out (while compensating for $\boldsymbol{\mathcal{I}}'$), the noise enhancement problem is resolved to a great extent.

Having formulated the NBI recovery procedure for the optimistic case of perfect grid alignment, we now turn our attention to the case when there exists a

mismatch between the grids of NBI sources and the SC-FDMA system. A fundamental requirement of sub-Nyquist sampling based reconstruction (as pursued in this work) is the sparsity of the unknown signal. Though there are only a few active NBI sources, the non-orthogonality of these sources to the SC-FDMA grid destroys the frequency domain sparsity of the unknown signal (see Fig. 4.1). To overcome this practical hindrance towards sparse NBI reconstruction, the subsequent discussion focuses on sparsity restoration techniques.

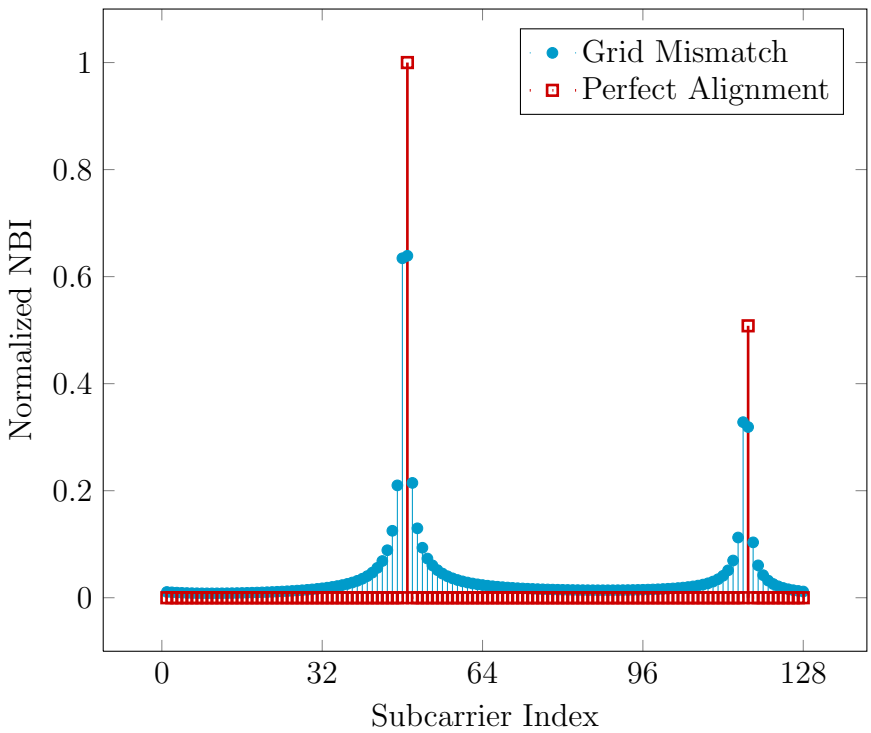

Figure 4.1: NBI spreading as a result of grid mismatch between NBI sources and the SC-FDMA system.

4.4.1 Sparsifying $\mathcal{I}'$

A well-known approach to spectrally contain an NBI signal experiencing energy spill-over (due to the grid mismatch) is *windowing* [62]. A windowing matrix

function $\mathbf{H}_{win} = \mathbf{F}_N \mathbf{\Lambda}_w \mathbf{F}_N^{\mathsf{H}}$ applied to the received signal sparsifies the unknown vector $\boldsymbol{\mathcal{I}}'$. Here $\mathbf{\Lambda}_w = \text{diag}(w(0), w(1), \cdots, w(N-1))$, and $w(n)$ is the nth sample of the window function. It is a common practice to window the received time domain signal before taking the DFT. However, as the sole purpose of introducing windowing is enhancing the sparsity of $\boldsymbol{\mathcal{I}}'$, we can postpone its inclusion till NBI reconstruction. To incorporate the windowing matrix function at NBI recovery stage we can re-write (4.11) as

$$\boldsymbol{\mathcal{X}}'_{\mathcal{T}} = \mathbf{\Psi}_{\mathcal{T}} \mathbf{H}_{win}^{-1} \mathbf{H}_{win} \boldsymbol{\mathcal{I}}', \tag{4.12}$$

where we assume the non-singularity of $\mathbf{H}_{win}$. Now, if we sense through $\mathbf{\Psi}_{\mathcal{T}} \mathbf{H}_{win}^{-1}$, we will be reconstructing $\mathbf{H}_{win} \boldsymbol{\mathcal{I}}'$, which is much more sparse compared to $\boldsymbol{\mathcal{I}}'$. As the formulation (4.12) requires only the non-singularity of $\mathbf{H}_{win}$, we are motivated to look for other possibilities towards sparsifying $\boldsymbol{\mathcal{I}}'$. Speaking in terms of time and frequency domain, as the signal $\boldsymbol{\mathcal{I}}'$ is no longer sparse in either, we seek another domain that has a sparse representation of $\boldsymbol{\mathcal{I}}'$. Any transformation possessing the three properties namely, i) linearity, ii) invertibility and iii) good sparsifying ability will serve the purpose. While choosing a sparsifying transform for NBI reconstruction, though property i) and ii) will be promptly evident, property iii) needs some consideration. To this end, note that though truly sparse signals are comparable by the number of active elements, compressible signals are not, as $\|\boldsymbol{\mathcal{I}}'\|_{\ell_0} = N$. As practical signals are seldom sparse, other sparsity measures e.g.,

Gini index (GI) [71] and *numerical sparsity* [72] have been put forth to compare compressible signals. In this work, we use GI (a normalized measure of sparsity) to compare sparsifying transforms. Given a vector $\underline{\boldsymbol{\mathcal{I}}}' = [\underline{\mathcal{I}}'(0), \underline{\mathcal{I}}'(1), \cdots, \underline{\mathcal{I}}'(N-1)]$, with its elements re-ordered, such that $|\underline{\mathcal{I}}'(0)| < |\underline{\mathcal{I}}'(1)| <, \cdots, < |\underline{\mathcal{I}}'(N-1)|$, then

$$\mathrm{GI}(\underline{\boldsymbol{\mathcal{I}}}') = 1 - 2\sum_{k=0}^{N-1} \frac{|\underline{\mathcal{I}}'(k)|}{\|\underline{\boldsymbol{\mathcal{I}}}'\|_{\ell_1}} \left(\frac{N-k-\frac{1}{2}}{N} \right), \tag{4.13}$$

where $\|\cdot\|_{\ell_1}$ represents the 1 norm. An important advantage of GI over the conventional norm measures is that it is normalized, and assumes values between 0 and 1 for any vector. Further, it is 0 for the least sparse signal with all the coefficients having an equal amount of energy and 1 for the most sparse signal which has all the energy concentrated in just one coefficient (for details see [71]). Numerical findings based on GI suggest that *Haar wavelet* transform [73] possesses the three desired characteristics. As the discussion of all the tested transforms will take us too far afield, we will confine our attention to the sparsifying ability of the Haar transform in comparison with windowing. The unitary Haar transform $\mathbf{H}_{haar}$ can be applied to $\boldsymbol{\mathcal{I}}'$ in a manner identical to (4.12), i.e.,

$$\boldsymbol{\mathcal{X}}'_{\mathcal{T}} = \boldsymbol{\Psi}_{\mathcal{T}} \mathbf{H}_{haar}^{\mathsf{H}} \mathbf{H}_{haar} \boldsymbol{\mathcal{I}}', \tag{4.14}$$

where $\mathbf{H}_{haar}^{\mathsf{H}} = \mathbf{H}_{haar}^{-1}$.

4.4.2 Simulation Results

A 512 sub-carrier SC-FDMA system is simulated, with 2 active users accessing the frequency resources in interleaved manner. The channel delay spread is quarter the symbol duration i.e., $N_c = N/4$ and 16-QAM modulation is utilized with SIR being -10dB. As the robustness of the SABMP reconstruction in the absence of statistical information has already been demonstrated in [51], we obtain $\boldsymbol{\mathcal{I}}_L$ from complex normal distribution without loss of generality. Two experiments are conducted in order to demonstrate the ability of the proposed reconstruction scheme to successfully recover the NBI. In first experiment no grid offset is assumed, whereas, the second experiment assumes the realistic grid mismatch case.

Experiment 1: Reconstruction with no Grid Offset

In this experiment, the number of active NBI sources vary from symbol to symbol with a maximum of 4 active NBI sources per symbol. The locations of the active NBI sources also vary, however, all NBI sources are restricted to fall on grid. Fig. 4.2 presents the BER results as a function of energy per bit (E_b/N_0) with 64 reserved tones per user (this makes the subsampling rate $\frac{|\mathcal{T}|}{N} = \frac{64}{256} = \frac{1}{4}$). The results depict the ability of the proposed scheme to recover not only the NBI but also the noise on weak channels, resulting in a BER that is much lower than the no NBI case. Fig. 4.3 depicts the BER performance as a function of reserved tones with E_b/N_0 fixed at 20dB. These results show the sensitivity of the proposed reconstruction scheme towards the number of reserved carriers and depict that

acceptable BER performance cannot be achieved by choosing an arbitrarily small number of reserved tones.

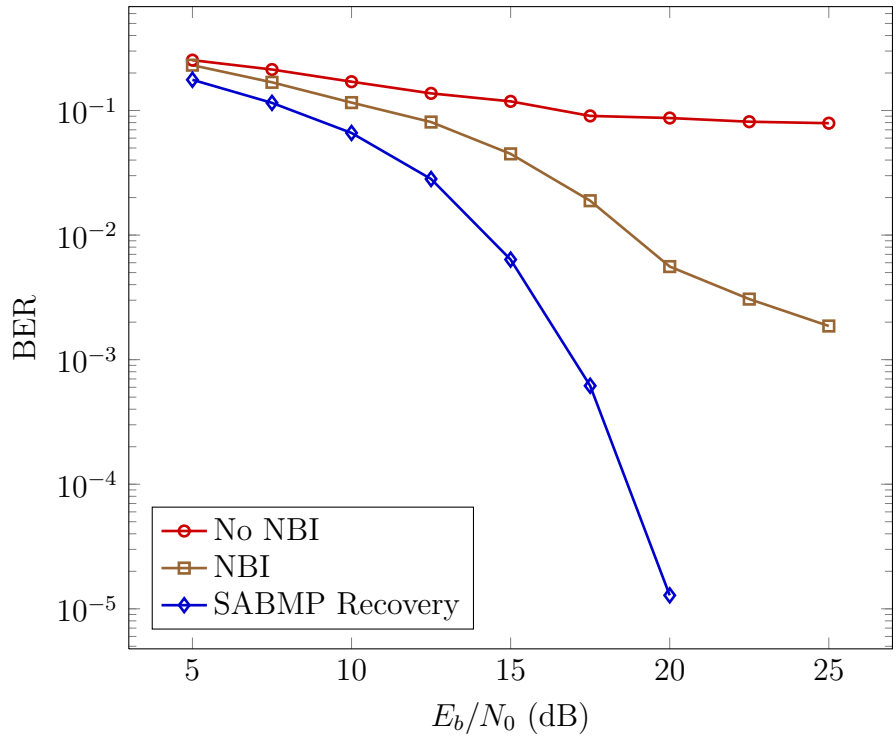

Figure 4.2: BER performance as a function of E_b/N_0 ($|\mathcal{T}| = 64$).

4.4.3 Experiment 2: Sparsifying usnig haar transform and reconstruction accuracy

In this experiement, first we compare the Haar transform and windowing (Hamming [62]) for their sparsifying ability. The average GI (as a function of active NBI sources) of $\boldsymbol{\mathcal{I}}'$, $\mathbf{H}_{win}\boldsymbol{\mathcal{I}}'$ and $\mathbf{H}_{haar}\boldsymbol{\mathcal{I}}'$ over 1000 runs is shown in Fig. 4.4. From the results it is clear that for small number of active sources (i.e., ≤ 4) the Haar transform has better sparsifying ability than windowing. As we expect the number of active NBI sources to be small, we conclude that Haar transform

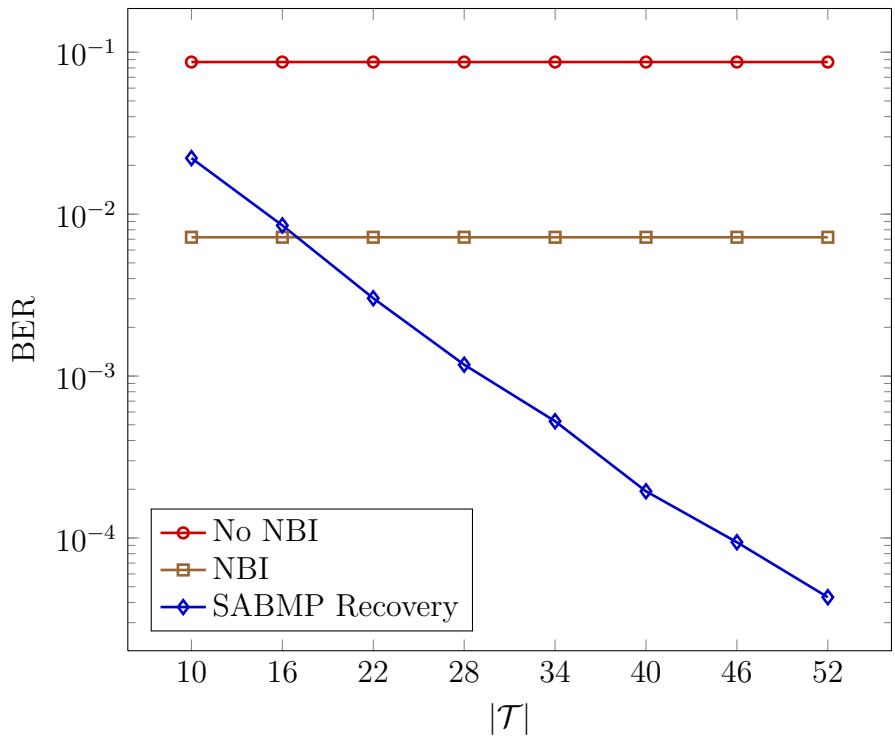

Figure 4.3: SABMP reconstruction results with no grid offset ($E_b/N_0 = 20$dB).

is a better choice towards sparsity restoration in the context of NBI recovery. Further, the BER performance of proposed reconstruction scheme for the cases of no sparsity restoration, windowing and Haar transform is shown in Fig. 4.5. These results also support the conclusion that Haar transform possesses better sparsifying characteristics. Fig. 4.6 shows the BER performance as a function of reserved tones. It is evident from the results that the advantage of using the Haar transform becomes significant as the number of measurements is increased.

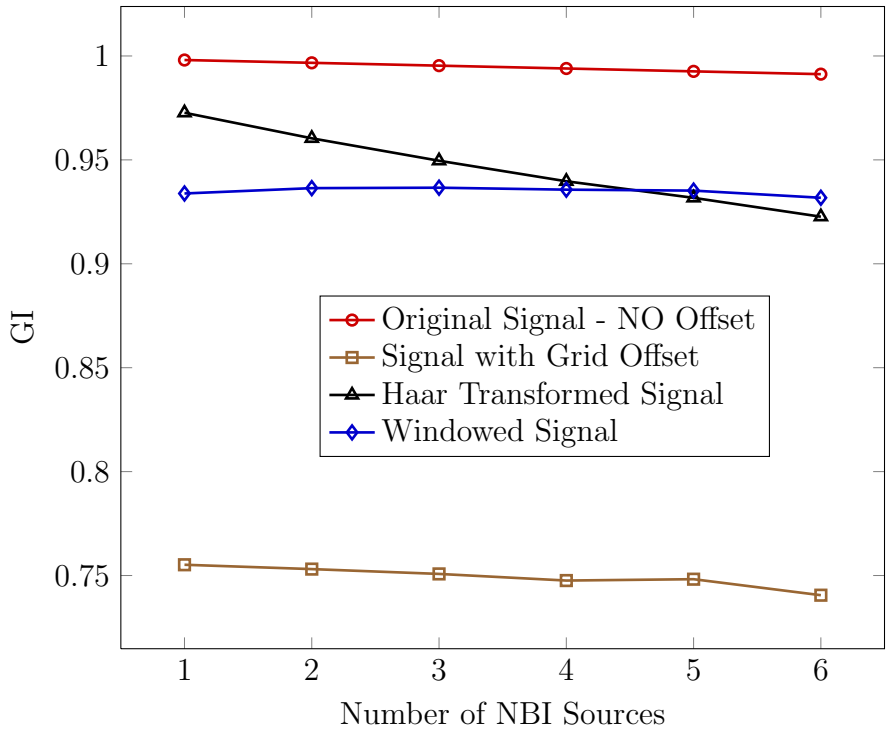

Figure 4.4: GI comparison of Haar transform and windowing method.

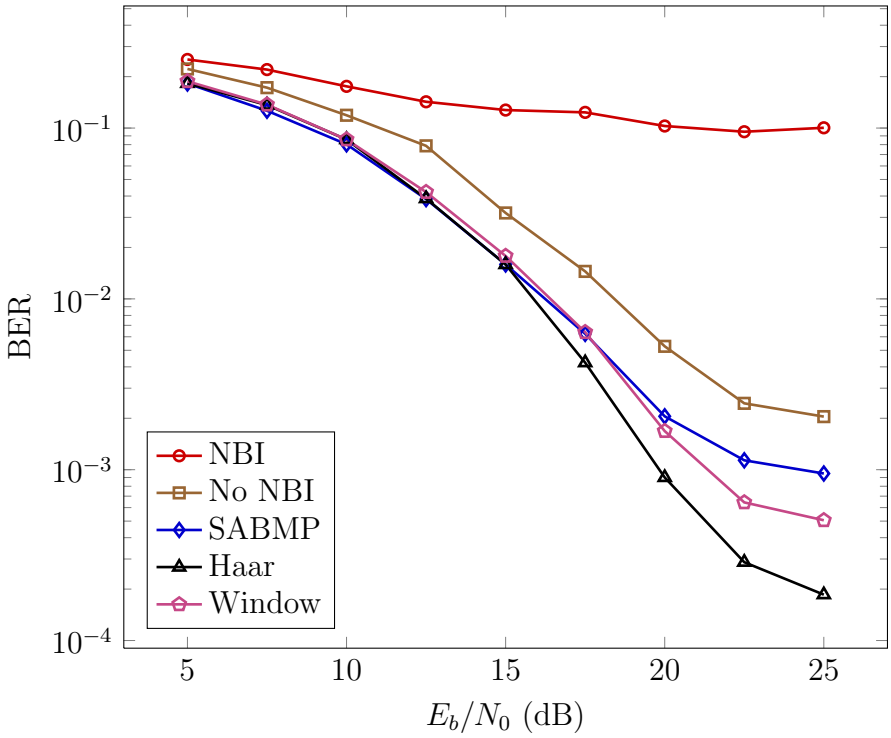

Figure 4.5: BER performance comparison of Haar transform and windowing ($|\mathcal{T}| = 64$).

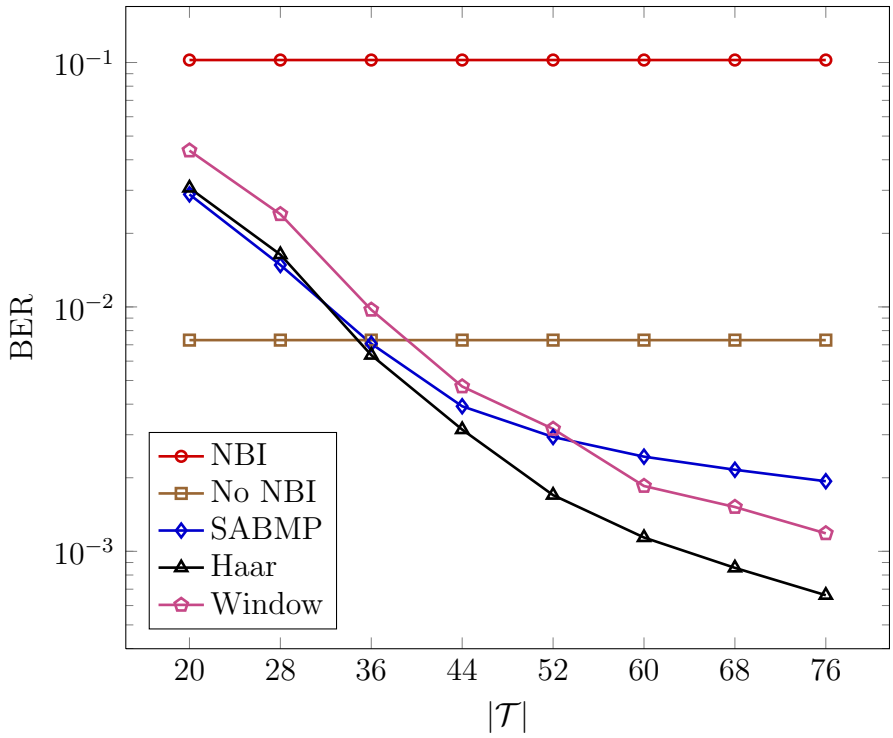

Figure 4.6: BER performance comparison of Haar transform and windowing ($E_b/N_0 = 20$dB).

4.5 Augmented NBI Recovery and the concept of Reliability

Reserved tones reduce the number of available data-carriers, hence, we attempt to improve the system spectral efficiency by minimizing the number of data free tones. First, we note that due to low SIR, a majority of data points in received NBI impaired signal are out of their correct decision regions (as demonstrated by the high BER of the NBI curves in Fig. 4.2,4.3,4.5,4.6). However, after subtracting

the NBI estimate from (4.10), we have

$$\widehat{\boldsymbol{\mathcal{X}}}_u = \boldsymbol{\mathcal{X}}_u + \mathbf{F}_P^{\mathsf{H}} \mathbf{R}_u^{\mathsf{T}} \boldsymbol{\Lambda}_u^{-1} \underbrace{(\boldsymbol{\mathcal{I}}' - \widehat{\boldsymbol{\mathcal{I}}}')}_{\widetilde{\boldsymbol{\mathcal{I}}}} = \boldsymbol{\mathcal{X}}_u + \boldsymbol{\mathcal{D}}_u, \tag{4.15}$$

where $\boldsymbol{\mathcal{D}}_u = \mathbf{F}_P^{\mathsf{H}} \mathbf{R}_u^{\mathsf{T}} \boldsymbol{\Lambda}_u^{-1} \widetilde{\boldsymbol{\mathcal{I}}}'$, and is henceforth called the *residual perturbation*. At this stage, it is reasonable to assume that the residual perturbation is not strong and a majority of data points are in their correct decision regions. Now we look for a subset of the data points that have not crossed their corresponding decision regions (with a high probability) and call them *reliable carriers*. Note that, the severe impact of the NBI disallows the use of data-aided NBI recovery from the outset (to completely eliminate the requirement of reserved tones). Nonetheless, reliable carriers can still be used in conjunction with reserved tones to significantly improve the system spectral efficiency and minimize the hit taken on the data rate. Further, we must highlight that the concept of using reliable data carriers is not new, (see e.g., [74, 75]). However, the *Euclidean distance* reliability criteria employed in [74, 75] is simplistic and relies solely on the relative distance of the received constellation point from its neighbours to determine the confidence level. In comparison, the reliability metric used in this work utilizes additional information about perturbations and is rigorous towards analyzing the reliability of the data points.

There are two fundamental questions associated with the use of data-aided approach: i) How to find a subset of data carriers that is reliable and ii) How to use this data set in conjunction with the reserved tones to improve the recon-

struction accuracy. We start by addressing the second question and later present a systematic procedure to select a subset of data points that is reliable.

Let us assume that a set of $|\mathcal{R}|$ reliable carriers indexed by $\mathcal{R}$ is available, where $\mathcal{R} \cup \mathcal{T} = \emptyset$. Now proceed by projecting (4.10) onto a binary selection matrix $\mathbf{S}_{\mathcal{R}}$ and obtain

$$\begin{aligned} \mathbf{S}_{\mathcal{R}}\widehat{\boldsymbol{\mathcal{X}}}_u &= \mathbf{S}_{\mathcal{R}}\boldsymbol{\mathcal{X}}_u + \mathbf{S}_{\mathcal{R}}\mathbf{F}_P^{\mathsf{H}}\mathbf{R}_u^{\mathsf{T}}\boldsymbol{\Lambda}_u^{-1}(\boldsymbol{\mathcal{I}} + \boldsymbol{\mathcal{Z}}), \\ \Longrightarrow \underbrace{\mathbf{S}_{\mathcal{R}}\widehat{\boldsymbol{\mathcal{X}}}_u - \mathbf{S}_{\mathcal{R}}\boldsymbol{\mathcal{X}}_u}_{\boldsymbol{\mathcal{X}}'_{\mathcal{R}}} &= \underbrace{\mathbf{S}_{\mathcal{R}}\mathbf{F}_P^{\mathsf{H}}\mathbf{R}_u^{\mathsf{T}}\boldsymbol{\Lambda}_u^{-1}}_{\boldsymbol{\Psi}_{\mathcal{R}}}\underbrace{(\boldsymbol{\mathcal{I}} + \boldsymbol{\mathcal{Z}})}_{\boldsymbol{\mathcal{I}}'}. \end{aligned} \tag{4.16}$$

The aforementioned equation has the same form as (4.11), where the unknown $\boldsymbol{\mathcal{I}}'$ is identical to (4.11) and the sensing matrix $\boldsymbol{\Psi}_{\mathcal{R}}$ is similar to the sensing matrix $\boldsymbol{\Psi}_{\mathcal{T}}$. Hence given the measurements $\boldsymbol{\mathcal{X}}'_{\mathcal{R}}$ are available, we can use the set of equation (4.16) in conjunction with (4.11) to find a better estimate of $\boldsymbol{\mathcal{I}}'$. A simple concatination of the the systems (4.11) and (4.16) yields

$$\underbrace{\begin{bmatrix} \boldsymbol{\mathcal{X}}'_{\mathcal{T}} \\ \boldsymbol{\mathcal{X}}'_{\mathcal{R}} \end{bmatrix}}_{\boldsymbol{\mathcal{X}}'} = \underbrace{\begin{bmatrix} \boldsymbol{\Psi}_{\mathcal{T}} \\ \boldsymbol{\Psi}_{\mathcal{R}} \end{bmatrix}}_{\boldsymbol{\Psi}} \boldsymbol{\mathcal{I}}', \Longrightarrow \boldsymbol{\mathcal{X}}' = \boldsymbol{\Psi}\boldsymbol{\mathcal{I}}'. \tag{4.17}$$

In comparison with (4.11) (which had $|\mathcal{T}|$ equations), the aforementioned system has $|\mathcal{T}| + |\mathcal{R}|$ equations, and hence the solution of (4.17) is expected to provide better NBI estimate. However, to solve (4.17), we require the set of measurements $\boldsymbol{\mathcal{X}}'_{\mathcal{R}} = \mathbf{S}_{\mathcal{R}}\widehat{\boldsymbol{\mathcal{X}}}_u - \mathbf{S}_{\mathcal{R}}\boldsymbol{\mathcal{X}}_u$. The term $\mathbf{S}_{\mathcal{R}}\widehat{\boldsymbol{\mathcal{X}}}_u$ is available, and to obtain $\mathbf{S}_{\mathcal{R}}\boldsymbol{\mathcal{X}}_u$, we

proceed by projecting (4.15) on $\mathbf{S}_{\mathcal{R}}$ and get

$$\mathbf{S}_{\mathcal{R}}\widehat{\boldsymbol{\mathcal{X}}}_u = \mathbf{S}_{\mathcal{R}}\boldsymbol{\mathcal{X}}_u + \mathbf{S}_{\mathcal{R}}\boldsymbol{\mathcal{D}}_u. \tag{4.18}$$

As the set $\mathcal{R}$ indexes the reliable carriers, the equality $\lfloor \mathbf{S}_{\mathcal{R}}\widehat{\boldsymbol{\mathcal{X}}}_u \rfloor = \mathbf{S}_{\mathcal{R}}\boldsymbol{\mathcal{X}}_u$ holds in (4.18), where $\lfloor \cdot \rfloor$ represents a maximum likelihood (ML) decision. Hence, now we have both components required for the evaluation of $\boldsymbol{\mathcal{X}}'_{\mathcal{R}}$ and hence (4.17) can be solved for $\boldsymbol{\mathcal{I}}'$.

The formulation (4.17) assumes that the index set $\mathcal{R}$ is available. To obtain this index set note that, in (4.15), we expect the following: for some sub-carriers, the perturbation $\mathcal{D}(i)$ is strong enough to take $\mathcal{X}(i)$ out of its correct decision region i.e., $\lfloor \widehat{\mathcal{X}(i)} \rfloor \neq \mathcal{X}(i)$, while for others with a milder perturbation, we expect to have $\lfloor \widehat{\mathcal{X}(i)} \rfloor = \mathcal{X}(i)$ (the subscript u is dropped for notational convenience). The subset of data carries which satisfy $\lfloor \widehat{\mathcal{X}(i)} \rfloor = \mathcal{X}(i)$ are the reliable carriers and fortunately constitute a major part of all data sub-carriers (after initial NBI compensation). To select this subset, we note that the major source of perturbation is the residual NBI distortion, especially for high signal-to-noise ratio (SNR). Hence, we can write the reliability function of the ith sub-carrier in terms of $\mathcal{D}(i)$ as

$$\mathfrak{R}(\mathrm{i}) = \frac{\mathrm{p}(\mathcal{D}(i) = \widehat{\mathcal{X}}(i) - \lfloor \widehat{\mathcal{X}}(i) \rfloor)}{\sum_{k=0,\mathcal{A}(k)\neq \lfloor \widehat{\mathcal{X}}(i) \rfloor}^{M-1} \mathrm{p}(\mathcal{D}(i) = \widehat{\mathcal{X}}(i) - \mathcal{A}(k))}, \tag{4.19}$$

where $\mathrm{p}(\cdot)$ represents the pdf of $\mathcal{D}$, which is assumed to be zero mean Gaussian with variance σ_D^2 (see [50] for details)[1]. In (4.19), the numerator is the proba-

bility that $\mathcal{D}(i)$ does not take $\mathcal{X}(i)$ beyond its correct decision region and the denominator sums the probabilities of all possible incorrect decisions that $\mathcal{D}(i)$ can cause. After obtaining the reliability $\mathfrak{R}(i)$ for each carrier i, we pick the $|\mathcal{R}|$ sub-carriers with highest reliability values and index them using $\mathcal{R}$. This index set is used in the previously discussed manner to reconstruct the unknown clipping vector. Further, it is observed that the set $\mathcal{R}$ constructed using the reliability metric (4.19) indexes non-uniformly placed tones and hence is fitting for CS based sparse recovery. In addition, it must be highlighted that the advantage of spectral efficiency expected by the use of data-aided approach comes at the expense of increased computational complexity. As the data-aided reconstruction is a two stage process, its complexity is roughly twice the computational complexity of the one stage (reserved tones only) reconstruction.

The selection of $|\mathcal{T}|$ and $|\mathcal{R}|$ is also critical for NBI mitigation and needs some consideration. From sparse signal reconstruction point of view, it is desirable to increase the measurements, however, other limitations render it infeasible to choose an arbitrarily large $|\mathcal{T}|$ and $|\mathcal{R}|$. The choice of $|\mathcal{T}|$ is mainly dictated by the desired data rate and the number of NBI sources that the system may experience. The selection of $|\mathcal{R}|$ is dependent on the conflicting interests associated with increasing or decreasing the number of utilized reliable tones. Note that, though a larger $|\mathcal{R}|$ promises improved estimation accuracy but at the same time the risk of feeding erroneous information to the reconstruction algorithm is also increased. In this regard, the study in [50] bounds the number of maximum reliable

carriers that can be used without risking incorrect measurements. Further, in the current framework, a sensible criteria towards selecting the cardinality of $\mathcal{R}$ is to choose $|\mathcal{R}| \propto |\mathcal{T}|$. This heuristic is based on the observation that an increased number of reserved tones will reduce the residual NBI and hence the proportion of reliable carriers also increases.

4.5.1 Simulation Results

Experiments are conducted to check the effectiveness of the proposed data-aided reconstruction scheme. The general simulation setup (i.e., sub-carriers, users, channel length, SIR, QAM order etc) is kept consistent with the previously explained setting (changes whenever made are highlighted in the description of experiments).

Experiment 1: data-aided CS for Spectral Efficiency

We start by choosing $|\mathcal{T}| = 32$ and use $|\mathcal{R}| = |\mathcal{T}| = 32$ for data-aided NBI reconstruction. This way, though the subsampling rate is still ($\frac{|\mathcal{T}|+|\mathcal{R}|}{N} = \frac{64}{256} = \frac{1}{4}$), the reserved tones rate ($\frac{\mathcal{T}}{N} = \frac{32}{256} = \frac{1}{8}$) is cut into half. It is evident from Fig. 4.7 that the signal reconstruction accuracy considerably improves by using reliable tones in conjunction with reserved tones. Further, the results of data-aided reconstruction for the optimistic case of no grid offset are shown in Fig. 4.8. The findings for the case of perfect grid alignment are inline with the observations for the grid offset case and the advantage of using the reliable tones is evident.

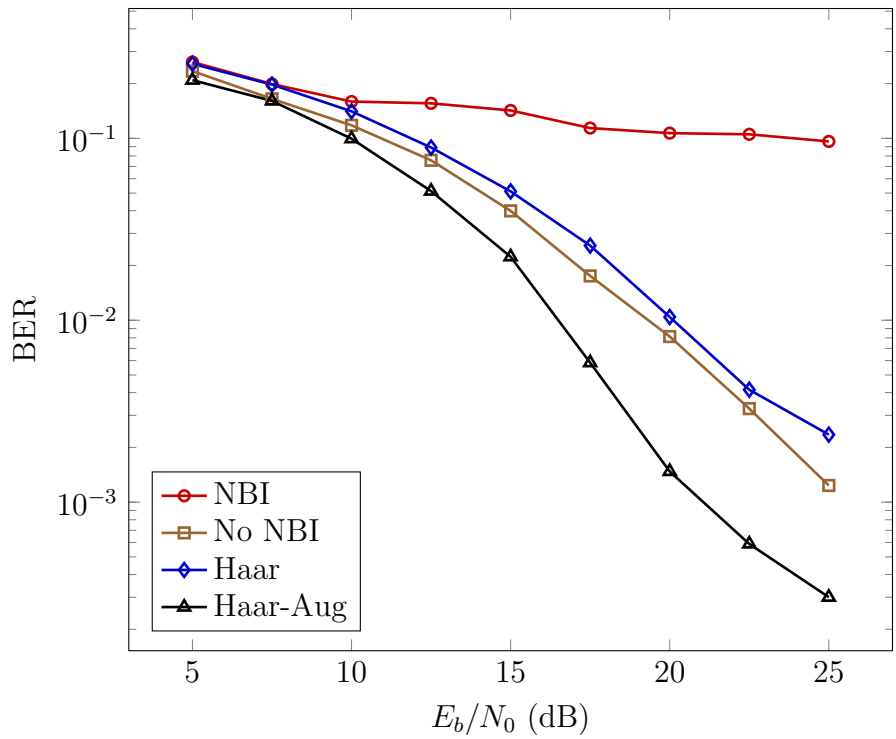

Figure 4.7: Reconstruction accuracy of the data-aided sparse recovery with grid offset.

Experiment 2: Proportionality between $|\mathcal{T}|$ and $|\mathcal{R}|$

This experiment is carried to demonstrate the relationship between the number of reliable tones available and the reserved tones. In Fig. 4.9, it is shown that the number of correct decisions made based on the utilized reliability criteria will significantly improve, if we choose more reserved tones. The format $|\mathcal{R}|\%/|\mathcal{T}|\%$, depicts the percentage of reliable carriers $|\mathcal{R}|\%$ chosen, when the reserved tones were $|\mathcal{T}|\%$. The results are obviously expected, as more reserved tones result in better NBI reconstruction in the first stage and hence lower residual perturbation, yielding more reliable carriers.

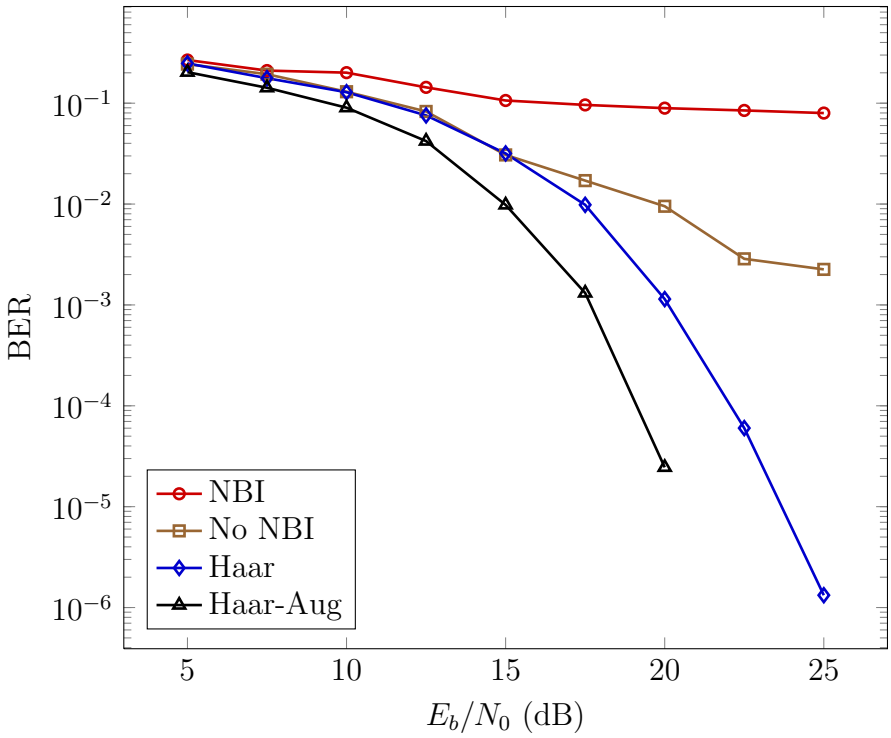

Figure 4.8: Reconstruction accuracy of the data-aided sparse recovery with no grid offset.

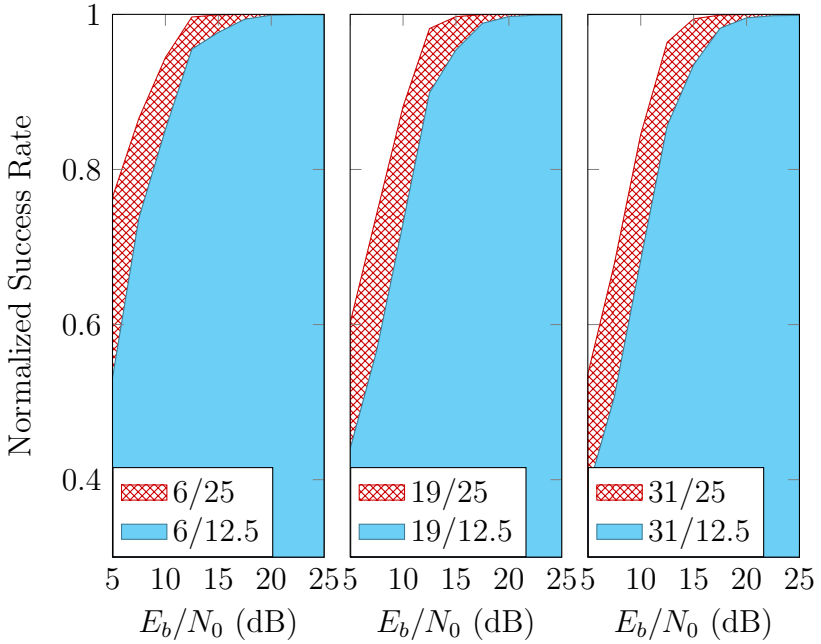

Figure 4.9: Reliability of the data-aided scheme as a function of reserved tones. The $|\mathcal{R}|\%/|\mathcal{T}|\%$ format represents the ratio of the percentage of reliable carriers picked $|\mathcal{R}|\%$ to the percentage of reserved tones $|\mathcal{T}|\%$.

4.6 Multiple Antenna Base-station

In this section, we consider the practical case of a BS equipped with multiple receiving antennas i.e., a SIMO setup. In this scenario, each antenna will receive the same transmitted signal impaired by NBI sources. While modelling NBI over multiple antennas, though it will be too restrictive to assume the same signal over all antennas, it is practical to expect the NBI signal to share a common support (i.e., to consider the received NBI signals *jointly sparse*). Further, the values of the active elements are considered to be varying across antennas. The common support property stems from the fact that the antenna elements are in close proximity and hence a distant NBI source will experience the same propagation delay (also true for multipaths). However, as the NBI sources may experience different fades to each antenna element, the values of the received signal will be different (i.e., both the phase and magnitude). Given an NBI impaired signal on each antenna element and the *a priori* information about the joint sparsity of the unknown, we propose to reconstruct it using the multiple measurement vector (MMV) based SABMP (i.e., MMV-SABMP) [76]. The main idea behind MMV-SABMP is to reconstruct the support of the unknown signal collaboratively, based on all measurement vectors and later reconstruct the amplitudes of the active elements individually.

4.6.1 Simulation Results

The performance of MMV based jointly sparse NBI reconstruction is compared against single measurement vector (SMV) based reconstruction. The number of receiver antennas is assumed to be 2 and received signals are combined using maximal ratio combining (MRC).

Experiment 1: SMV vs MMV reconstruction for jointly sparse NBI

In this experiment, the number of reserved tones is kept fixed at $|\mathcal{T}| = 32$ and the BER performance of MMV and SMV reconstruction is compared for varying E_b/N_0. The results are presented in Fig. 4.10, and demonstrate the ability of the MMV reconstruction to improve the BER performance for a wide range of E_b/N_0.

4.7 Chapter Conclusion

The problem of NBI reconstruction is addressed in this chapter. The proposed NBI cancellation scheme exploits the frequency domain sparsity of the unknown signal and adopts a low complexity Bayesian sparse recovery procedure. At the transmitter a few non-uniformly placed sub-carriers are kept data free to sense the NBI signal at the receiver. Further, it is noted that in practice, the sparsity of the NBI signal is destroyed by a grid mismatch between NBI sources and the system under consideration. Towards this end, first an accurate grid mismatch model is presented that is capable of assuming independent offsets for multiple

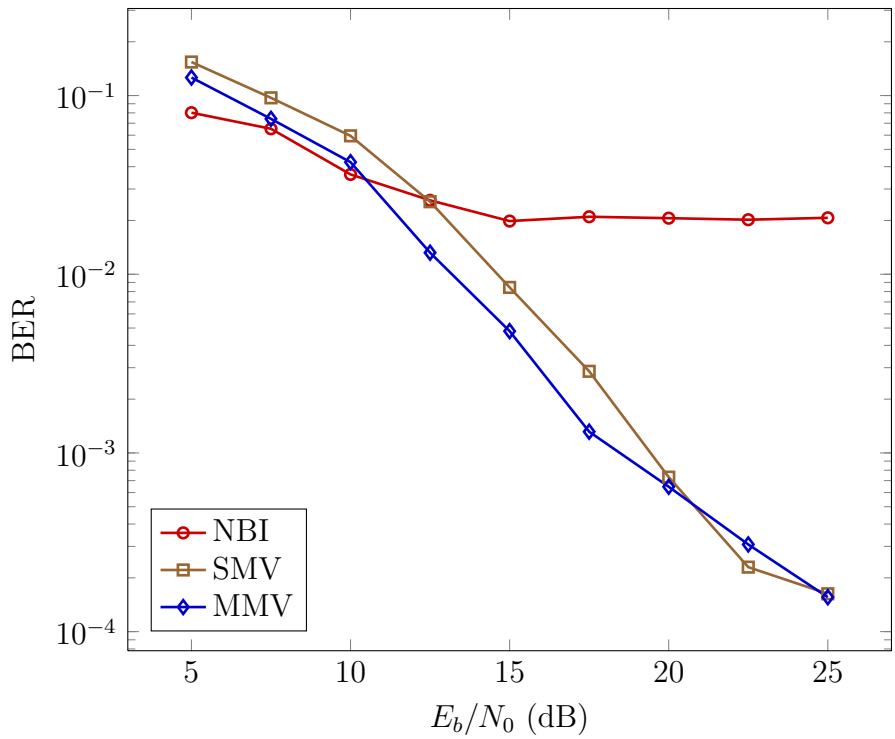

Figure 4.10: Reconstruction accuracy of the MMV scheme ($|\mathcal{T}| = 32$).

NBI sources. Secondly, prior to NBI reconstruction, the sparsity of the unknown signal is restored by employing a sparsifying transform. To improve the spectral efficiency of the proposed scheme, a data-aided NBI recovery procedure is outlined. This data-aided scheme relies on adaptively selecting a subset of data carriers and using them as additional measurements to enhance the NBI estimation. Numerical results are presented that depict the suitability of the proposed scheme for NBI mitigation.

CHAPTER 5

CONCLUSION AND FUTURE WORK

5.1 Concluding Remarks

In this thesis, fundamental problems with physical layer of multicarrier communications based on OFDM systems are addressed. These include power amplifier nonlinearity, peak-to-average power ratio reduction, channel estimation and the narrow band interference cancellation.

We started by presenting a power efficient OFDMA-CR system. Power efficiency is achieved by applying the proposed joint-compensation technique to an amplifier operating beyond saturation. Such an operation caused over-drive distortions which required to be estimated at the receiver. Hence sparse signal reconstruction scheme was employed at the receiver for distortion estimation. It was shown by numerical results for the entire communication system including channel

effects, that proposed formulation leads to improved EVM and BER performance. Further, the proposed technique was successfully applied in SIMO configuration. The results illustrate that, compared to the SISO case, additional performance enhancement can be obtained when multiple antennas are used at the receiver with MRC.

Next, we presented the problem of PAPR reduction. To this end, a low complexity Bayesian clipping recovery scheme was presented. The proposed WPA-SABMP scheme utilizes the undistorted phase property and weighting for enhanced clipping recovery. The proposed approach is agnostic to the non-Gaussian distribution of the clipping signal and so outperforms other traditional Bayesian approaches and ℓ_1 sparse recovery schemes. The WPA-SABMP scheme also utilizes the available statistics for enhanced recovery, however, when these statistics were unavailable the proposed scheme bootstrapped itself and successfully estimated the clipping distortions. Simulation results showed significant performance enhancement for WPA-SABMP scheme in both the error rate and complexity. The proposed scheme was then extended for the SIMO-OFDM systems and numerical findings were presented. In addition, a multi-user clipping recovery scheme was proposed and channel estimation strategies were presented for clipped OFDM signal. The simulation results for OFDMA clipping mitigation and data aided channel estimation also showed favourable results.

Finally we addressed the narrowband interference problem and a novel narrow band interference (NBI) mitigation scheme was proposed for SC-FDMA systems.

The proposed NBI cancellation scheme exploits the frequency domain sparsity of the unknown signal and adopts a low complexity Bayesian sparse recovery procedure. At the transmitter a few non-uniformly placed sub-carriers are kept data free to sense the NBI signal at the receiver. Further, it is noted that in practice, the sparsity of the NBI signal is destroyed by a grid mismatch between NBI sources and the system under consideration. Towards this end, first an accurate grid mismatch model is presented that is capable of assuming independent offsets for multiple NBI sources. Secondly, prior to NBI reconstruction, the sparsity of the unknown signal is restored by employing a sparsifying transform. To improve the spectral efficiency of the proposed scheme, a data-aided NBI recovery procedure is outlined. This data-aided scheme relies on adaptively selecting a subset of data carriers and using them as additional measurements to enhance the NBI estimation. Numerical results are presented that depict the suitability of the proposed scheme for NBI mitigation.

5.2 Future Work

The work we have presented in this thesis represents nodes with many potential branches. Here, we try to highlight some of the most important branches.

1. Amplifier Linearization: The proposed linearization approach doesn't use any information about the characteristics of the power amplifier and assumes any linearized power amplifier will behave as a limiter. An alternative approach might be to remove the DPD from the transmitter and utilize the power spectral

density of the power amplifier output for its linearization at the receiver.

2. PAPR Reduction: Bayesian recovery produces the estimate of the clipping signal in one go, appreciates the sparsity and incorporates the *a priori* information about the structure of the problem. On the contrary, a class of clipping recovery schemes, rely on iterative decoding and clipping of the received signal to mitigate the distortions (e.g., iterative maximum likelihood (ItML)). However, these schemes do not acknowledge the sparsity of the unknown or the available phase information. It appears that iterative thresholding based sparse reconstruction lies at the verge of the aforementioned techniques and can combine the advantage of iterative reconstruction while exploiting the available information.

3. Narrow Band Interference: Though there is numerical evidence towards the sparsifying ability of Haar transform in comparison with windowing. This brings up an important question about the availability/design of sparifying transforms. Keeping the sparsity of unknown signal as the cost function and looking for a transform that minimizes this lost function will not only help deepen the understanding of the characteristics that make Haar transform a suitable choice, but also lead to better linear sparsifying transforms.

REFERENCES

[1] A. Stamoulis, S. N. Diggavi, and N. Al-Dhahir, "Intercarrier interference in MIMO-OFDM," *IEEE Trans. Signal Process.*, vol. 50, no. 10, pp. 2451–2464, 2002.

[2] S. H. Han and J. H. Lee, "An overview of peak-to-average power ratio reduction techniques for multicarrier transmission," *IEEE Wireless Commun.*, vol. 12, no. 2, pp. 56–65, 2005.

[3] L. Wang and C. Tellambura, "An Overview of peak-to-average power ratio reduction techniques for OFDM systems," in *Proc. IEEE ISSPIT*, 2006, pp. 840–845.

[4] T. Jiang and Y. Wu, "An overview: peak-to-average power ratio reduction techniques for OFDM signals," *IEEE Trans. Broadcast.*, vol. 54, no. 2, pp. 257–268, 2008.

[5] D. W. Lim, S. J. Heo, and J. S. No, "An overview of peak-to-average power ratio reduction schemes for OFDM signals," *J. Commun. Netw.*, vol. 11, no. 3, pp. 229–239, 2009.

[6] F. M. Ghannouchi and O. Hammi, "Behavioral modeling and predistortion," *IEEE Microw. Mag.*, vol. 10, no. 7, pp. 52–64, 2009.

[7] O. Hammi, J. Sirois, S. Boumaiza, and F. M. Ghannouchi, "Design and performance analysis of mismatched Doherty amplifiers using an accurate load-pull-based model," *IEEE Trans. Microw. Theory Techn.*, vol. 54, no. 8, pp. 3246–3254, 2006.

[8] H.-H. Chen, C.-H. Lin, P.-C. Huang, and J.-T. Chen, "Joint polynomial and look-up-table predistortion power amplifier linearization," *IEEE Trans. Circuits Syst. II, Exp. Briefs*, vol. 53, no. 8, pp. 612–616, 2006.

[9] X. Cai and G. B. Giannakis, "Error probability minimizing pilots for OFDM with M-PSK modulation over Rayleigh-fading channels," *IEEE Trans. Veh. Technol.*, vol. 53, no. 1, pp. 146–155, 2004.

[10] K. Z. Islam, T. Y. Al-Naffouri, and N. Al-Dhahir, "On optimum pilot design for comb-type OFDM transmission over doubly-selective channels," *IEEE Trans. Commun.*, vol. 59, no. 4, pp. 930–935, 2011.

[11] T. Y. Al-Naffouri, K. Z. Islam, N. Al-Dhahir, and S. Lu, "A model reduction approach for OFDM channel estimation under high mobility conditions," *IEEE Trans. Signal Process.*, vol. 58, no. 4, pp. 2181–2193, 2010.

[12] Z. Wu and C. R. Nassar, "Narrowband interference rejection in OFDM via carrier interferometry spreading codes," *IEEE Trans. Wireless Commun.*, vol. 4, no. 4, pp. 1491–1505, 2005.

[13] R. Nilsson, F. Sjoberg, and J. P. LeBlanc, "A rank-reduced LMMSE canceller for narrowband interference suppression in OFDM-based systems," *IEEE Trans. Commun.*, vol. 51, no. 12, pp. 2126–2140, 2003.

[14] A. Batra and J. R. Zeidler, "Narrowband interference mitigation in BICM OFDM systems," in *IEEE Int. Conf. on Acous. Speech and Sig. Process. (ICASSP)*. IEEE, 2009, pp. 2605–2608.

[15] G. Taubock and F. Hlawatsch, "A compressed sensing technique for OFDM channel estimation in mobile environments: Exploiting channel sparsity for reducing pilots," in *IEEE Int. Conf. on Acous. Speech and Sig. Process. (ICASSP)*. IEEE, 2008, pp. 2885–2888.

[16] G. Caire, T. Y. Al-Naffouri, and A. K. Narayanan, "Impulse noise cancellation in OFDM: an application of compressed sensing," in *IEEE Int. Symp. on Inf. Theory (ISIT)*. IEEE, 2008, pp. 1293–1297.

[17] E. B. Al-Safadi and T. Y. Al-Naffouri, "Peak reduction and clipping mitigation in OFDM by augmented compressive sensing," *IEEE Trans. Signal Process.*, vol. 60, no. 7, pp. 3834–3839, 2012.

[18] J. L. Paredes, G. R. Arce, and Z. Wang, "Ultra-wideband compressed sensing: channel estimation," *IEEE J. Sel. Topics Signal Process.*, vol. 1, no. 3, pp. 383–395, 2007.

[19] G. Shi, J. Lin, X. Chen, F. Qi, D. Liu, and L. Zhang, "UWB echo signal detection with ultra-low rate sampling based on compressed sensing," *IEEE Trans. Circuits Syst. II, Exp. Briefs*, vol. 55, no. 4, pp. 379–383, 2008.

[20] M. A. Figueiredo, R. D. Nowak, and S. J. Wright, "Gradient projection for sparse reconstruction: Application to compressed sensing and other inverse problems," *IEEE J. Sel. Topics Signal Process.*, vol. 1, no. 4, pp. 586–597, 2007.

[21] M. Lustig, D. L. Donoho, J. M. Santos, and J. M. Pauly, "Compressed sensing MRI," *IEEE Signal Process. Mag.*, vol. 25, no. 2, pp. 72–82, 2008.

[22] M. Herman and T. Strohmer, "Compressed sensing radar," in *IEEE Radar Conf.* IEEE, 2008, pp. 1–6.

[23] M. A. Herman and T. Strohmer, "High-resolution radar via compressed sensing," *IEEE Trans. Signal Process.*, vol. 57, no. 6, pp. 2275–2284, 2009.

[24] E. J. Candès and M. B. Wakin, "An introduction to compressive sampling," *IEEE Signal Process. Mag.*, vol. 25, no. 2, pp. 21–30, 2008.

[25] S. Ji, Y. Xue, and L. Carin, "Bayesian compressive sensing," *IEEE Trans. Signal Process.*, vol. 56, no. 6, pp. 2346–2356, 2008.

[26] P. Schniter, L. C. Potter, and J. Ziniel, "Fast Bayesian matching pursuit," in *Proc. Inform. Theory & Appl. Workshop, Feb. 2008.*

[27] A. A. Quadeer and T. Y. Al-Naffouri, "Structure-Based Bayesian Sparse Reconstruction," *IEEE Trans. Signal Process.*, vol. 60, no. 12, pp. 6354–6367, 2012.

[28] T. Blumensath and M. E. Davies, "Gradient pursuits," *IEEE Trans. Signal Process.*, vol. 56, no. 6, pp. 2370–2382, 2008.

[29] J. A. Tropp and A. C. Gilbert, "Signal recovery from random measurements via orthogonal matching pursuit," *IEEE Trans. Inf. Theory*, vol. 53, no. 12, pp. 4655–4666, 2007.

[30] D. Needell and J. A. Tropp, "CoSaMP: Iterative signal recovery from incomplete and inaccurate samples," *Appl. Computat. Harmon. Anal.*, vol. 26, no. 3, pp. 301–321, 2009.

[31] I. F. Akyildiz, W.-Y. Lee, M. C. Vuran, and S. Mohanty, "NeXt generation/dynamic spectrum access/cognitive radio wireless networks: a survey," *Computer Networks*, vol. 50, no. 13, pp. 2127–2159, 2006.

[32] F. S. P. T. Force, "Report of the spectrum efficiency working group," 2002.

[33] D. Kivanc, G. Li, and H. Liu, "Computationally efficient bandwidth allocation and power control for OFDMA," *IEEE Trans. Wireless Commun.*, vol. 2, no. 6, pp. 1150–1158, 2003.

[34] K. Rawat, M. Rawat, and F. Ghannouchi, "Compensating I–Q imperfections in hybrid RF/digital predistortion with an adapted lookup table implemented

in an FPGA," *IEEE Trans. Circuits Syst. II, Exp. Briefs*, vol. 57, no. 5, pp. 389–393, 2010.

[35] A. Ghadam, S. Burglechner, A. Gokceoglu, M. Valkama, and A. Springer, "Implementation and performance of DSP-oriented feedforward power amplifier linearizer," *IEEE Trans. Circuits Syst. I, Reg. Papers*, vol. 59, no. 2, pp. 409–425, 2012.

[36] S.-C. Jung, O. Hammi, and F. M. Ghannouchi, "Design optimization and DPD linearization of GaN-based unsymmetrical Doherty power amplifiers for 3G multicarrier applications," *IEEE Trans. Microw. Theory Techn.*, vol. 57, no. 9, pp. 2105–2113, 2009.

[37] T. Liu, S. Boumaiza, and F. M. Ghannouchi, "Deembedding static nonlinearities and accurately identifying and modeling memory effects in wide-band RF transmitters," *IEEE Trans. Microw. Theory Techn.*, vol. 53, no. 11, pp. 3578–3587, 2005.

[38] A. A. Quadeer, S. F. Ahmed, and T. Y. Al-Naffouri, "Structure based Bayesian sparse reconstruction using non-Gaussian prior," in *Proc. 49th Annu. Allerton Conf. Commun., Control, Comput.*, 2011, pp. 277–283.

[39] J. Boutros and E. Viterbo, "Signal space diversity: a power-and bandwidth-efficient diversity technique for the Rayleigh fading channel," *IEEE Trans. Inf. Theory*, vol. 44, no. 4, pp. 1453–1467, 1998.

[40] M. Masood and T. Al-Naffouri, "A Fast Non-Gaussian Bayesian Matching Pursuit Method for Sparse Reconstruction," *IEEE Trans. Signal Process*, to appear.

[41] M. D. McKinley, K. A. Remley, M. Myslinski, J. S. Kenney, D. Schreurs, and B. Nauwelaers, "EVM calculation for broadband modulated signals," in *64th ARFTG Conf. Dig*, 2004, pp. 45–52.

[42] S. Forestier, P. Bouysse, R. Quere, A. Mallet, J.-M. Nebus, and L. Lapierre, "Joint optimization of the power-added efficiency and the error-vector measurement of 20-GHz pHEMT amplifier through a new dynamic bias-control method," *IEEE Trans. Microw. Theory Techn.*, vol. 52, no. 4, pp. 1132–1141, 2004.

[43] B. G. Lee and S. Choi, *Broadband wireless access and local networks: mobile WiMAX and WiFi*. Artech House Publishers, 2008.

[44] D. Kim and G. L. Stuber, "Clipping noise mitigation for ofdm by decision-aided reconstruction," *IEEE Commun. Lett.*, vol. 3, no. 1, pp. 4–6, 1999.

[45] D. Tse and P. Viswanath, *Fundamentals of wireless communication*. Cambridge university press, 2005.

[46] F. F. J. MacWilliams and N. N. J. A. Sloane, *The Theory of Error-correcting Codes: Part 2*. Elsevier, 1977, vol. 16.

[47] J. Armstrong, "Peak-to-average power reduction for OFDM by repeated clipping and frequency domain filtering," *Elect. Lett.*, vol. 38, no. 5, pp. 246–247, 2002.

[48] L. Wang and C. Tellambura, "A simplified clipping and filtering technique for PAR reduction in OFDM systems," *IEEE Signal Process. Lett.*, vol. 12, no. 6, pp. 453–456, 2005.

[49] Y. C. Wang and Z. Q. Luo, "Optimized iterative clipping and filtering for PAPR reduction of OFDM signals," *IEEE Trans. Commun.*, vol. 59, no. 1, pp. 33–37, 2011.

[50] E. B. Al-Safadi and T. Y. Al-Naffouri, "Pilotless Recovery of Nonlinearly Distorted OFDM Signals by Compressive Sensing over Reliable Data Carriers," in *Proc. IEEE Int. Workshop on Signal Process. Advances in Wireless Commun. (SPAWC)*, 2012.

[51] M. Masood and T. Y. Al-Naffouri, "Sparse Reconstruction Using Distribution Agnostic Bayesian Matching Pursuit," *IEEE Trans. Signal Process.*, vol. 61, no. 21, pp. 5298–5309, 2013.

[52] B. Wu, S. Cheng, and H. Wang, "Iterative channel estimation and signal detection in clipped OFDM," in *Proc. IEEE GLOBECOM*, 2005.

[53] A. H. Sayed, *Fundamentals of adaptive filtering*, 2003: Wiley.

[54] A. Ali, A. Al-Zahrani, T. Y. Al-Naffouri, and A. Naguib, "Receiver based PAPR reduction in OFDMA," *submitted to ICASSP 2014.*

[55] H. G. Myung, J. Lim, and D. Goodman, "Single carrier FDMA for uplink wireless transmission," *IEEE Veh. Technol. Mag.*, vol. 1, no. 3, pp. 30–38, 2006.

[56] D. Gerakoulis and P. Salmi, "An interference suppressing OFDM system for ultra wide bandwidth radio channels," in *proc. IEEE conf. ultra wideband syst. and tech.*, 2002, pp. 259–264.

[57] J. Zhang and J. Meng, "Robust narrowband interference rejection for power-line communication systems Using IS-OFDM," *IEEE Trans. Power Del.*, vol. 25, no. 2, pp. 680–692, 2010.

[58] Y. Wang, X. Dong, and I. J. Fair, "Spectrum shaping and NBI suppression in UWB communications," *IEEE Trans. Wireless Commun.*, vol. 6, no. 5, pp. 1944–1952, 2007.

[59] J. Coon, "Narrowband interference avoidance for ultra-wideband single-carrier block transmissions with frequency-domain equalization," *IEEE Trans. Wireless Commun.*, vol. 7, no. 10, pp. 4032–4039, 2008.

[60] D. Darsena, "Successive narrowband interference cancellation for OFDM systems," *IEEE Commun. Lett.*, vol. 11, no. 1, pp. 73–75, 2007.

[61] D. Darsena and F. Verde, "Successive NBI cancellation using soft decisions for OFDM systems," *IEEE Signal Process. Lett.*, vol. 15, pp. 873–876, 2008.

[62] A. Gomaa and N. Al-Dhahir, "A sparsity-aware approach for NBI estimation in MIMO-OFDM," *IEEE Trans. Wireless Commun.*, vol. 10, no. 6, pp. 1854–1862, 2011.

[63] M. S. Sohail, T. Y. Al-Naffouri, and S. N. Al-Ghadhban, "Narrow Band Interference Cancellation in OFDM: A Structured Maximum Likelihood Approach," in *IEEE SPAWC*, 2012.

[64] L. Mei, Q. Zhang, X. Sha, and N. Zhang, "WFRFT Precoding for Narrowband Interference Suppression in DFT-Based Block Transmission Systems," *IEEE Commun. Lett.*

[65] A. J. Redfern, "Receiver window design for multicarrier communication systems," *IEEE J. Sel. Areas Commun.*, vol. 20, no. 5, pp. 1029–1036, 2002.

[66] G. Tang, B. Bhaskar, P. Shah, and B. Recht, "Compressed Sensing Off the Grid," *IEEE Trans. Inf. Theory*, vol. 59, no. 11, pp. 7465–7490, 2013.

[67] S. D. Babacan, R. Molina, and A. K. Katsaggelos, "Bayesian compressive sensing using Laplace priors," *IEEE Trans. Image Process*, vol. 19, no. 1, pp. 53–63, 2010.

[68] N. O'Donoughue and J. M. Moura, "On the product of independent complex Gaussians," *IEEE Trans. Signal Process.*, vol. 60, no. 3, pp. 1050–1063, 2012.

[69] G. Berardinelli, B. E. Priyanto, T. B. Sorensen, and P. Mogensen, "Improving SC-FDMA performance by turbo equalization in UTRA LTE uplink," in *Proc. IEEE Veh. Technol. Conf.*, 2008.

[70] G. Huang, A. Nix, and S. Armour, "Decision feedback equalization in SC-FDMA," in *Proc. IEEE PIMRC*, 2008.

[71] D. Zonoobi, A. A. Kassim, and Y. V. Venkatesh, "Gini index as sparsity measure for signal reconstruction from compressive samples," *IEEE J. Sel. Topics Signal Process.*, vol. 5, no. 5, pp. 927–932, 2011.

[72] M. Lopes, "Estimating Unknown Sparsity in Compressed Sensing," in *Proc. 30th ICML*, 2013.

[73] A. Haar, "Zur theorie der orthogonalen funktionensysteme," *Mathematische Annalen*, vol. 69, no. 3, pp. 331–371, 1910.

[74] A. Ali, O. Hammi, and T. Y. Al-Naffouri, "Compressed Sensing Based Joint-Compensation of Power Amplifier's Distortions in OFDMA Cognitive Radio Systems," *IEEE J. Emerg. Sel. Topic Circuits Syst.*, vol. 3, no. 4, pp. 508–520, 2013.

[75] D. S. Owodunni, A. Ali, A. A. Quadeer, E. B. Al-Safadi, O. Hammi, and T. Y. Al-Naffouri, "Compressed sensing techniques for receiver based post-compensation of transmitter's nonlinear distortions in OFDM systems," *Signal Process.*, vol. 97, pp. 282–293, 2014.

[76] M. Masood and T. Y. Al-Naffouri, "Support Agnostic Bayesian Recovery of Jointly Sparse Signals," in *Proc. EUSIPCO*, 2014.

Vitae

- Anum Ali
- Born in Chakwal, Pakistan on Sep. 22nd, 1989.
- Received Bachelor of Science (B.S.) degree in Electrical Engineering from COMSATS Institute of Information Technology, Islamabad, Pakistan in July 2011.
- Research Associate in COMSATS Institute of Information Technology, Islamabad, Pakistan from Aug. 2011 to Aug. 2012.
- Joined the Electrical Engineering Department at King Fahd University of Petroleum and Minerals in Sep. 2012.
- Email: anumali@ieee.org

List of Publications

- **Anum Ali**, Oualid Hammi and Tareq Y. Al-Naffouri, "Compressed Sensing based Joint-Compensation of Power Amplifier's Distortions in OFDMA Cognitive Radio Systems", *IEEE Journal on Emerging and Selected Topics in Circuits and Systems (JETCAS)*, vol. 3, no. 4, pp. 508-520, Dec. 2013.

- **Anum Ali**, Abdullatif Al-Rabah, Mudassir Masood and Tareq Y. Al-Naffouri, "Receiver-based Recovery of Clipped OFDM Signals for PAPR Reduction: A Bayesian Approach", submitted to *IEEE Transactions on Signal Processing.*

- **Anum Ali**, Mudassir Masood, Muhammad S. Sohail, Samir Al-Ghadhban and Tareq Y. Al-Naffouri "Narrowband Interference Mitigation in SC-FDMA Using Bayesian Sparse Recovery", submitted to *IEEE Transactions on Signal Processing.*

- **Anum Ali**, Ali Al-Zahrani, Tareq Y. Al-Naffouri and Ayman Naguib "Receiver Based PAPR Reduction in OFDMA", in Proceedings of *IEEE International Conference on Acoustics, Speech, and Signal Processing (ICASSP)*, 2014.

- **Anum Ali**, Damilola S. Owodunni, Oualid Hammi and Tareq Y. Al-Naffouri, "System and method for joint compensation of power amplifier's distortions", US patent pending.

- Damilola S. Owodunni, **Anum Ali**, Ahmed A. Quadeer, Ebrahim B. Al-Safadi, Oualid Hammi and Tareq Y. Al-Naffouri, "Compressed Sensing Techniques for Receiver based Post-Compensation of Transmitter's Nonlinear Distortions in OFDM Systems", *Signal Processing*, vol. 97, pp. 282-293, Apr. 2014.

- Ebrahim B. Al-Safadi, Tareq Y. Al-Naffouri, Mudassir Masoor and **Anum Ali**, "Nonlinear Distortion Reduction in OFDM from Reliable Perturbations in Data Carriers", to be submitted to *Signal Processing*.

- Abdullatif Al-Rabah , Mudassir Masood, **Anum Ali** and Tareq Y. Al-Naffouri, "Receiver-Based Bayesian PAPR Reduction in OFDM", in Proceedings of *European Signal Processing Conference (EUSIPCO)*, 2013.